Bacterial Migration and Motion In a Fluid Phase and Near a Solid Surface

---

A Dissertation

Presented to

the Faculty of the School of Engineering and Applied Science

University of Virginia

In Partial Fulfillment

of the Requirements for the Degree

Doctor of Philosophy (Chemical Engineering)

by

Paul D. Frymier Jr.

January, 1995

APPROVAL SHEET

This dissertation is submitted in partial fulfillment of the

requirements for the degree of

Doctor of Philosophy (Chemical Engineering)

Paul Inzmier

Author

This dissertation had been read and approved by the Examining Committee:

Roseanne M. Ford

Peter T. Cummings

Dissertation Co-Advisors

John McConnell

Eric J. Fernandez

Arthur D. Brell

Accepted for the School of Engineering and Applied Science:

R. W. Hill

Dean, School of Engineering and
Applied Science
January, 1995

Abstract

An understanding of the migration and motion of bacteria in a fluid phase and near solid surfaces is necessary to characterize processes such as the bioremediation of hazardous waste, the pathogenesis of infection, industrial biofouling and wastewater treatment, among others.

This study addresses three questions concerning the prediction of the distribution of a population of bacteria in a fluid phase and the motion of bacteria near a solid surface: Under what conditions does a one-dimensional phenomenological model for the density of a population of chemotactic bacteria yield an adequate representation of the migration of bacteria subject to a one-dimensional attractant gradient? How are the values of transport coefficients obtained from experimental data affected by the use of the one-dimensional phenomenological model and also by the use of different descriptions of bacterial swimming behavior in a mathematically rigorous balance equation? How is the characteristic motion of bacteria swimming in a fluid affected by the presence of a solid phase?

A computer simulation that rigorously models the movement of a large population of individual chemotactic bacteria in three dimensions is developed to test the validity of a one-dimensional phenomenological model for bacterial migration in a fluid. It is found that, to within the precision of the simulation technique, the one-dimensional model yields solutions very similar to the rigorous simulation technique for a wide range of conditions relevant to experimental studies in a stopped-flow diffusion chamber.

The finite element method (FEM) is used to obtain solutions to a more rigorous equation for the migration of a population of bacteria in response to a one-dimensional attractant gradient. FEM solutions are compared to solutions of a one-dimensional phenomenological model to determine the error incurred when this model is used to obtain the value of the chemotactic sensitivity coefficient, a macroscopic transport coefficient. It is

found that the value of the chemotactic sensitivity obtained from experimental data using the FEM solutions and solutions using the one-dimensional model can be significantly different. The chemotactic sensitivity coefficient is also shown to be sensitive to the choice of the model for down gradient swimming behavior, leading to errors as large as 100% in the chemotactic sensitivity coefficient.

The motion of *Escherichia coli* near a solid surface is studied using a microscope that tracks individual bacteria in three dimensions. The experimental data is compared to two analytical solutions: one for the motion of a sphere propelled by a single flagellum rotating at a constant speed and the other for a sphere moving perpendicularly toward the surface and opposing a constant force. It is found that the change in the cell swimming speed as a function of the surface-to-cell distance is in agreement with the change predicted by the two theories. The tendency of flagellated bacteria to swim in 30 - 50 μm circles when moving along a solid, planar surface is demonstrated in orthogonal projections of the tracking data that show the position of the solid surface relative to the bacterium. It is observed that bacteria turn parallel to a surface when swimming toward it instead of colliding with the surface. The Derjaguin-Landau and Verwey-Overbeek (DLVO) theory of colloid stability is applied to the experimentally measured electrostatic parameters for the system to offer an explanation for the tendency of cells to swim very close to the surface without becoming irreversibly adsorbed to it.

Acknowledgments

I would like to thank the following programs, institutions and individuals:

- The U. S. Department of Energy and the Oak Ridge Institute for Science Education for financial support through the Environmental Restoration and Waste Management Fellowship Program.

- The IBM Corporation for computing hardware support through the IBM Environmental Research Program.

- Dr. Howard Berg for the many helpful suggestions and technical assistance.

- Dr. Roseanne Ford and Dr. Peter Cummings for their advise and guidance.

- Kerri for constant support, suggestions, and motivation.

Contents

	page
1 Introduction	**1**
2 Cellular Dynamics Simulations of Bacterial Chemotaxis	**4**
2.1 Introduction	4
2.2 Background	6
2.3 Simulation Methodology	15
2.4 Results	20
2.4.1 Simulation conditions	20
2.4.2 Values of the parameter ε	24
2.4.3 Simulation and balance equation solutions	26
2.5 Conclusion	30
3 Numerical Solution of a Balance Equation for One-Dimensional Attractant Gradients	**32**
3.1 Introduction	32
3.2 Balance Equations	34
3.3 Methodologies	36
3.3.1 Finite element method solution	37
3.3.2 Stopped-flow diffusion chamber assay	40
3.3.3 Cellular dynamics simulation	42
3.4 Results	43

3.4.1 Comparison of models 44

3.4.2 Effect of model selection on the chemotaxis transport coefficient 48

3.5 Conclusion 56

4 Bacteria-Surface Interactions 58

4.1 Introduction 58

4.2 Background 60

4.3 Methods and Materials 66

4.3.1 Preparation of samples 67

4.3.2 Measurement of electrophoretic mobility 68

4.3.3 Tracking microscope 69

4.3.4 Data analysis algorithm 77

4.4 Results 79

4.4.1 Bulk tracking experiments 79

4.4.2 Near surface tracking experiments 88

4.4.3 Effect of the solid surface on the swimming speed 98

4.4.4 Comparison of experimental data to solutions of theories for spheres: Wild type cells 102

4.4.5 Comparison of experimental data to solutions of theories for spheres: Smooth swimming cells 109

4.5 Discussion 121

4.6 Conclusion 125

5 Summary and Concluding Remarks 127

5.1 Comparison and Validation of Models 127

5.2 Bacteria-Surface Interactions 129

5.3 Concluding Remarks 131

A Relating Mean Run Time and Attractant Gradient 141

B Turn Angle Probability Distribution 145

C Direction Change Distribution 147

D Genotype of HCB437 149

E Growth Media and Buffer Solution Compositions 151

F Additional Wild Type and Smooth Swimming Bacterial Traces 153

List of Symbols

Symbols

a	attractant concentration	mol/cm^3
a_0	initial attractant concentration	cells/cm^3
A_{123}	Hamaker constant for the buffer-bacteria-glass system	J
b	bacterial density sphere radius	cells/cm cm
b_0	initial bacterial density	cells/cm^3
c	bacterial density	cells/cm^3
D	diffusion coefficient	cm^2/s
e	charge on an electron	C
F	force function	
G	shape function	
G_A	Van der Waals interaction potential	J
G_E	electrostatic interaction potential	J
G_T	total interaction potential	J
h	depth of simulation box or separation distance	cm
$\mathbf{J}_b^{\text{diff}}$	diffusive bacterial flux	cells/cm^2-s
k	turn angle distribution	
$k_{+-/-+}$	one-dimensional turn angle distributions	
K	reduced turn angle distribution	
K_d	dissociation constant for receptor binding	mol/cm^3
k_B	Boltzmann's constant	J/K

l	length of simulation box	cm
L	length of finite element domain	
M_i	concentration of ion i	mol/l
n	number of samples angle-dependent bacterial density	cells/cm^3
n^+	number of bacteria moving in the $+z$ direction	
n^-	number of bacteria moving in the $-z$ direction	
N	number of bacteria	
N_A	Avagadro's number	1/mol
N_b	number of bound receptors	
N_T	total number of receptors	
O	on the order of	
$p^{+/-}$	one-dimensional direction change probabilities	1/s
p_r	probability of reversing direction	
$\mathbf{r}$	position vector	
S	sample variance	
$\hat{\mathbf{s}}$	direction coordinate vector	
s	one-dimensional swimming speed	cm/s
S	sample variance	
t	time	s
$t_{\alpha/2}$	value of the Student t with a 100(1-α)% confidence interval	
T	temperature	K
U	speed of a sphere in Brenner's solution	cm/s
v	three-dimensional bacterial swimming speed	cm/s
$\langle X \rangle$	sample mean	

x, y, z	direction coordinates	
z_i	charge on ion i	

Greek Symbols

α	turn angle parameter of velocity solution	
β	tumbling probability	1/s
β_0	tumbling probability in the absence of an attractant gradient	1/s
$\beta^{\pm}$	one-dimensional tumbling probabilities	1/s
χ_0	chemotactic sensitivity coefficient	cm^2/s
ε	parameter of turn angle distribution	
ε_r	relative permittivity	
ε_0	permittivity of a vacuum	C/V-cm
ϕ	surface potential	J
Φ	difference angle	
γ	constant in a bilinear interpolation for a property	
κ	reciprocal Debye length	1/cm
λ	parameter in Brenner's solution for the velocity of a sphere	
μ	viscosity electrophoretic mobility	g/cm-s μm-cm/V-s
μ_0	random motility coefficient	cm^2/s
μ_i	mean of population i	
θ	angle between bacterial direction and z-axis	
$\dot{\theta}$	angular speed	1/s
Θ	Heaviside operator	
ρ	random number	

σ	bacterial density in Alt's cell balance	cells/cm^3
τ	run length	s
$\langle \tau^{\pm} \rangle$	mean run time in the +/- direction	s
$\langle \tau_0 \rangle$	mean run time in the absence of an attractant gradient	s
υ	proportionality constant in the definition of the chemotactic sensitivity	
ω	weighting parameter for the finite element algorithm	
Ω	mean squared displacement	cm^2
ψ	mean cosine of the turn angle	
ζ	zeta potential	mV
$\vec{\nabla}_r$	gradient operator	

Superscripts

+	in the positive direction
-	in the negative direction
e	element index
3D	three-dimensional
1D	one-dimensional

Subscripts

0	in the absence of an attractant gradient, an initial value, or the result of a perturbation analysis
1, 2, 3, 4	indices
i, *j*, *k*, *l*, *m*	indices
z	in the *z* direction

List of Figures

page

2.1 Schematic representation of the SFDC used by Ford and co-workers. Impinging flow from the upper and lower ports creates an initial step change in attractant concentration at the center of the chamber and a uniform distribution of bacteria. The approximate dimensions of the chamber are 4 cm × 2 cm × 0.2 cm. On the right is an exploded view of the simulation box which is referred to later in the text. 11

2.2 Logic diagram for the CD simulation methodology. 18

2.3 Planar projections of a sample three-dimensional trace of a simulated bacterium moving in the absence of an attractant gradient. Ignoring the partial initial and final runs, the bacterium executed 46 runs in 244.2 s for an average run time of 5.3 s. 19

2.4 Mean squared displacement Ω as a function of t. 22

2.5 Summary plot of cases presented. 25

2.6 Values in $z-t$ space where ε_1 is significant. Shown are regions in the $z-t$ plane inside which the quantity ε_1 has ranges $\varepsilon_1 > 1$, $\varepsilon_1 > 0.5$ and $\varepsilon_1 < 0.5$. 26

2.7 Comparison of RTBL and simulation results for $a_0 = 0.2$ mM and $\chi_0^{3D} = 3.5 \times 10^{-4}$ cm²/s at t = 0.5, 3, 6, and 12 minutes. The smoother of the curves represents the results from RTBL. 27

2.8 Comparison of RTBL and simulation results for $a_0 = 0.2$ mM and $\chi_0^{3D} = 105 \times 10^{-4}$ cm²/s at t = 0.5 and 6 min. Note the change of scale on the vertical axis. 28

2.9 Comparison of RTBL and simulation results for $a_0 = 1.2$ mM and $\chi_0^{3D} = 3.5 \times 10^{-4}$ cm²/s at t = 0.5 and 6 min. 29

2.10 Comparison of RTBL and simulation results for $a_0 = 0.02$ mM and $\chi_0^{3D} = 3.5 \times 10^{-4}$ cm²/s at t = 0.5 and 6 min. Note the change of scale on the vertical axis. 29

3.1 This is an example of the type of grid used in obtaining the finite element solutions presented in this paper. The actual grids used contained 200 divisions in the z direction and 10 divisions in the θ direction. The length L was 1.2 cm. 38

3.2 This is an example of a single element in the grid. The "nodes" of the grid are the corners of the elements. The values of dependent variable $n_z(z, \theta, t)$ at the nodes are $n_{z(i)}$, $n_{z(j)}$, $n_{z(k)}$ and $n_{z(l)}$. 39

3.3 Schematic representation (left) of the SFDC used by Ford and co-workers. Impinging flow from the upper and lower ports creates an initial step change in attractant gradient at the center of the chamber and a uniform distribution of bacteria. The approximate dimensions of the chamber are 4 cm × 2 cm × 0.2 cm. On the right is an exploded view of the region of the SFDC used by the theoretical methodologies in this work to generate solutions for the cell density profile. 41

3.4 Comparison of the finite element solution of the balance equation for one-dimensional gradients. Shown are solutions to Equation 3.1 (solid line), CD simulation (squares) and the RTBL model (dashed line) for $\chi_0^{3D} = 3.5 \times 10^{-4}$ cm²/s. Dimensionless bacterial density, c/c_0 is plotted

as a function of the position z along the SFDC for times of 1, 2, 4, and 6 min. Position $z = 0$ corresponds to the position of the initial step change in the attractant concentration at $t = 0$ with a fucose concentration of 0.2 mM initially in the bottom of the SFDC ($0 < z \leq 0.4$ cm in the graphs). 46

3.5 Comparison of the finite element solution of the balance equation for one-dimensional gradients. Shown are solutions to Equation 3.1 (solid line), CD simulation (squares) and the RTBL model (dashed line) for $\chi_0^{3D} = 105 \times 10^{-4}$ cm²/s. Solutions are shown at 1, 2, 4 and 6 min. 47

3.6 The area between the dimensionless bacterial density curve and $c \setminus c_0 = 1$ in the SFDC. The area under the bacterial density curve for the half of the SFDC with a high concentration of attractant is plotted as a function of $\sqrt{t}$ for the case shown in Figure 3.8. The value of χ_0 used to produce the model results is $\chi_0^{3D} = 1.9 \times 10^{-4}$ cm²/s and yields the same slope as a linear least squares regression of the experimental data. In this comparison the offset time has been included in the simulation solutions [71]. 49

3.7 Finite element solutions to the balance equation for one-dimensional gradients using $\chi_0^{3D} = 105 \times 10^{-4}$ cm²/s. In the first case (solid line), the tumbling frequency β is allowed to increase above its basal level β_0 for populations of bacteria moving against the attractant gradient according to Equation 3.3. In the second case (dashed line), the tumbling frequency is assumed to return to its basal value for bacteria moving against an attractant gradient according to Equation 3.4. 51

3.8 Comparison of FEM solutions to experimental data. FEM solutions to the balance equation for one-dimensional gradients (solid line) and experimental data [72] (circles) for the response of *E. coli* to α-methylaspartate in the SFDC with a 0.01 mM initial concentration of α-methylaspartate in the bottom of the SFDC (right side of figure) are

shown. Also shown (dashed line) is the dimensionless attractant concentration, a/a_0. In the FEM model solution, the tumbling frequency β is allowed to increase above its basal level β_0 for populations of bacteria moving against the attractant gradient according to Equation 3.3. The value of χ_0^{3D} used in the model solution was 1.9×10^{-4} cm²/s. 53

3.9 Comparison of FEM solutions to experimental data. FEM solutions of the balance equation for one-dimensional gradients (solid line) and experimental data [72] (circles) for the response of *E. coli* to α-methylaspartate in the SFDC are shown. In the FEM model solution, the tumbling frequency βreturns to its basal value β_0 for populations of bacteria moving against the attractant gradient according to Equation 3.4. The value of χ_0^{3D} used in the model solution was 3.8×10^{-4} cm²/s. 54

3.10 Finite element solutions to the balance equation for one-dimensional gradients. In the first case (solid line), the partial derivative with respect to time is included in the substantial derivative of the number of bound receptors (Equation 6). In the second case (dashed line), the partial derivative with respect to time is omitted (Equation 7). Only a slight difference between the solutions is seen at 1 and 2 min and the two solutions are identical at 4 and 6 min on the scale of this graph. Both cases assume that the tumbling frequency returns to its basal value for cells moving in a direction against the attractant gradient.}. 55

4.1 Perpendicular motion of a sphere toward a plane surface. A sphere of radius b moves perpendicularly toward a solid surface with speed U at a separation distance of $h-b$. 63

4.2 Solution of Stokes' equation by Ramia *et. al.* The boundary element method (BEM) is used to solve Stokes' equation for a sphere with a flagellum rotating at constant rate moving toward a solid surface at 3

different orientation angles. Also shown is the solution to Equation 4.11, based on Brenner's solution for the force on a sphere perpendicularly approaching a solid surface. The dimensionless speed is the instantaneous speed divided by the speed in an unbounded fluid. The dimensionless distance is $(h-b)/b$. 65

4.3 Orientation angle definitions. This diagram illustrates the orientation angles referred to in the text. The orientation angle is defined such that 0° is coincident with the surface normal, 90° is parallel to the surface, and 180° is perpendicular to the surface and opposite in direction to the surface normal. 66

4.4 Schematic of the tracking microscope used in this study. Adapted from Berg [8]. 70

4.5 Close-up of the stage and coil arrangement on the microscope. Adapted from Berg [8]. 71

4.6 Alignment of the ends of the optical fibers. This is the alignment of the ends of the optical fibers as the would appear viewed from the chamber along the light path to the three mirrors in Figure 4.4. Adapted from Berg [8]. The z_1 and z_2 fibers appear superimposed on the center of the array viewed from this perspective. 72

4.7 Chamber type 1. This is a diagram of the type of chamber used in tracking experiments performed on bacteria in the bulk fluid. 74

4.8 Chamber type 2. The type of chamber was used in tracking experiments performed on bacteria near the surface is shown above (not to scale). 75

4.9 Dot array on top window of chamber type 2. Shown is an exploded view of the underside of the top window used in tracking experiments near the surface of the glass window. An array of dots was printed on the

underside of the window to allow the position of the surface of the glass to be determined (not to scale). 76

4.10 Wild type bacterium in bulk. Shown is the trace of a bacterium tracked in the bulk fluid. Each sample point is represented by a sphere. Yellow spheres represent sample points for which the analysis determined the bacterium was executing a run. Tumbles are indicated by purple spheres. 80

4.11 Wild type bacterium in bulk. This is another example of a trace from a bacterium tracked in the bulk fluid. 81

4.12 Speed of a wild type bacterium in the bulk fluid. Shown is the speed of the bacterium in Figure 4.10 as a function of time. 82

4.13 Close-up of bacterial swimming speed. Shown above is the region from 20 s to 30 s in Figure 4.12 above to illustrate the variation in swimming speed. Points where the analysis determined that tumbles occurred are shown as solid dots on the speed trace. 83

4.14 Run time distribution with methylcellulose. The distribution of run times from a tracking experiment is shown in which 0.18% (w/v) Methocel was added to the motility buffer. In this experiment 100 bacteria were tracked. The solid line is the Poisson interval distribution whose mean is the same as the experimental mean. 84

4.15 Turn angle distribution with Methocel. This figure shows the distribution of turn angles for the same experiment shown in Figure 4.14. The solid line is a curve fit to the data. 85

4.16 Run speed distribution with Methocel. This figure shows the distribution of run speeds for the same experiment shown in Figure 4.14. The solid line is a curve fit to the data. 86

4.17 Run time distribution without Methocel. This figure shows the distribution of run times from a tracking experiment in which no Methocel

was added to the motility buffer. In this experiment 130 bacteria were tracked. The solid line is the Poisson interval distribution whose mean is the same as the experimental mean. 86

4.18 Turn angle distribution without Methocel. This figure shows the distribution of turn angles for the same experiment shown in Figure 4.17. The solid line is a curve fit to the data. 87

4.19 Run speed distribution without Methocel. Shown is the distribution of run speeds for the same experiment shown in Figure 4.17. The solid line is a curve fit to the data. 88

4.20 Wild type bacterial trace 1. In this figure is shown the trace of a wild type bacterium that was tracked near the surface of the upper window of the tracking chamber. The red plane with a white border represents the position of the glass surface as determined by the position of the array of calibration dots as discussed in the text. The normal to the surface is shown as a white line. Yellow spheres represent sample points that are part of a run, while purple points represent points where the analysis algorithm indicated a tumble occurred. 90

4.21 Distance and speed for wild type bacterium 1. The swimming speed and the surface-to-cell distance as a function of time are plotted for the bacterium shown in Figure 4.20. The solid circles along the distance line indicate points where the bacterium tumbled. 91

4.22 Distance and orientation for wild type bacterium 1. The orientation and surface-to-cell distance are plotted as a function of time for the bacterium shown in Figure 4.20. The solid circles along the distance line indicate points where the bacterium tumbled. 91

4.23 Time variation in the apparent distance from the surface to a point known to be on the surface. The initial error of about 0.3 μm at the start of the

trial is due to the error in obtaining the position of the surface by focusing on the array of dots as discussed in the text. 92

4.24 Wild type bacterial trace 2. Shown is the trace of a wild type bacterium moving near the surface. The circular portions of the cell's path occurred when the cell was closest to the glass surface. 94

4.25 Distance and speed for wild type bacterium 2. The surface-to-cell distance and swimming speed are plotted for the bacterium shown in Figure 4.24. 95

4.26 Wild type bacterial trace 3. Shown is a cell trace from a wild type cell tracked near the glass surface. 96

4.27 Distance and speed for wild type bacterium 3. Note that the data analysis algorithm identified this trail as a single continuous run. 97

4.28 Distance and orientation for wild type bacterium 3. 97

4.29 Mean swimming speed as a function of orientation. The four distance values plotted in the figure are the midpoints of the regions identified in the legend. 99

4.30 Mean swimming speed as a function of orientation. The data shown in Figure 4.29 is plotted as a function of distance. Data for distances greater than 30 μm is omitted. 100

4.31 Mean swimming speed in bulk versus orientation. The data in the distance range 0-10 μm for the surface tracking experiments is also shown for comparison. 100

4.32 95% confidence intervals on the difference in mean swimming speeds. The difference in the values of the mean swimming speeds are plotted with brackets to indicate the 95% confidence interval on the population parameter, $\mu_1 - \mu_2$. 102

4.33 Wild type bacterial trace 4. This bacterium executes a single tumble, shown as a purple sphere at the lower center of the figure. 103

4.34 Distance and orientation for wild type bacterium 4. The single tumble is indicated by the solid dot at approximately 4 s. The bacterium can be seen to approach the surface at an orientation of between 135° and 180° at approximately 4 s and again at approximately 22 s. 104

4.35 Speed versus separation distance for wild type bacterium 4, first run. The experimental data (•) is plotted with the BEM solutions of Ramia *et al.* at 180° and 135° and the solution of Equation 4.11. The dimensionless distance is $(h-b)/b$ where b is the radius of the cell body and h is the distance from the center of the cell to the surface. The dimensionless speed is the instantaneous speed divided by the speed in an unbounded fluid, U_∞. For the experimental data, the velocity closest to 10 μm was used as U_∞. The dimensionless distance for the experimental data was calculated assuming a representative cell radius of 1 μm. 105

4.36 Speed versus separation distance for wild type bacterium 4, second run. The experimental data (•) is plotted with the BEM solutions of Ramia *et al.* and the solution of Equation 4.11. 106

4.37 Distance and speed for wild type bacterium 4. The single tumble is indicated by the solid dot at approximately 4 s. 106

4.38 Wild type bacterial trace 5. Shown is the trace of a wild type bacterium moving near the surface. The circular portions of the cell's path occurred when the cell was closest to the glass surface. 107

4.39 Distance and speed for wild type bacterium 5. 108

4.40 Distance and orientation for wild type bacterium 5. 108

4.41 Speed versus separation distance for wild type bacterium 5. The experimental data is plotted for the region in Figure 4.39 just prior to 2 s. 109

4.42 Smooth swimming bacterial trace 1, view 1. The smooth swimming bacteria have a deletion in the gene responsible for the tumbling behavior

in *E. coli.* As expected, the data analysis does not predict tumbles in the traces of these bacteria. 110

4.43 Smooth swimming bacterial trace 1, view 2. The bacterium whose trace is shown here is the same as that shown in Figure 4.42. The drift in the distance measurement causes error in the distance measurement which makes the bacteria in this trace appear to be a significant distance above the surface. Since it was observed that the calibration dots were in clear focus while bacteria were circling on the surface, the actual surface-to-cell distance for cells moving along the surface was less than 2 μm as discussed in the text. 111

4.44 Smooth swimming bacterial trace 1, view 3. The same trace as in Figures 4.42 and 4.43 is shown, viewed from the along the normal. The nearly perfect circles that bacteria often make when swimming along a solid surface can be seen plainly here. 112

4.45 Distance and speed for smooth swimming bacterium 1. The line indicating the distance to the surface oscillates between 5 s and 35 s, when the bacterium was observed to move along the surface in circles. The oscillations in the surface distance are the result of a nonuniform surface calibration. As the cell circles in this figure, its surface-to-cell distance appears to oscillate between approximately 4 and 5 μm. 113

4.46 Distance and orientation for smooth swimming bacterium 1. The bacterium begins to swim toward the surface at approximately 135°. 114

4.47 Speed versus distance for smooth swimming bacterium 1. 115

4.48 Close-up of orientation for smooth swimming bacterium 1. Here, data for each sample point is shown as a circle (on the distance curve) or as a square (on the orientation curve). 115

4.49 Smooth swimming bacterial trace 2. Tracking began for the bacterium whose trace is shown here at approximately 35 μm from the surface. The bacterium approached the surface and then began swimming in circles on the surface. 117

4.50 Speed versus orientation for smooth swimming bacterium 2. 118

4.51 Speed versus distance for smooth swimming bacterium 2. 118

4.52 Smooth swimming bacterial trace 3. The bacterium whose trace is shown here, approached the surface and began swimming along it, without showing significant curvature in its path. Essentially straight bacterial paths across the surface were observed, although not as frequently as circular paths. 119

4.53 Distance and speed for smooth swimming bacterium 3. 120

4.54 Speed versus distance for smooth swimming bacterium 3. 121

4.55 DLVO interaction potential as a function of separation distance. The potentials shown are those for van der Waals interaction G_A, electrostatic interaction G_E, and the sum of the two, G_T. for the wild type bacteria and glass in the phosphate buffer solution of ionic strength 0.19 M. The interaction potentials are normalized by k_BT. 123

4.56 Expanded view of the DLVO interaction potential shown in Figure 4.55. A secondary minimum $7k_BT$ deep exists at approximately 4.5 nm from the solid surface. 124

C.1 This is an illustration of the relationship between the direction vectors, $\hat{\mathbf{s}}$ and $\hat{\mathbf{s}}'$ and the angles θ and. θ'. 147

F.1 Wild type bacterial trace 6. 154

F.2 Wild type bacterial trace 7. 155

F.3 Wild type bacterial trace 8. 156

F.4 Smooth swimming bacterial trace 4. 157

F.5 Smooth swimming bacterial trace 5. 158

F.6 Smooth swimming bacterial trace 6. 159

F.7 Smooth swimming bacterial trace 7. 160

List of Tables

		page
2.1	Summary of constants used in the CD simulations.	21
3.1	Values of constants used in solutions shown in Figures 3.4 and 3.5. These are the values of the constants used in the CD simulation and in solving Equation 3.1 and the RTBL equation.	45
3.2	Conditions for experimental measurement of the response of *E. coli* to α-methylaspartate [72].	52
3.3	Comparison of χ_0^{3D} values for different models. These values of χ_0^{3D} were obtained from fitting to experimental data for various models, tumbling mechanisms and inclusion/exclusion of temporal gradient in tumbling probability.	57
4.1	Electrostatic parameters for the wild type bacteria and finely crushed microscope cover slip glass.	69

Chapter 1

Introduction

The presence of bacteria in natural systems affects our lives in both positive and negative ways. Bacteria can detoxify synthetic compounds released into the environment as well as breakdown and mineralize contaminants in industrial and domestic waste water. However, they can also cause disease, produce compounds which are toxic, and foul industrial processes and marine surfaces. In order to determine the extent to which these processes occur, it is necessary to determine, among other things, the distribution of bacteria in the system of interest. Accurate predictions of the distribution and migration of bacteria in these systems make it possible to augment the beneficial aspects of a bacterial presence and to reduce the negative aspects.

This study attempts to answer the following three questions concerning the prediction of the distribution of a population of bacteria in a natural environment: To what extent do approximations implicit in a one-dimensional phenomenological model for the migration of a population of chemotactic bacteria in a fluid medium affect the ability of the model to accurately predict the distribution of bacteria? How are the values of transport coefficients obtained from experimental data affected by the use of the one-dimensional phenomenological model and also by the use of different descriptions of bacterial swimming behavior in a mathematically rigorous balance equation? How is the

characteristic motion of bacteria swimming in a solid phase affected in the presence of a solid phase?

Chapters 2 and 3 deal primarily with mathematical models for the migration of a population of chemotactic bacteria in a bulk fluid medium. In order to probe the validity of a one-dimensional phenomenologically-based model equation for the time evolution of the density of a population of chemotactic bacteria, a cellular level simulation is developed in Chapter 2. The simulation incorporates the constitutive relationships of the model equation, but is a mathematically much more accurate representation of the phenomena that the one-dimensional balance equation attempts to model. The simulation therefore allows the validity of the balance equation used in the model equation to be tested apart from the accuracy of the constitutive relationships integral to the model.

A priori knowledge of the characteristics of bacterial motion is necessary to develop the proper constitutive relationships for inclusion in the model equation. However, in many situations, balance equations are applied to experimental studies in order to obtain the values of population-based transport coefficients with incomplete knowledge of the behavior of the bacteria being modeled or the extrapolation of the behavior of one type of bacteria to another type. Chapter 3 examines the use of balance equations and constitutive relationships in the analysis of experimental data on bacterial chemotaxis in the stopped-flow diffusion chamber. In the analysis of these experimental studies, the macroscopic transport coefficient χ_0^{3D}, the chemotactic sensitivity coefficient, is obtained from experimental data by matching the experimental data for the accumulation of bacteria around a gradient of a chemical attractant to solutions of mathematical models for the migration of bacteria in the presence of an attractant. This study shows the effect of different constitutive relationships for the tumbling response of bacteria to a negative attractant gradient on the value of χ_0 obtained from the experiment. In addition, this research also shows the effect of the use of a phenomenologically based, one-dimensional model

compared to a mathematically rigorous three-dimensional analogue on the value of χ_0 obtained from experiment.

Chapter 4 deals with the experimental observations of the changes in the characteristic motion of bacteria near a solid surface. These experiments were performed using both a wild type and a smooth swimming mutant of *E. coli*. The motion of cells near a plane surface is studied through the analysis of the paths of individual cells as they approach a surface. Distributions of the mean swimming speeds of cells are analyzed to determine if significant differences in the swimming speed are present for particular surface-to-cell distance regions or cell orientations (i.e.; toward or away from the surface). The swimming speeds of individual cells as function of the surface-to-cell distance are measured and compared to theoretical solutions to the equations of motion of a sphere moving toward a solid surface through a viscous fluid. Comparisons are made to two such theoretical solutions in order to determine if models that consider only hydrodynamic interactions are appropriate for application to bacterial motion near a surface and at what distances these models are valid. Calculation of the DLVO interaction potential for the wild type cells offer a possible explanation the interesting tendency of bacteria to "track" a solid surface, often executing nearly perfect circles as they swim.

Chapter 5 summarizes the results of this study and presents concluding remarks to address the significance of this study and suggests a next step in the study of bacterial migration in the presence of solid surfaces.

Chapter 2

Cellular Dynamics Simulations of Bacterial Chemotaxis

2.1 Introduction

The migration of bacterial populations plays an important role in many ecological processes such as nitrogen fixation, pathogenesis of infection, formation of biofilms and the degradation of chemical wastes in the environment (bioremediation) [21]. However, the extent to which migration affects these natural processes is not well understood. One approach toward quantifying this behavior is through the development and application of accurate mathematical models. The transport properties contained within these models are needed for the design of effective processes which would exploit the migration and redistribution of bacterial populations in natural environments. For example, bacterial migration is important for facilitating contact between the bacteria and the contaminant to be degraded for *in situ* applications of bioremediation.

Rivero and co-workers [62] have proposed a mathematical model (hereafter referred to as the RTBL model) describing the migration of bacteria in the presence of chemical gradients. Their model includes two transport coefficients: one to characterize random motion in the absence of chemical gradients and another representing the directed motion

associated with the presence of a chemical gradient. An experimental apparatus was designed by Ford *et al.* [30] to determine values for the transport properties which are utilized in the RTBL model. However, the model was derived for the case of motion in only one dimension while bacteria within the experimental apparatus actually move in three dimensions. Although the RTBL model was shown to agree well with experiments under conditions of steep one-dimensional chemical gradients, it has been subsequently shown [28] that the RTBL model cannot be reconciled with a more mathematically rigorous (but more difficult to apply in practice) three-dimensional cell balance approach except in one limiting case- specifically, the limit of a small one-dimensional attractant gradient implying symmetry in the remaining two dimensions. It is our objective in this paper to study the effect of simplifying assumptions implicit in the RTBL model on solutions obtained under the conditions of steep chemical gradients realized in the experiments of Ford *et al.* This is accomplished through the application of a cellular level simulation technique to problems where we expect the model to perform the least satisfactorily based on the series expansion analysis of Ford and Cummings [28]. Since the transport properties will be used for design of improved processes, it is critical that the models we use to interpret experimental data for determining these coefficients be accurate. With these tools available, those processes which most strongly influence bacterial behavior in natural settings can be identified and appropriate strategies for design and control can be implemented.

In Section 2.2, some of the previous work in the area of bacterial chemotaxis is reviewed. In Section 2.3, the methodology of the computer simulation program is described . The simulation results are compared with RTBL in Section 2.4 for conditions similar to those in the experimental apparatus developed by Ford and co-workers [30] to study the migration of bacterial populations. The comparisons are performed over a range of parameters characterizing the attractant concentration and bacterial sensitivity to the attractant in order to delineate the regions where the RTBL model is valid.

2.2 Background

Peritrichous bacteria such as *Escherichia coli* and *Salmonella typhimurium* are able to move in a fluid medium via the coordinated rotation of approximately 6-8 flagella attached to the perimeter of the cell. The movement of these bacteria can be described as alternating between two distinct phases: "running" and "tumbling" [11, 46, 70]. During the running phase, the cell's flagellar bundle rotates counterclockwise in a coordinated fashion and the cell moves in a nearly straight path. The duration of a typical run is of the order of 1 to 10 s. In the tumbling phase, the rotation of the flagella reverses and the bundle uncoils so that no coordinated linear motion occurs and the cell spins in place. The duration of the tumbling phase is of the order of 0.1 s. As a result of tumbling the cell reorients itself according to a turn angle distribution, which has a slight bias in the direction the cell was moving prior to tumbling [11, 47] and then begins a new run. In a uniform environment, the swimming pattern resembles a three-dimensional random walk similar to Brownian motion in molecular diffusion. This motion is described by the term random motility.

In the presence of a concentration gradient of an attractant (food sources such as sugars or amino acids, for example), bacteria are able to bias their random walk by changing their tumbling frequency [46, 70]. When moving toward an area of increasing (decreasing) attractant concentration, cells decrease (increase) their tumbling frequency, thereby increasing (decreasing) the lengths of their runs in the direction of increasing (decreasing) attractant concentration. In this way, a population of cells moving within an attractant gradient will exhibit a net movement toward the attractant source. This overall directed motion is called chemotaxis. The ability of chemotactic bacteria to direct their motion enables them to move to more favorable environments by swimming toward increasing concentrations of nutrients, giving these bacteria a competitive advantage over nonmotile bacteria [40].

A complete mathematical description of the motion of a population of chemotactic bacteria requires a set of cell balance equations along with constitutive relationships which relate the quantities in the cell balance equation to the properties of the cells and their motion. The three-dimensional cell balance equations of Alt [5] are the most general. Letting $\sigma(\mathbf{r},\hat{\mathbf{s}},\tau,t)$ be the number density of cells per unit volume at position $\mathbf{r}$ moving in direction $\hat{\mathbf{s}}$ with run time τ (i.e., the time since the preceding tumble), at time t, Alt's fundamental equation is:

$$\frac{\partial\sigma(\mathbf{r},\hat{\mathbf{s}},\tau,t)}{\partial t}=\frac{\partial\sigma(\mathbf{r},\hat{\mathbf{s}},\tau,t)}{\partial\tau}-\hat{\mathbf{s}}\bullet\vec{\nabla}_{\mathbf{r}}\left[v(\mathbf{r},t)\sigma(\mathbf{r},\hat{\mathbf{s}},\tau,t)\right]-\beta(\mathbf{r},\hat{\mathbf{s}},\tau,t)\sigma(\mathbf{r},\hat{\mathbf{s}},\tau,t) \quad (2.1)$$

for $\tau>0$ and:

$$\sigma(\mathbf{r},\hat{\mathbf{s}},0,t)=\int_0^{\infty}\int\beta(\mathbf{r},\hat{\mathbf{s}}',\tau,t)\,\sigma(\mathbf{r},\hat{\mathbf{s}}',\tau,t)k(\mathbf{r},\hat{\mathbf{s}}',t;\hat{\mathbf{s}})d\hat{\mathbf{s}}'d\tau \quad (2.2)$$

for $\tau=0$. Here, $\beta(\mathbf{r},\hat{\mathbf{s}},\tau,t)$ is the probability per unit time that a cell moving in direction $\hat{\mathbf{s}}$ at $\mathbf{r}$ at time t with run time τ tumbles at $\mathbf{r}$ at time t. The probability that a cell chooses the direction $\hat{\mathbf{s}}_2$ as its new direction after tumbling is $k(\mathbf{r},\hat{\mathbf{s}}_1,t;\hat{\mathbf{s}}_2)$. The subscript $\mathbf{r}$ emphasizes that the operator $\vec{\nabla}_{\mathbf{r}}$ is with respect to the spatial coordinate $\mathbf{r}$. The swimming speed of the bacteria is v and is known from experimental observations to be relatively constant over a range of attractant concentrations [11, 56]. Equation 2.1 states that the rate of change in the population of cells at $\mathbf{r}$ at time t moving in direction $\hat{\mathbf{s}}$ with run time τ is given by a term which reflects the change in the population due to changes in the run time, a term that reflects the change due to convection, and a term that reflects the loss to the population due to cells tumbling with probability β. Equation 2.2 states that one obtains an initial ($\tau=0$) population of cells moving in direction $\hat{\mathbf{s}}$ by considering cell populations which were moving in another direction $\hat{\mathbf{s}}'$ with run time τ, which tumbled at time t,

represented by the product $\beta(\mathbf{r},\hat{\mathbf{s}}',\tau,t)\sigma(\mathbf{r},\hat{\mathbf{s}}',\tau,t)$, and multiplying by the probability that the cell moves in the direction $\hat{\mathbf{s}}$ after tumbling, given by $k(\mathbf{r},\hat{\mathbf{s}}',t;\hat{\mathbf{s}})$. This product is integrated over all directions $\hat{\mathbf{s}}'$ and all run times τ.

Segel [66] and Rivero *et al.* [62] have developed simpler phenomenological models based on individual cell motion in one direction only. The one-dimensional balance equations of Segel are:

$$\frac{\partial n^+}{\partial t} = -\frac{\partial (sn^+)}{\partial t} + p^- n^- - p^+ n^+ \tag{2.3}$$

$$\frac{\partial n^-}{\partial t} = \frac{\partial (sn^-)}{\partial t} + p^+ n^+ - p^- n^- \tag{2.4}$$

where $n^+(z,t)$ is the density of cells at point z at time t moving in the positive z direction and $n^-(z,t)$ is the density of cells at point z at time t moving in the negative z direction, s is the one-dimensional, scalar swimming speed of the bacteria, $p^+ = p^+(z,t)$ is the probability per unit time that a cell moving in the positive z direction tumbles and becomes a cell moving in the negative z direction and $p^- = p^-(z,t)$ is the probability per unit time that a cell moving in the negative z direction tumbles and becomes a cell moving in the positive z direction.

The RTBL model is based on the cell balance equations of Segel. Under the assumption that the phenomenon of tumbling is a Poisson process [9], the tumbling probability β is equal to the inverse of the mean run time,

$$\beta = \frac{1}{\langle \tau \rangle} \tag{2.5}$$

This assumption is supported by the experimental work of Berg and Brown [11]. Rivero *et al.* write this equation in one dimension as:

$$\beta^{\pm} = \frac{1}{\langle \tau^{\pm} \rangle} \tag{2.6}$$

where $\beta^{\pm} = \beta^{\pm}(z,t)$ is the probability that a cell moving in the $\pm z$ direction tumbles and $\langle \tau^{\pm} \rangle$ is the mean run time for cells moving in the $\pm z$ directions, respectively. In addition, Rivero *et al.* propose:

$$p^{\pm} = \beta^{\pm} p_r \tag{2.7}$$

where p_r is the probability that a cell reverses direction after tumbling. The mean run times $\langle \tau^{\pm} \rangle$ are then related to the attractant concentration a and its gradient by:

$$\ln \frac{\langle \tau^{\pm} \rangle}{\langle \tau_0 \rangle} = \pm \frac{\chi_0^{1D}}{s} \frac{K_d}{(K_d + a)^2} \frac{\partial a}{\partial z} \tag{2.8}$$

where $\langle \tau_0 \rangle$ is the mean run time in the absence of a chemical gradient, K_d is the dissociation constant for the attractant-receptor binding and χ_0^{1D} is the one-dimensional chemotactic sensitivity parameter. In the RTBL model, Equations 2.6-2.8 form a set of constitutive equations for Segel's cell balance equations.

As shown in Appendix A, Equation 2.8 is a mathematical simplification of the expression for bacterial motion in three dimensions given by:

$$\ln \frac{\langle \tau \rangle}{\langle \tau_0 \rangle} = \frac{\chi_0^{3D}}{v} \frac{K_d}{(K_d + a)^2} \hat{\mathbf{s}} \cdot \vec{\nabla}_{\mathbf{r}} a \tag{2.9}$$

where χ_0^{3D} is the three-dimensional analogue of χ_0^{1D}. For a discussion of the derivation of Equation 2.9 above we refer the reader to Appendix A. Substituting Equation 2.5 into Equation 2.9 and rearranging, we have:

$$\beta = \beta_0 \exp\left[-\frac{\chi_0^{3D}}{v} \frac{K_d}{(K_d + a)^2} \hat{\mathbf{s}} \cdot \nabla a \right] \tag{2.10}$$

where:

$$\beta_0 = \frac{1}{\langle \tau_0 \rangle} \tag{2.11}$$

In the one-dimensional RTBL model:

$$\beta^{\pm} = \beta_0 \exp\left[\mp \frac{\chi_0^{1D}}{s} \frac{K_d}{(K_d + a)^2} \frac{\partial a}{\partial z} \right] \tag{2.12}$$

so the complete RTBL model is the set of Equations 2.3, 2.4, 2.6, 2.7, 2.11 and 2.12. For a discussion of the approximate nature of Equation 2.12 we refer the reader to Appendix A.

The RTBL model was applied to the interpretation of experimental data by Ford *et al.* [30] for *E. coli* K12 responding to fucose. The experiments were carried out in a stopped-flow diffusion chamber (SFDC) shown schematically in Figure 2.1. For assays of chemotactic bacteria in the SFDC, a suspension of bacteria at concentration b_0 is pumped at a uniform rate into the upper port of the chamber and a mixture of attractant at concentration a_0 and bacteria at concentration b_0 is pumped at a uniform rate into the lower port. Fluid exits through ports at the centerline of the chamber and the flow rates are controlled by a dual piston syringe pump so that for times $t < 0$, the two impinging streams form a step change in the attractant concentration at the center of the chamber. At time $t = 0$, flow into and out of the SFDC is stopped and the attractant begins to diffuse into the upper half of the chamber generating a time-dependent gradient. As bacteria sense the

gradient a band of high cell density forms where the gradient is large and moves downward in the chamber to regions of higher attractant concentration. The experimental geometry is one of symmetry in two dimensions (the x and y directions in Figure 2.1) with an attractant gradient in the third dimension (the z direction).

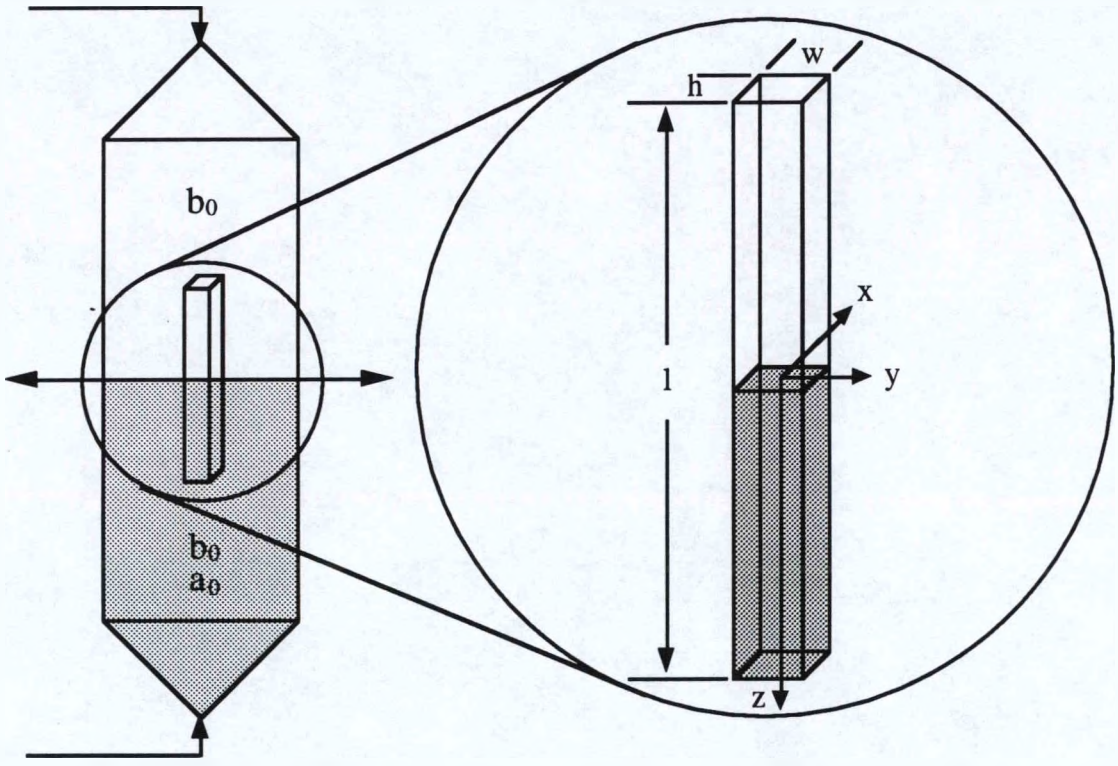

Figure 2.1: Schematic representation of the SFDC used by Ford and co-workers. Impinging flow from the upper and lower ports creates an initial step change in attractant concentration at the center of the chamber and a uniform distribution of bacteria. The approximate dimensions of the chamber are 4 cm × 2 cm × 0.2 cm. On the right is an exploded view of the simulation box which is referred to later in the text.

Ford and Cummings [28] studied in detail the relationship between the three-dimensional balance equations of Alt, Equations 2.1 and 2.2, and the one-dimensional equations of Segel, Equations 2.3 and 2.4, the latter being the basis for the RTBL model. Ford and Cummings showed that the Segel equations could only be derived rigorously from Alt's equations when the motion of the bacteria is confined to one dimension. They

considered three-dimensional systems with an attractant gradient in the z-coordinate direction and symmetry in the other two (x and y) coordinate directions so that:

$$\vec{\nabla}_r a = (0,0,\partial a / \partial z) \tag{2.13}$$

For cases of symmetry (as opposed to confinement to one-dimension), Ford and Cummings showed that the Alt equations could not be reduced to the Segel equations except in the limit of small ε, where ε is defined by:

$$\beta = \beta_0 \exp(-\varepsilon) \tag{2.14}$$

By comparing Equation 2.15 to Equation 2.10 and making use of Equation 2.13, ε can be written as

$$\varepsilon = \frac{\chi_0^{3D}}{v} \frac{K_d}{(K_d + a)^2} \frac{\partial a}{\partial z} \cos\theta \tag{2.15}$$

where θ is the angle made by the direction vector $\hat{\mathbf{s}}$ with the z axis. By perturbatively expanding in ε a reduced form of the Alt equation (obtained by integrating over τ, x and y) Ford and Cummings obtained:

$$\frac{\partial n_0^+}{\partial t} = -\frac{\partial}{\partial z}\left(\frac{v_0}{2} n_0^+\right) - \beta_1 n_0^+ k_{+-} + \beta_1 n_0^- k_{-+} \tag{2.16}$$

$$\frac{\partial n_0^-}{\partial t} = -\frac{\partial}{\partial z}\left(\frac{v_0}{2} n_0^-\right) - \beta_1 n_0^- k_{-+} + \beta_1 n_0^+ k_{+-} \tag{2.17}$$

where β_1 is the tumbling probability, k_{+-} is the probability that a cell moving in the positive z direction becomes a cell moving in the negative z direction after tumbling and k_{-+} is the probability that a cell moving in the negative z direction becomes a cell moving in the

positive z direction. The subscript 0 indicates that these are the leading order terms from series expansions in the parameter ε. This analysis clarifies the relationship between the one-dimensional cell speed s in the Segel equations and the three-dimensional cell speed v that is determined experimentally.

From this analysis, it is apparent that the correct speed to use in the one-dimensional equations is the observable three-dimensional cell speed v divided by 2 rather than $\sqrt{3}$ recommended by Segel [67] and used in the analysis of Ford and co-workers [29, 30]. Ford and Cummings noted that although this correction to the cell speed is small it would affect the value of the population parameters obtained from experiment. Using Equations (A.6) and (A.9) from Appendix A and the relationship

$$v = 2s \tag{2.18}$$

we have:

$$\chi_0^{3D} = \upsilon v^2 N_T = 4\chi_0^{1D} \tag{2.19}$$

where υ is a proportionality constant describing the fractional change in mean run time per unit time rate of change in cell surface receptors that are bound to attractant molecules. We note that using the relationship $s = v/\sqrt{3} = 0.557v$ instead of the correct relationship $s = 0.5v$ results in s being overestimated by 15.5%. It would consequently result in the χ_0^{3D} obtained from experiment being underestimated by 25% according to the relationship in Equation 2.19.

The studies of Ford *et al.* [30] and Ford and Lauffenburger [29] involved comparison of the experimentally measured bacterial density with the predictions of the RTBL model. For appropriately chosen values of χ_0^{1D}, there is good agreement between RTBL and experiment. Several approximations and/or assumptions are implicit in using

the RTBL model: first, use of the approximate one-dimensional balance equations, Equations 2.3 and 2.4; second, the diffusion approximation [62] which enables the RTBL model equations to be solved numerically at the macroscopic level; third, the model for the tumbling probability, Equation 2.10, which involves a proposed mechanism for the way in which bacteria sense and respond to their environment; and fourth, the simplification of the tumbling probability to the one-dimensional form, Equation 2.12, as described at the end of Appendix A. Of these four, three are mathematical approximations (first, second and fourth) and one is a phenomenological assumption. One role for the cellular dynamics simulations is to test the validity of the mathematical approximations and is the focus of this chapter. The validity of the phenomenological assumptions can be tested by comparing the simulation results with experiments, however this is not the subject of this chapter.

Since the RTBL model does agree well with experiment, a question then naturally arises. Is the agreement of RTBL with experiment fortuitously caused by cancellation of two or more sources of error introduced by the phenomenological assumption for the tumbling probability and the mathematical approximations? The most straightforward way to answer this question is to perform a cellular level simulation of bacterial motion corresponding to the experimental situation (bacteria moving in three-dimensional space in the presence of a one-dimensional attractant gradient) that eliminates the mathematical approximations by using the general (three-dimensional) tumbling probability model, Equation 2.10. The degree to which the RTBL model predictions and the simulation agree is then a measure of the validity of the mathematical approximations, and thus the validity of the RTBL model in describing real three-dimensional systems with attractant gradients in one spatial direction.

Computer simulations of the motion of individual bacteria have been reported by several researchers. Berg [9, 10] performed simulations to illustrate the random walks generated by single cells assuming Poisson statistics for the tumbling probability and a simple approximation to the bias in the turn angle distribution. Bornbusch and co-workers

[16, 17] investigated the effect of limiting the turning field size of a cell on its ability to locate an attractant source. Tankersley and Conner [73] performed simulations of single cell migration to illustrate how the differences between various cell types in the mechanisms used to move toward an attractant source resulted in markedly different patterns of migration. In the present work, we develop a computer simulation methodology which rigorously describes the three-dimensional motion of individual chemotactic bacteria for the situation present in the SFDC experiments. Unlike the previous computer simulations just described, a large population of bacteria (20,000 cells) are simulated and the experimentally measured turn angle distribution is incorporated into the mechanism for reorienting the cells after tumbling. The results of the simulation are compared with those obtained using the RTBL model which involves the assumptions and approximations detailed above.

2.3 Simulation Methodology

After setting the appropriate initial conditions, bacterial movement is simulated by performing three calculations for each individual bacterium at each time step. First, it is determined whether or not the cell tumbles. Second, if the cell tumbles then its new direction is chosen; if it does not tumble, its direction is maintained. Third, the cell's new position is computed based on its direction vector, swimming speed and the time step. The implementation of these three steps and other details of the simulation are described in this Section.

The simulation "box" is given an initial uniform random distribution of bacteria. Letting $b(\mathbf{r},t)$ be the bacterial density at position $\mathbf{r}$ at time t, then the initial concentration $b(\mathbf{r},t=0)$ (see Figure 2.1) is given by:

$$b(\mathbf{r},t=0)=b_0, \quad \begin{array}{l} -\frac{h}{2} \le x \le \frac{h}{2} \\ -\frac{w}{2} \le x \le \frac{w}{2} \\ -\frac{l}{2} \le x \le \frac{l}{2} \end{array} \tag{2.20}$$

An initial bacterial concentration of $b_0 = 2 \times 10^7$ cells/cm^3 was used in the experiments of Ford *et al.* [30]; however, for the simulation results presented here, we used an initial concentration of bacteria of $b_0 = 2 \times 10^6$ cells/cm^3 in order to reduce the calculations necessary at each time step by an order of magnitude. The bacteria are assigned initial direction vectors at random. A step change along the z-axis at time $t = 0$ in the concentration of an attractant, a, exists such that:

$$\begin{aligned} a(z, t=0) &= 0, \quad -\tfrac{l}{2} \le z < 0 \\ a(z, t=0) &= a_0, \quad 0 < z \le \tfrac{l}{2} \\ a(z,t) &= \frac{a_0}{2}\left[1 + \operatorname{erf}\left(\frac{z}{\sqrt{4Dt}}\right)\right], \quad t > 0, -\tfrac{l}{2} \le z \le \tfrac{l}{2} \end{aligned} \tag{2.21}$$

where a_0 is the initial attractant concentration introduced into one half of the chamber, D is the diffusion coefficient of the attractant, z is the position along the z axis and t is time. The solution given above for $t > 0$ can be found in Crank [23]. For $t > 0$, the motion of each bacterium is modeled as an independent, three-dimensional, biased random walk.

That the motion of each bacterium can be considered independent of the motion of other bacteria is justified by noting that the cell densities used in the SFDC experiments are low enough that intercellular distances are at least an order of magnitude greater than cellular diameters. However at much higher cell densities (by an order of magnitude or more), hydrodynamic interactions among swimming bacteria may be significant [33] In such cases, the application of this simulation technique would require additional terms in the equations of motion to account for hydrodynamic interactions between the bacteria. The position $\mathbf{r}_i$ of the bacterium i at time $t + \Delta t$, where Δt is the time step in the simulation, is given by:

$$\mathbf{r}_i(t + \Delta t) = \mathbf{r}_i(t) + v\hat{\mathbf{s}}_i \Delta t \tag{2.22}$$

where v is the three-dimensional swimming speed of the bacterium and $\hat{\mathbf{s}}_i$ is the unit vector in the direction of motion of the bacterium. The simulation box employs periodic boundary conditions [4]. If the cell moves out of the box, it is repositioned so that it reenters at the opposite wall, retaining a constant number of cells in the simulation box. The length of the simulation box in the direction of the attractant gradient (the z direction) is 0.8 cm. This is sufficiently large to ensure that the attractant concentration is uniform at the ends of the box ($z = \pm 0.4$ cm), at which points the cell density returns to the bulk density b_0.

The unit direction vectors for the bacteria evolve in time according to:

$$\hat{\mathbf{s}}_i(t+\Delta t) = \lambda_i \hat{\mathbf{s}}_i(t) + (1-\lambda_i)\hat{\mathbf{s}}_i' \tag{2.23}$$

where:

$$\lambda_i = \Theta[\rho_i(t+\Delta t) - \beta \Delta t] \tag{2.24}$$

In this equation, ρ_i is a random number chosen at time $t+\Delta t$ from a uniform distribution on [0,1], β is the tumbling probability, $\hat{\mathbf{s}}_i'$ is chosen randomly from the distribution for the change in direction after tumbling obtained by experimental observations of single cells by Berg and Brown [11], and Θ is the Heaviside function, defined as:

$$\Theta(x) = \begin{cases} 0, & x < 0 \\ 1, & x > 0 \end{cases} \tag{2.25}$$

Details on the method of choosing $\hat{\mathbf{s}}_i'$ are provided in Appendix B. Equation 2.24 implies that:

$$\lambda_i = 1 \quad \text{if } \rho_i \geq \beta \Delta t \tag{2.26}$$

$$\lambda_i = 0 \quad \text{if} \quad \rho_i < \beta\Delta t \tag{2.27}$$

so that a bacterium has probability $\beta\Delta t$ of tumbling and probability $(1-\beta\Delta t)$ of continuing its run. Thus, the tumbling probability in a zero gradient is constant and consistent with a Poisson distribution. The time step used in the simulation is $\Delta t = 0.1$ sec, the time corresponding to τ_t, the experimentally observed duration of a tumble. Therefore the tumbling process is effectively instantaneous in our simulation.

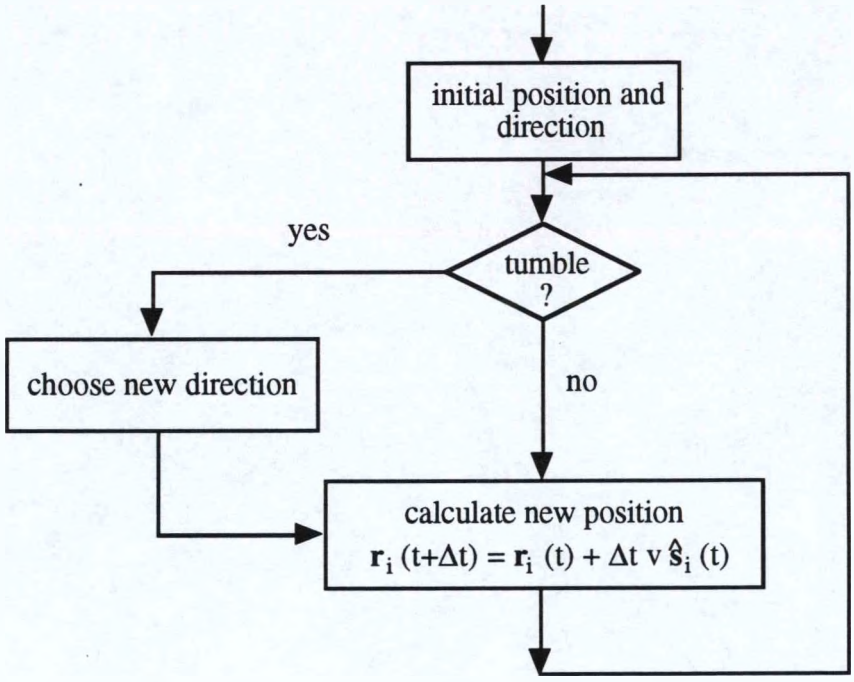

Figure 2.2: Logic diagram for the CD simulation methodology.

The logic diagram in Figure 2.2 summarizes the methodology described in this section. The simulation box is first initialized. At the start of the simulation loop, each bacterium decides whether or not to tumble (according to Equation 2.24). Based on whether or not it tumbles, either a new direction is chosen or the bacterium continues its

run in the same direction. Finally the bacterium moves to a new position based on its swimming speed and direction vector using an Euler's integration of the equation of motion. Figure 2.3 shows the path of a single cell generated by applying the simulation algorithm in the absence of a chemical gradient over a period of $2500\Delta t$ where $\Delta t = 0.1$ s. The cell swimming speed 22 μm/s and zero gradient tumbling probability (0.17 s^{-1}) are the same as for the simulations reported in Section 2.4. Periodic boundary conditions were not implemented in this sample trace.

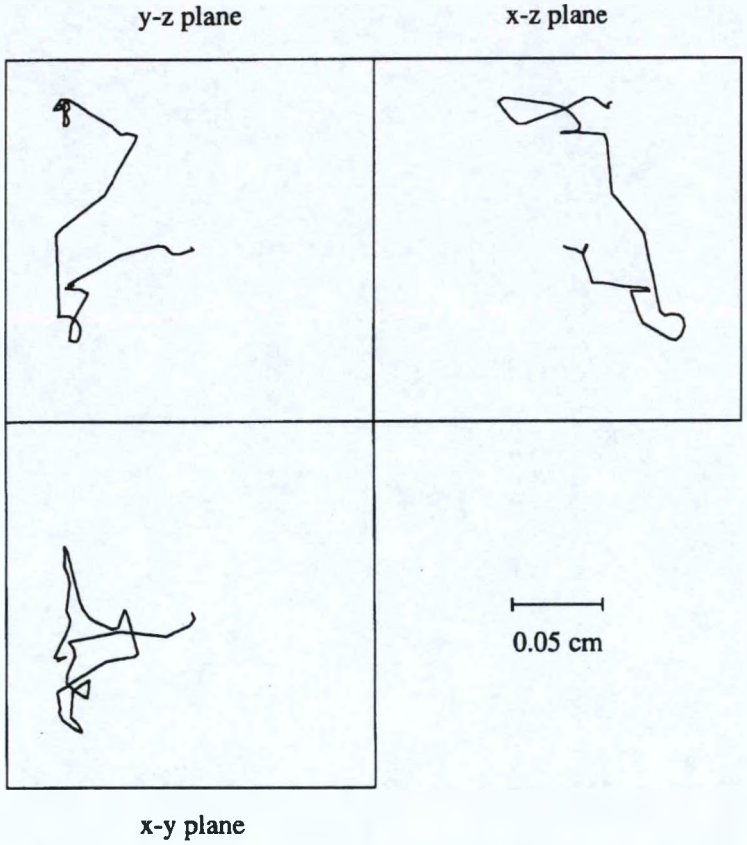

Figure 2.3: Planar projections of a sample three-dimensional trace of a simulated bacterium moving in the absence of an attractant gradient. Ignoring the partial initial and final runs, the bacterium executed 46 runs in 244.2 s for an average run time of 5.3 s.

In the next section, we discuss the results of the simulation.

2.4 Results

The goal of this section is to compare the results of the simulation outlined in Section 2.3 with those of the RTBL model over relatively large ranges of values for the chemotactic sensitivity, χ_0, and the attractant concentration gradient as determined by the initial attractant concentration, a_0. A statement of the conditions under which the simulations were performed are given and then the results obtained in each case are presented.

2.4.1 Simulation conditions

The experimental situation modeled in the simulations is that of the response of *E. coli* bacteria to a gradient of fucose in the SFDC of Ford *et al.* [30] (see Figure 2.1) with the conditions given in Table 2.1. The dimensions of the simulation box are 0.1 cm $\times$ 0.1 cm $\times$ 0.8 cm. At bacterial densities similar to those in the SFDC of 2.5×10^7 cells/cm^3, this would require 2×10^5 individual bacteria. As discussed in Section 2.3, a bacterial density of 2.5×10^6 cells/cm^3, corresponding to 2×10^4 individual cells, was used in the simulation. Since the bacteria are assumed to be independent of each other, using a density of 2.5×10^6 cells/cm^3 yields the same results as a density of 2.5×10^7 cells/cm^3 as long as densities are computed relative to the bulk value. The lower density (corresponding to fewer cells in the simulation box) decreases the computer time required for the calculation (proportional to N where N is the number of bacteria) at the cost of some increased statistical uncertainty (which is $O(N^{-1/2})$). The attractant concentration is modeled by Equation 2.21 presented in the previous section with the initial concentration of fucose in the lower half of the chamber equal to a_0. The diffusivity D of fucose given in Table 2.1 is the value reported by Ford and co-workers. A typical three-dimensional cell speed of 22 μm/s was used to be consistent with the one-dimensional speed of 11 μm/s used by

Ford *et al.* In their experimental studies, Ford and co-workers reported values for the random motility coefficient in the absence of an attractant, μ_0 of between 0.47×10^{-5} and 1.5×10^{-5} cm²/s. Lovely and Dalquist [44] derived the following relationship between the random motility coefficient, μ_0, the cell speed v, the mean run time in the absence of an attractant gradient $\langle\tau_0\rangle$:

$$\mu_0 = \frac{v^2\langle\tau_0\rangle}{3(1-\psi)} \tag{2.28}$$

where ψ is the average value of $\cos(\alpha)$, α being the angle between the direction vectors of a cell before and after tumbling. This is a general result for three-dimensional motion of bacteria; the only assumptions are a constant swimming speed, straight line runs between tumbles, and a Poisson distribution for run lengths. It is therefore consistent with the simulation algorithm and with Alt's general three-dimensional cell balance equations, 2.1 and 2.2, under the additional assumption of a constant cell swimming speed.

p_{t_0} (1/s)	v (μm/s)	a_0 (mM)	$\chi_0^{3D}\times10^4$ (cm²/s)	$D\times10^6$ (cm²/s)	K_d (mM)
0.17	22	0.02-1.2	3.5-105	6.9	0.08

Table 2.1: Summary of constants used in the CD simulations.

A seventh order polynomial fit (see Appendix B for further details) to the experimental data of Berg and Brown [11] was used and it was determined that $\psi = 0.36$. Using this value of ψ and values of 1.5×10^{-5} cm²/s for μ_0 and 22 μm/s for v, yields a value for $\langle\tau_0\rangle$ of 6.0 s by Equation 2.28. For a Poisson process, this corresponds to a tumbling probability in the absence of a gradient of $p_{t_0} = 0.17$ 1/s, which is the value that was used in the simulations. A time step of $\Delta t = 0.1$ s was used. For this time step, a

bacterium in the simulation moving in a isotropic medium will, on the average, tumble every 58 time steps. The values of the parameters used in the simulation are summarized in Table 2.1.

One test of the simulation methodology is to calculate the random motility μ_0 from the simulation and check that it matches the value given by Equation 2.28. A simulation was performed in the absence of an attractant gradient and the mean squared displacement $\Omega(t)$ of the bacteria was calculated from the definition:

$$\Omega(t) = \frac{1}{N}\sum_{i=1}^{N}\left[\mathbf{r}_i(t) - \mathbf{r}_i(0)\right]^2 \tag{2.29}$$

According to the Einstein relation [4]:

$$\Omega(t) \rightarrow 6\mu t \tag{2.30}$$

so that at long times Ω should become linear in t with slope 6μ.

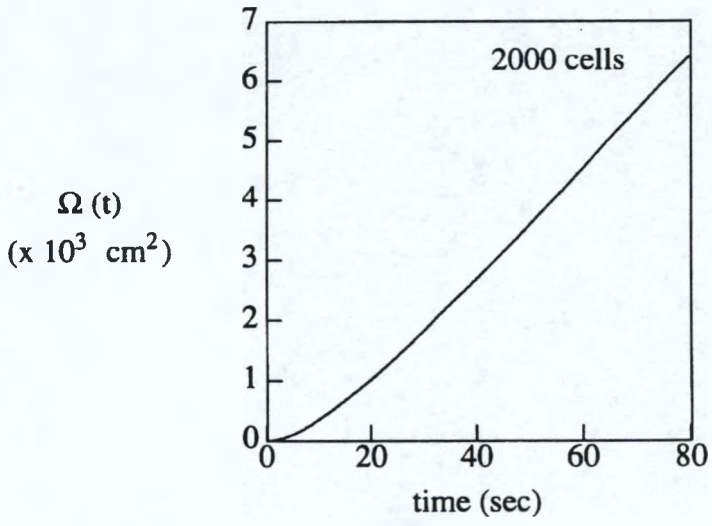

Figure 2.4: Mean squared displacement Ω as a function of t.

As can be seen in Figure 2.4, $\Omega(t)$ is linear in t at large t. The slope implies a value of 1.55×10^{-5} cm^2/s for μ which is within 3% of the correct value. This suggests that the simulation methodology is very accurate. Note that at short times Ω is quadratic in t. By fitting $\Omega(t)$ to at^2 for $t<2$ s, we find a is found to be equal to 452 μm^2/s^2 which is within 7% of v^2, consistent with the short time analysis of the RTBL model as presented by Othmer *et al.* [57]. The crossover from $\Omega(t)\sim t^2$ to $\Omega(t)\sim t$ corresponds to the transition to the diffusion regime in which the diffusion approximation, discussed by Rivero *et al.* [62], is valid. Hence, the fact that $\Omega(t)$ becomes linear in t for $t>10$s suggests that the diffusion approximation is satisfied at relatively short times. The diffusion approximation is utilized in the macroscopic version of the RTBL model solved by Ford *et al.* [30] and the simulation results suggest that the diffusion approximation should be accurate.

The macroscopic form of the RTBL model which follows from the diffusion approximation [62] was implemented in a finite difference program using a predictor-corrector method [26]. As discussed in Section 2.2 the RTBL model is expected to show the most deviation from the simulation for large attractant gradients and large values of the chemotactic sensitivity coefficient since the three-dimensional equations simplify to an analogue of the one-dimensional phenomenological model only in the limit of small ε, Equation 2.15. The range of values of the parameters χ_0 and a_0 over which we performed simulations and comparisons with the RTBL model include the lower (0.01 mM) and upper (1.0 mM) ranges of a_0 studied experimentally with the SFDC and the lower (3.5×10^{-4} cm^2/s) and upper (105×10^{-4} cm^2/s) limits on χ_0^{3D} measured experimentally [27, 50]. The cases that are considered in this study are summarized in Figure 2.5. Higher values of a_0 were not considered since for attractant concentrations significantly above ten times the dissociation constant for the attractant-receptor binding, K_d the receptors available for sensing concentration gradients become saturated [41] and

the cell no longer responds chemotactically. Simulations were also performed for intermediate values of the parameters a_0 and χ_0^{3D} to determine if significant differences could be observed between the simulation and the RTBL model. The results yielded similar trends to those presented here.

2.4.2 Values of the parameter ε

In view of the analysis of Ford and Cummings, it is interesting to consider the relative values of ε (see Equation 2.15) implied by the four cases considered. The parameter ε can be written in the form:

$$\varepsilon = \varepsilon_0 \cos\theta \frac{\partial(a/a_0)}{\partial(z/l)} \tag{2.31}$$

where ε_0, which is dimensionless and angle-independent, is given by:

$$\varepsilon_0 = \frac{\chi_0^{3D}}{vl} \frac{K_d a_0}{(K_d + a)^2} \tag{2.32}$$

Clearly, because of the gradient term $\partial(a/a_0)/\partial(z/l)$, which varies from $+\infty$ at $z=0$ and $t=0$ to essentially zero at $z=\pm l/2$, the value of ε can be very large and will be dependent on position and time. As the attractant profile relaxes with time, ε will become small at all positions. Thus, for given values of χ_0^{3D} and a_0 there will be a t-dependent range of z centered on $z=0$ which contracts as t increases and inside of which ε will be large. Based on the Ford and Cummings analysis, this might be the region for which the RTBL model may not be successful since the Alt equations simplify to the Segel equations only under the assumption of small ε. The larger ε_0 is, the greater will be the range of z and t included in this region. By evaluating ε_0 at $z=0$ where $a=a_0/2$ for all t, a dimensionless measure of the expected applicability of the RTBL model can be obtained,

larger values of ε_0 implying a smaller region of z and t over which RTBL might be applicable.

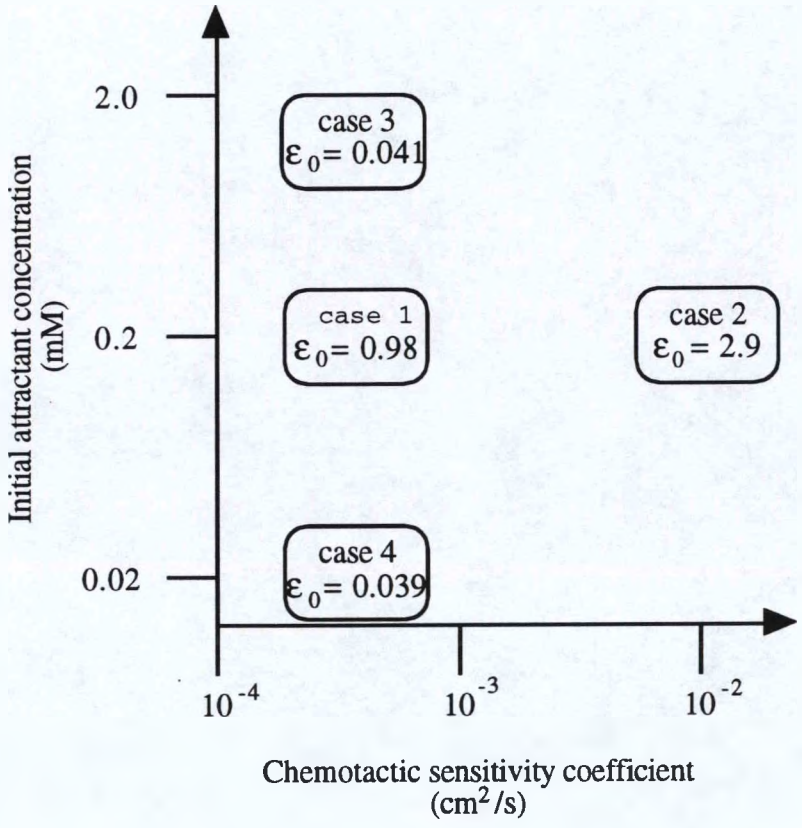

Figure 2.5: Summary plot of cases presented.

For the four cases shown in Figure 2.5, Cases 1, 2, 3 and 4 yield values for ε_0 of 0.098, 2.9, 0.041 and 0.039 respectively. On this basis, it might be expected that RTBL would be least applicable to Case 2 and most applicable in Cases 3 and 4. It should also be noted that ε_0 has its maximum value as a function of a_0 at $a_0 = 2K_d = 0.16$ mM which is near the value of 0.2 mM for Cases 1 and 2. In Figure 2.6, the quantity $\varepsilon_1 = \varepsilon / \cos\theta$ is shown as a function of z and t for Case 1. As is evident from this figure, ε_1 is significantly larger than zero over significant ranges of z and t. Thus, *a priori* one would expect that the RTBL model would not be very accurate.

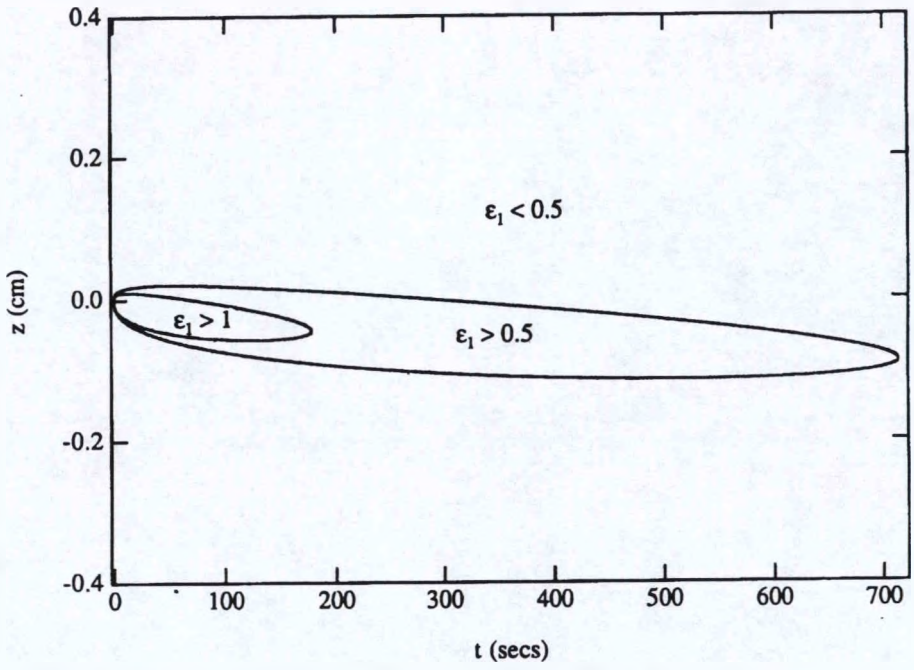

Figure 2.6: Values in $z-t$ space where ε_1 is significant. Shown are regions in the $z-t$ plane inside which the quantity ε_1 has ranges $\varepsilon_1 > 1$, $\varepsilon_1 > 0.5$ and $\varepsilon_1 < 0.5$.

2.4.3 Simulation and balance equation solutions

First, values of a_0 and χ_0^{3D} are considered that are similar to those used in the SFDC experiments of Ford *et al.* [30]. In Figure 2.7 the RTBL model with $s = v/2$ and $\chi_0^{1D} = \chi_0^{3D}/4$ is compared to the simulation results for $a_0 = 0.2$ mM and $\chi_0^{3D} = 3.5\times10^{-4}$ cm^2/s. These relationships are the proper ones between the three-dimensional and one-dimensional parameters as discussed previously in Section 2.2. They are used in the results for all cases presented in this work.

The points at which cell densities from the simulation are plotted in the figure are the average of the density in a "sampling bin" 0.01 cm wide centered around the point. Sampling is implemented over 50 time steps (which corresponds to 5 s) so the density reported for a point at a given time is the average density in the sampling bin over the

sampling period. The statistical error associated with the simulation causes the curve representing the simulation results to be a little noisy.

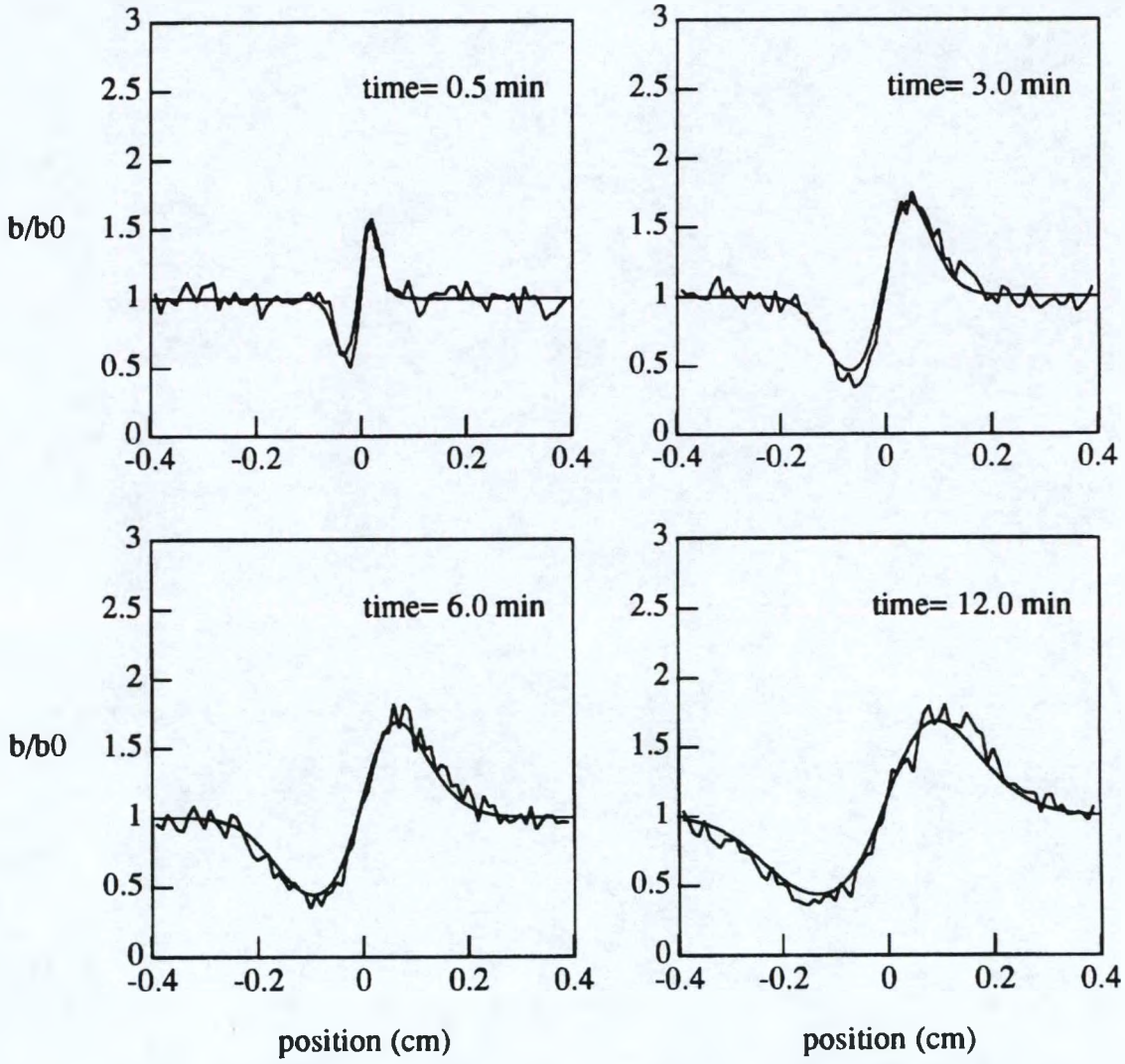

Figure 2.7: Comparison of RTBL and simulation results for $a_0 = 0.2$ mM and $\chi_0^{3D} = 3.5 \times 10^{-4}$ cm^2/s at t = 0.5, 3, 6, and 12 minutes. The smoother of the curves represents the results from RTBL.

The RTBL model agrees closely with the simulation in this case. The peak in the cell density profile is the result of a high density band of cells that forms where the concentration gradient is high. The trough in the density profile is the result of cell

depletion in the region behind the advancing concentration gradient as cells move with the gradient. These phenomena are also observed in experimental studies [30].

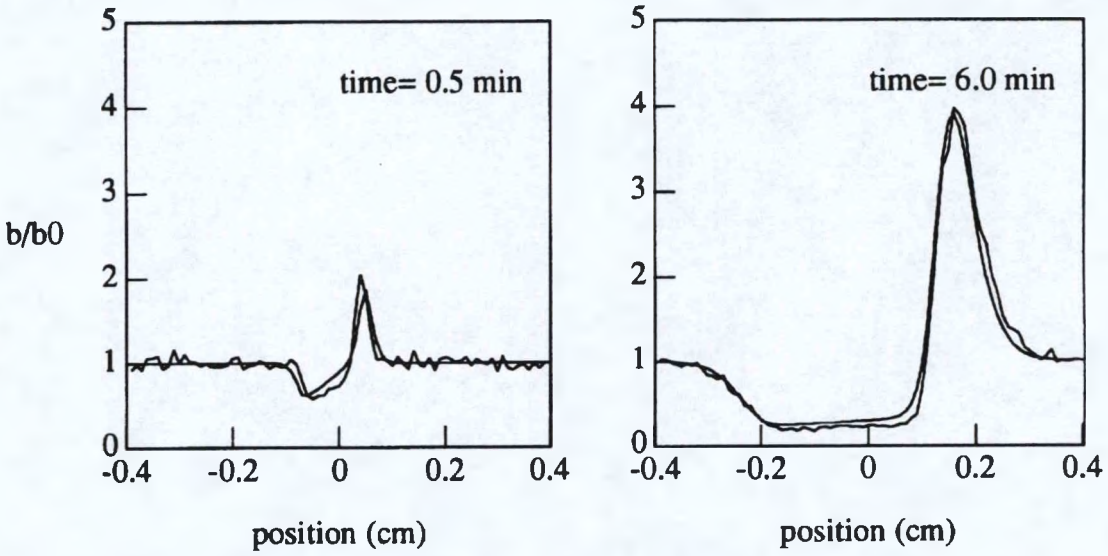

Figure 2.8: Comparison of RTBL and simulation results for $a_0 = 0.2$ mM and $\chi_0^{3D} = 105 \times 10^{-4}$ cm^2/s at $t = 0.5$ and 6 min. Note the change of scale on the vertical axis.

For the second case, shown in Figure 2.8, a value of $\chi_0^{3D} = 105 \times 10^{-4}$ cm^2/s was used , which is thirty times larger than the first case and the same initial attractant concentration a_0 as the previous case. Note that the scale on the vertical axis has been changed to allow for the higher peak value of the bacterial density at this value of χ_0^{3D}. Again, the simulation results agree well with those of the RTBL model.

Next the effect of the initial concentration, a_0 on the simulation and the RTBL model results are examined . In Figure 2.9, χ_0^{3D} is held fixed at $\chi_0^{3D} = 3.5 \times 10^{-4}$ cm^2/s as in the initial case and a_0 is increased to 1.2 mM, six times the value used in the first case. As in the two previous cases, the agreement between the two solutions is very good.

In Case 4, the effect of lowering the value of a_0 is examined . Figure 2.10 shows the results obtained using $a_0 = 0.02$ mM while holding χ_0^{3D} fixed. The simulation results show a larger maximum value of the bacteria density than does the RTBL model, but taking

into account statistical inaccuracies the deviation of the RTBL model from the simulation is quite small.

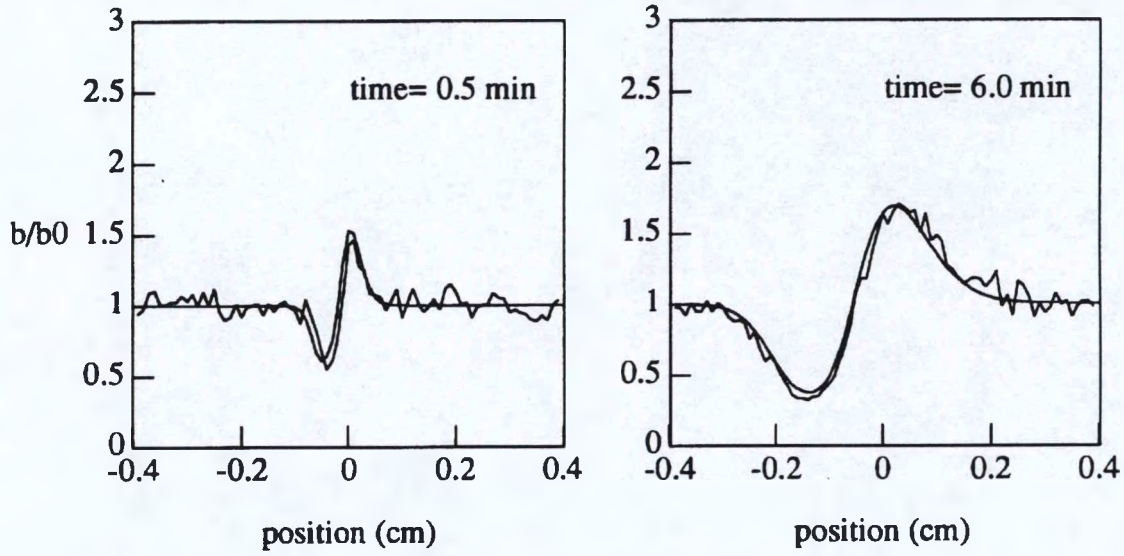

Figure 2.9: Comparison of RTBL and simulation results for $a_0 = 1.2$ mM and $\chi_0^{3D} = 3.5 \times 10^{-4}$ cm²/s at $t = 0.5$ and 6 min.

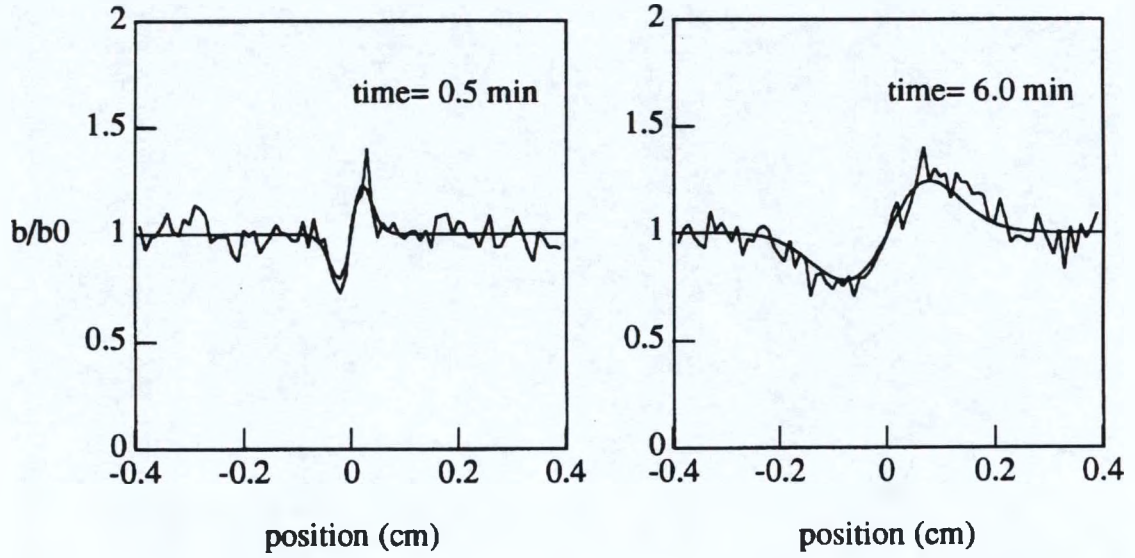

Figure 2.10: Comparison of RTBL and simulation results for $a_0 = 0.02$ mM and $\chi_0^{3D} = 3.5 \times 10^{-4}$ cm²/s at $t = 0.5$ and 6 min. Note the change of scale on the vertical axis.

The earlier discussion of the expected accuracy of the RTBL model suggested that the RTBL model would agree least with the simulation for Case 2, agree most for cases 3 and 4, but for all cases show some deviation for a range of z and t depending on the values of a_0 and χ_0^{3D}. However, it is apparent that the RTBL model agrees very well with the simulation for all the cases and for most values of z and t. This suggests that the validity of the Segel equations cannot be judged solely on the basis of the magnitude of the perturbation parameter ε.

2.5 Conclusion

In Section 2.4, the effect of the parameters a_0 and χ_0^{3D} on the simulation and the RTBL model was examined to determine the range of validity of one-dimensional phenomenological models for conditions involving symmetry in two dimensions. The range of χ_0^{3D} was varied from 3.5×10^{-4} cm^2/s to 105×10^{-4} cm^2/s. The initial concentration a_0 was varied from 0.02 mM to 1.2 mM. In all cases presented here, the results of the three-dimensional simulation and the one-dimensional RTBL model compare favorably. There are three possible explanations for this favorable comparison: the first is that the ranges of z and t over which ε is large are in practice small compared to the full ranges of z and t; the second is that in the regions where z and t are large, the motion of the bacteria becomes effectively one-dimensional so that a one-dimensional model is appropriate; the third is that the coefficients of the higher order terms in the perturbative expansion are small so that the higher order terms are negligible even when ε is large. It is probable that some combination of these mechanisms is involved. In any event, the comparisons show that the assumption of small ε necessary to reduce the more rigorous, three-dimensional equations of Alt to the one-dimensional phenomenological RTBL model does not inhibit its use in accurately modeling situations involving two dimensions of symmetry. However, any real differences between the simulation and the RTBL model

results may be masked by the significant noise level of the simulation results. This possibility is explored in Chapter 3.

It should be emphasized that the agreement between the one-dimensional model and the three-dimensional simulation only follows when one uses the relationships between the three-dimensional chemotactic sensitivity and cell swimming speed and their one-dimensional analogues that follow from the Ford and Cummings analysis. These relationships should be used in all future work when parameters for one-dimensional phenomenological models are obtained by experimental measurement.

Chapter 3:

Numerical Solution of a Balance Equation for One-Dimensional Attractant Gradients

3.1 Introduction

To quantitatively study the migration behavior of motile bacteria, recourse is made to cell balance equations which are analogous to mass balances in the study of mass transport. The ability of the bacteria to move in both random and coordinated fashions must be accounted for in the cell balance equations. For a review of the details of the motion of flagellated bacteria see Section 2.2.

As bacteria move about exploring their surroundings, they monitor changes in chemical concentrations through receptor proteins located on the cell surface. These receptors, like enzymes, have specific binding sites to which only a narrow range of structurally similar chemical substrates can bind. It is the change in the number of bound receptors over time that provides information to the cell regarding chemical gradients [46]. In the presence of a gradient in an attractant (a chemical species to which bacteria favorably respond, such as a nutrient), bacteria are able to bias their random walk by decreasing their

tumbling frequency when moving toward higher attractant concentrations thus extending the run lengths in that direction. This results in a net bias of movement toward more favorable conditions and is known as chemotaxis. It is important to note that experimental evidence suggests that this is the *only* mechanism by which chemotactic bacteria respond to an attractant. For example, the turn angle distribution is unaffected by the presence of an attractant [45].

A cell balance equation for bacteria responding to one-dimensional gradients was derived by Ford and Cummings [28] from Alt's general three-dimensional balance equations [5] which are based on Berg's physical picture of bacterial motion. This balance equation for one-dimensional gradients can be contrasted with the equations appropriate to motion of bacteria in one dimension used by Ford and co-workers [29, 30] to analyze experimental data from the stopped-flow diffusion chamber assay.

In this article, a finite element method is applied to the numerical solution of the balance equation derived by Ford and Cummings [28] for conditions relevant to experimental studies [29, 30] which involve only one-dimensional attractant gradients. We then compare solutions of this balance equation to those obtained using a phenomenological one-dimensional model [62] and to simulations of populations of individual bacteria [31]. The finite element solution is then used to probe the affects on the bacterial migration of two different models of how bacteria respond when moving against an attractant gradient. Our results show that the two models for down-gradient behavior give significantly different solutions. In addition, the importance of a commonly neglected temporal derivative term in the relationship between the attractant gradient and the tumbling probability is numerically evaluated. Finally, impact of each of these alternatives- the choice of balance equation, the model for down-gradient swimming behavior, and the neglect of the temporal derivative- on the experimentally measured transport coefficient for chemotaxis is examined .

3.2 Balance Equations

In this section, the balance equation for one-dimensional gradient derived by Ford and Cummings is briefly described . This balance equation is a simplification of the full three-dimensional cell balance equation of Alt [5] for bacteria moving in three dimensions subject to one-dimensional attractant gradients. The simpler phenomenological one-dimensional balance equations developed by Rivero *et al* are also describe in order to contrast the two models.

Alt's cell balance equations, Equations 2.1 and 2.2, apply to bacteria moving in three dimensions and are valid in the presence of multi-dimensional attractant gradients. In Alt's equations, the speed is still assumed to be a function of time and position and that tumbling probability is a function of position, direction, run time and time. These equations would be difficult to solve numerically for two reasons. First, the experimentally determined three-dimensional direction change probability distribution would have to be tabulated for a sufficient number of all the possible directions $\hat{\mathbf{s}}$ and $\hat{\mathbf{s}}'$ so that interpolations could be done with sufficient accuracy. In addition, there would be six independent variables in the full three-dimensional problem making this a very computationally intensive problem to solve.

The full three-dimensional equation was simplified for the migration of bacteria in response to one-dimensional gradients of chemical attractants by Ford and Cummings [28]. The resulting cell balance equation is:

$$\frac{\partial n_z(z,\theta,t)}{\partial t} = -s_z \frac{\partial v(z,t) n_z(z,\theta,t)}{\partial z} - \beta(z,\theta,t) n_z(z,\theta,t) + \int_0^{\pi} \beta(z,\theta',t) n_z(z,\theta',t) K(\theta',\theta) \sin\theta' d\theta' \tag{3.1}$$

where $K(\theta',\theta)$ is the probability per unit angular measurement that a bacterium moving the direction θ' will change its direction to θ after tumbling. Equation 3.1 states that the time rate of change in the number density of bacteria at position z moving in the direction θ with respect to the z-axis (see Figure C.1 in Appendix C) at time t is given by the sum of two loss terms (taking into account loss through convective motion away from the point z and through tumbling with probability density $\beta(z,\theta,t)$ and a gain term (taking into account bacteria which were moving in another direction θ' before tumbling and then moving in the direction θ.

The bacterial density that would be measured in an experiment is the angle independent density, $c(z,t)$, and is related to the angle dependent density, $n_z(z,\theta,t)$ by:

$$c(z,t) = \int_0^{\pi} n_z(z,\theta,t)\sin\theta\, d\theta \tag{3.2}$$

Equation 3.1 involves only three independent variables (z, θ and t) and requires as input the angle change distribution which is a function only of the two angles θ and θ'. In order to solve the cell balance equation, the functional form of the tumbling probability, β, must be specified.

As noted previously, the tumbling probability is a function of the attractant gradient ($\bar{\nabla}_r a$, where a is the concentration of the attractant) and the direction in which the bacterium is swimming. For a Poisson process, the probability of tumbling $\beta(\mathbf{r},\hat{\mathbf{s}},t)$ is given by:

$$\beta(\mathbf{r},\hat{\mathbf{s}},\tau,t) = \frac{1}{\langle\tau\rangle} = \beta_0 \exp\left[-\frac{\chi_0^{3D}}{v}\frac{K_d}{(K_d+a)^2}\hat{\mathbf{s}}\cdot\bar{\nabla}_r a\right] \tag{3.3}$$

For a discussion of the development of Equation 3.3, see Section 2.2.

For the special case of a one-dimensional attractant gradient in the z-direction, $\hat{\mathbf{s}} \cdot \vec{\nabla}_{\mathbf{r}} a$ reduces to $(\partial a / \partial z)\cos\theta$ and $\beta(\mathbf{r}, \hat{\mathbf{s}}, \tau, t) = \beta(z, \theta, t)$. Depending on the swimming behavior of the particular bacterial species, an alternate form of Equation 3.3 may be appropriate which is given by:

$$\beta(z,\theta,t) = \begin{cases} \beta_0 \exp(-\varepsilon), & \varepsilon > 0 \\ \beta_0, & \varepsilon < 0 \end{cases} \tag{3.4}$$

where:

$$\varepsilon = \frac{\chi_0^{3D}}{\nu} \frac{K_d}{(K_d + a)^2} \hat{\mathbf{s}} \cdot \vec{\nabla}_{\mathbf{r}} a = \frac{\chi_0^{3D}}{\nu} \frac{K_d}{(K_d + a)^2} \frac{\partial a}{\partial z} \cos\theta \tag{3.5}$$

That is, for some bacterial species the probability of tumbling does not increase when the bacteria are moving in the direction of a decreasing attractant gradient but simply returns to β_0, the basal tumbling frequency in the absence of a gradient [11].

In contrast to Equation 3.1, Segel [66] and Rivero *et al.* [62] have developed simpler phenomenological models based on individual cell motion in one direction only. The one-dimensional cell balance of Segel is given by Equations 2.3 and 2.4. Inherent in the development of these equations is the assumption that the bacteria are constrained to motion only in two directions, the $\pm z$ directions. In the RTBL model, Equations 2.2, 2.7 and 2.12 form a set of constitutive equations for Segel's cell balance equations. See Section 2.2 for the development of these equations.

3.3 Methodologies

In this section, the details of the finite element method (FEM) applied to the solution of the balance equation for a one-dimensional attractant gradient are described. The

experimental assay (whose function is modeled here using the finite element and cellular dynamics methods) and the cellular dynamics (CD) simulation methodology is also briefly reviewed.

3.3.1 Finite element method solution

The numerical solutions of the balance equation for one-dimensional attractant gradients, Equation 3.1, presented here utilized Galerkin's method on finite elements [3] for integration over the spatial variables z and θ. The solution of Equation 3.1 represents an unusual application of the finite element technique because it is an integro-partial differential equation, in contrast to the typical application to purely partial differential equations. Thus, a standard finite element package could not be used and the program used to solve Equation 3.1 was developed by the author. A weighted implicit/explicit finite difference method was used for the integration over time. With the definition

$$F(z,\theta,t) = -s_z \frac{\partial v(z,t) n_z(z,\theta,t)}{\partial z} - \beta(z,\theta,t) n_z(z,\theta,t) + \int_0^{\pi} \beta(z,\theta',t) n_z(z,\theta',t) K(\theta',\theta) \sin\theta' d\theta' \tag{3.6}$$

and first order differencing in time, Equation 3.1 gives:

$$\frac{n_z(z,\theta,t_m) - n_z(z,\theta,t_{m-1})}{\Delta t} = \omega F_m + (1-\omega) F_{m-1} \tag{3.7}$$

where the subscript m indicates that F is evaluated at the current time step $\left(t = t_m = t_0 + m\Delta t\right)$ and the subscript $m-1$ indicates that F is evaluated at the previous time step. The weighting parameter ω can be varied from 1 (resulting in a fully implicit

method) to 0 (resulting in a fully explicit method). The $z-\theta$ space was divided into finite rectangular elements as shown in Figure 3.1.

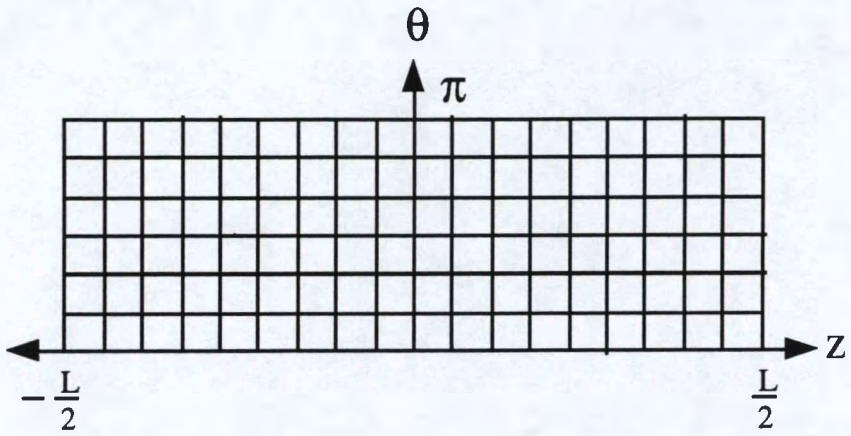

Figure 3.1: This is an example of the type of grid used in obtaining the finite element solutions presented in this paper. The actual grids used contained 200 divisions in the z direction and 10 divisions in the θ direction. The length L was 1.2 cm.

The initial conditions used in the solutions presented in this work correspond to those of the stopped-flow diffusion chamber (SFDC) assay of Ford and co-workers (see the description of the stopped-flow diffusion chamber in the following section). An initial uniform bacterial density and an initial step gradient of an attractant are assumed, that is:

$$n_z(z,\theta,t=0)=n_{z,0}, \quad -\tfrac{L}{2}\le z\le \tfrac{L}{2}, \quad 0\le\theta\le\pi \tag{3.8}$$

and

$$\begin{aligned} a(z,t=0)&=0, \quad -\tfrac{L}{2}\le z<0 \\ a(z,t=0)&=a_0, \quad 0<z\le\tfrac{L}{2} \\ a(z,t)&=\frac{a_0}{2}\left[1+\operatorname{erf}\left(\frac{z}{\sqrt{4Dt}}\right)\right], \quad t>0, -\tfrac{L}{2}\le z\le\tfrac{L}{2} \end{aligned} \tag{3.9}$$

where a_0 is the initial attractant concentration introduced into one half of the chamber, D is the diffusion coefficient of the attractant, z is the position along the z axis and t is time.

The time dependent solution given above for the attractant concentration profile can be found in Crank [23].

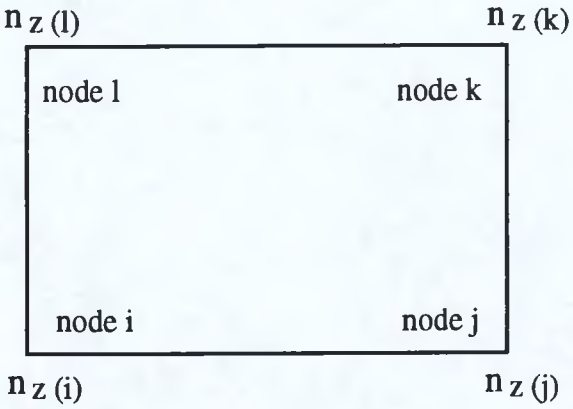

Figure 3.2: This is an example of a single element in the grid. The "nodes" of the grid are the corners of the elements. The values of dependent variable $n_z(z,\theta,t)$ at the nodes are $n_{z(i)}$, $n_{z(j)}$, $n_{z(k)}$ and $n_{z(l)}$.

A bilinear function was used to approximate $n_z(z,\theta,t)$ on the elements, that is:

$$n_z(z,\theta,t)^{(e)} = \gamma_1^{(e)} + \gamma_2^{(e)} z + \gamma_3^{(e)} \theta + \gamma_4^{(e)} z\theta \tag{3.10}$$

where the superscript e denotes the element e. The constants γ_1, γ_2, $\gamma_3$and γ_4 are related to the (unknown) nodal values of the dependent variable $n_z(z,\theta,t)$. The interpolation function for $n_z(z,\theta,t)$ can also be approximated by the more convenient form

$$n_z^{(e)}(z,\theta,t) = G_i^{(e)} n_{z(i)} + G_j^{(e)} n_{z(j)} + G_k^{(e)} n_{z(k)} + G_l^{(e)} n_{z(l)} \tag{3.11}$$

where the constants $n_{z(i)}$, $n_{z(j)}$, $n_{z(k)}$ and $n_{z(l)}$ are the values of $n_z(z,\theta,t)$ at the "nodes" of the element e (see Figure 2) and $G_i^{(e)}$, $G_j^{(e)}$, $G_k^{(e)}$, and $G_l^{(e)}$ are called the shape functions of e and are related to γ_1, γ_2, γ_3 and γ_4. The shape functions are constructed so that

$n_z(z,\theta,t)$ varies linearly along the sides of the element and takes on its nodal values at the nodes i, j, k, and l.

The integration over θ' indicated in Equation 3.1 was calculated using a two-point Gaussian integration on each element. Because of the sufficiently small variation of the integrand over the width of an element in θ-space ($\pi/10$), a two-point Gaussian quadrature was found to be sufficiently accurate; higher order Gaussian quadrature did not lead to significantly more accurate results. The values of θ and θ' for which the direction change is needed are therefore known at the beginning of the solution method permitting $K(\theta',\theta)$ to be calculated at the outset of the solution procedure and tabulated so that it need not be recalculated at each time step (see the Appendix). The solutions to the balance equation presented here were obtained using a grid of 2000 elements in the $z-\theta$ space. A typical finite element solution to the balance equation for one-dimensional attractant gradients requires about 40 CPU minutes on an IBM RS/6000 Powerstation 320.

3.3.2 Stopped-flow diffusion chamber assay

The stopped-flow diffusion chamber (SFDC) assay was developed by Ford and co-workers [30] to permit measurement of the two bacterial transport properties, the random motility coefficient, μ_0, and the chemotactic sensitivity coefficient, χ_0. The SFDC is shown schematically in Figure 3.3 along with the region of the chamber used to generate the theoretical solutions in this work. Recall from Equation 2.28 that in the absence of an attractant gradient, the random motility coefficient can be expressed in terms of the cellular quantities cell swimming speed v and mean run time $\langle\tau_0\rangle$ as:

$$\mu_0 = \frac{v^2\langle\tau_0\rangle}{3(1-\psi)} \tag{3.12}$$

where ψ is the average value of $\cos(\alpha)$, α being the angle between the direction vectors of a cell before and after tumbling. This is a general result for three-dimensional motion of bacteria assuming only a constant swimming speed, straight line swimming between tumbles, and a Poisson distribution for run lengths.

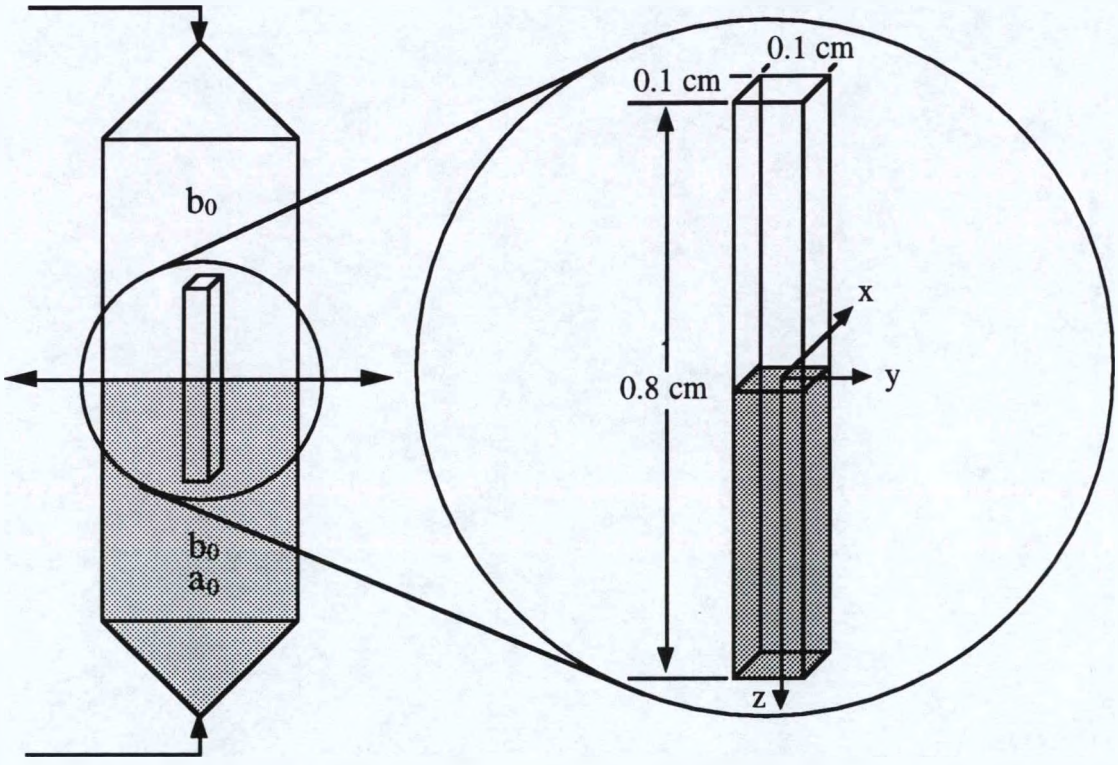

Figure 3.3: Schematic representation (left) of the SFDC used by Ford and co-workers. Impinging flow from the upper and lower ports creates an initial step change in attractant gradient at the center of the chamber and a uniform distribution of bacteria. The approximate dimensions of the chamber are 4 cm × 2 cm × 0.2 cm. On the right is an exploded view of the region of the SFDC used by the theoretical methodologies in this work to generate solutions for the cell density profile.

The random motility coefficient is analogous to the diffusion coefficient in Fickian diffusion, and in fact one can show at the macroscopic level that the diffusive part of the bacterial flux, $\mathbf{J}_b^{\text{diff}}$, is given by [39, 62]:

$$\mathbf{J}_b^{\text{diff}} = -\mu_0 \vec{\nabla}_{\mathbf{r}} c(\mathbf{r},t) \tag{3.13}$$

where $c(\mathbf{r},t) = \int n(\mathbf{r},\hat{\mathbf{s}},t)d\hat{\mathbf{s}}$ is the bacterial density.

A description of the experiments performed by Ford and co-workers in the SFDC are given in Section 2.2 and in the original work by Ford *et al.* [30] and Ford and Lauffenburger [29].

3.3.3 Cellular dynamics simulation

Cellular dynamics (CD) simulation methodology was developed in Chapter 2 as a method for studying the collective transport properties of populations of bacteria essentially by simulating the dynamics of large populations of individual bacteria [31]. It thus shares considerable common philosophical ground with molecular dynamics simulations methods used to predict the many-body thermophysical properties of liquids [4]. In essence, the stochastic differential equation which describes the dynamics of an individual bacterium is solved for 10^4-10^5 bacteria in a geometry appropriate to a small subvolume (1 mm × 1 mm × 8 mm) of the SFDC located at its center with the long axis parallel to the coordinate direction z in which there is an attractant gradient. Periodic boundary conditions are used at each face since the bacterial density is observed experimentally to have remained at the uniform initial value at these distances from the center of the SFDC during the course of a typical experiment (6-12 min).

The stochastic differential equation solved in the CD embodies the same individual cell dynamics as are assumed in Alt's equations and the general balance equation for one-dimensional gradients, Equation 3.1. Hence, from the mathematical point of view, the density profiles obtained from the CD simulations should be the same as those obtained from the FEM solution provided the same boundary conditions (i.e., SFDC geometry), operating conditions and sensing mechanisms are used in both cases. [This equivalence is

exactly the same as that between Brownian dynamics simulations of kinetic theory models of polymeric molecules at infinite dilution and the corresponding "diffusion equation" solutions for the phase space density [15].] The advantage of the FEM solution to Equation 3 over CD simulation is that the numerical computation involved is considerably less. This is because the error in CD simulations is $O(N^{-1/2})$ while the computation time is $O(N)$, where N is the number of bacteria simulated. Obtaining results from CD simulation with errors similar to those of FEM (around 1%) would be computationally expensive. For example, with 20,000 bacteria the noise in CD appears to be around 5%, so reducing this to 1% would require 25 times this number (or 500,000) bacteria and would require 26 h of CPU time on a IBM RS/6000 Powerstation 320 for a simulation corresponding to 6 min of real time. The advantage of the CD method is that it permits visualization of the individual bacterial motion as well as the collective motion of the population.

3.4 Results

In this Section, the results of the numerical solution of the balance equation for one-dimensional attractant gradients, Equation 3.1, using the finite element method (FEM) discussed in the previous section are presented. These results are then compared to the RTBL model and CD simulation results.

Before doing so, it is instructive to summarize the relationship between the three approaches being used to describe bacterial migration in this chapter: RTBL, the FEM solution to the balance equation for one-dimensional attractant gradients and CD simulations. All three approaches have the same conceptual basis: that tumbling in bacteria is governed by a stochastic Poisson process and is related to the attractant gradient by the experimentally derived relationship Equation 3.3. The CD simulation method is, in essence, a brute force Monte Carlo method for solving Alt's equations, Equations 3.1

and 3.2. The FEM solution is for the reduced form of Alt's equations derived by Ford and Cummings [28] for the case of a one-dimensional attractant gradient by exploiting symmetry in two of three coordinate directions. Thus, CD and FEM are alternative methods for solving the same model- that is, the same equations for the same physical situation- and thus should yield equivalent results. Note that the CD method involves the solution of the dynamical equations for individual cells and thus, unlike the FEM solution, is unable to take advantage of the overall symmetry of the population as it responds to a one-dimensional attractant gradient. This is one sense in which the FEM solution is more efficient. In contrast to the model underlying the CD simulation and the FEM solution, the RTBL model involves an additional physical assumption, namely that the bacteria are confined to one dimension in their motion [28].

The FEM solution is compared to that obtained by CD simulations and to that obtained from the RTBL model for two of the cases studied in Chapter 2 which contained CD simulations of *E. coli* in the presence of a gradient in fucose. Both the bacterial density profiles and the resulting bacterial transport coefficient for chemotaxis are compared. Then the variations on the cell sensory mechanism beyond those studied in the previous chapter using either CD simulation or RTBL are examined by comparing FEM solutions incorporating these variations to experimental data for the response of *E. coli* bacteria to a gradient of α-methylaspartate.

3.4.1 Comparison of models

The first comparison of FEM, CD and RTBL is performed for the set of conditions shown in Table 3.1 and $\chi_0^{3D} = 3.5 \times 10^{-4}$ cm²/s (equivalent to $\chi_0^{1D} = 0.88 \times 10^{-4}$ cm²/s. Note that the RTBL quantities for cell speed s and chemotactic sensitivity coefficient χ_0 in Table 3.1 are one-dimensional quantities and are related to the corresponding three-

dimensional quantities used in the CD and FEM calculations according to the relationship derived by Ford and Cummings [28]:

$$v^{3D} = 2v^{1D} = 2s \tag{3.14}$$

which leads to the following relationship between χ_0^{1D} and χ_0^{3D} [31]:

$$\chi_0^{3D} = 4\chi_0^{1D} \tag{3.15}$$

These relationships were verified in Chapter 2 as being essential to obtain consistency between the one-dimensional RTBL and three-dimensional descriptions. The attractant concentration, diffusivity and dissociation constant a_0, D and K_d) and bacterial properties (β_0, v and p_t) in Table 3.1 correspond to those in SFDC experiments measuring the response of *E. coli* bacteria to a gradient of fucose reported by Ford *et al.* [30]. The value $\chi_0^{3D} = 3.5\times10^{-4}$ cm^2/s corresponds to the experimentally measured value for this system. The value of $\chi_0^{3D} = 105\times10^{-4}$ cm^2/s is high, but is consistent with values measured experimentally for bacteria cultured in limited nutrient conditions [50].

Model	β_0 (s^{-1})	v (μm/s)	a_0 (mM)	$\chi_0\times10^{-4}$ (cm^2/s)	$D\times10^6$ (cm^2/s)	K_d (mM)	p_r
Eq. 3.1 & CD	0.17	22.	0.2	3.5, 105	6.9	0.08	---
RTBL	0.17	11.	0.2	0.88, 26.	6.9	0.08	0.32

Table 3.1: Values of constants used in solutions shown in Figures 3.4 and 3.5. These are the values of the constants used in the CD simulation and in solving Equation 3.1 and the RTBL equation.

In Figures 3.4 and 3.5, the FEM solution of Equation 3.1 is compared to the CD simulation and to the solution of the RTBL model for the conditions given in Table 1 with

$\chi_0^{3D} = 3.5 \times 10^{-4}$ cm²/s over a period corresponding to 6 min of elapsed time. The bacterial density $c(z,t)$ given by Equation 3.2 is plotted in dimensionless form as a function of position.

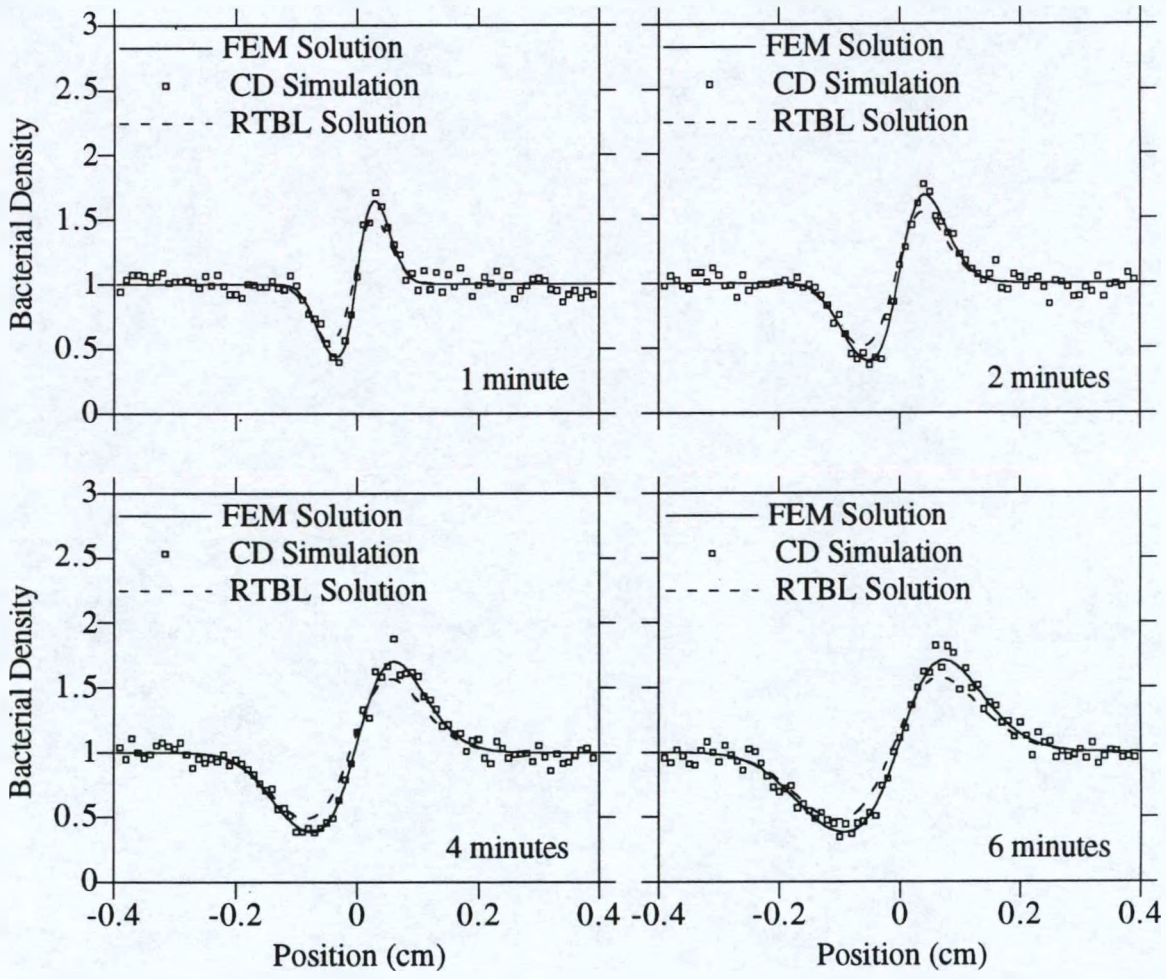

Figure 3.4: Comparison of the finite element solution of the balance equation for one-dimensional gradients. Shown are solutions to Equation 3.1 (solid line), CD simulation (squares) and the RTBL model (dashed line) for $\chi_0^{3D} = 3.5 \times 10^{-4}$ cm²/s. Dimensionless bacterial density, c/c_0 is plotted as a function of the position z along the SFDC for times of 1, 2, 4, and 6 min. Position $z = 0$ corresponds to the position of the initial step change in the attractant concentration at $t = 0$ with a fucose concentration of 0.2 mM initially in the bottom of the SFDC ($0 < z \leq 0.4$ cm in the graphs).

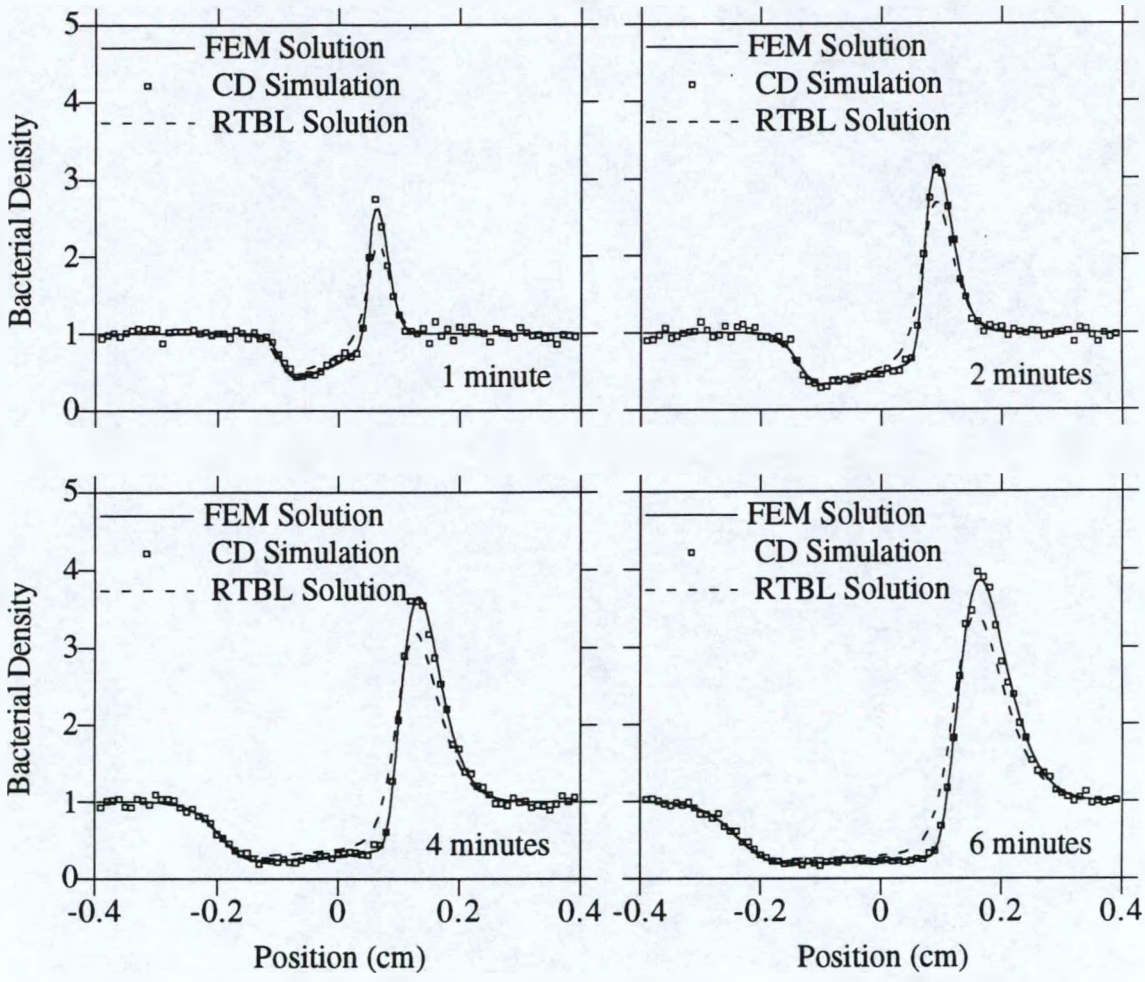

Figure 3.5: Comparison of the finite element solution of the balance equation for one-dimensional gradients. Shown are solutions to Equation 3.1 (solid line), CD simulation (squares) and the RTBL model (dashed line) for $\chi_0^{3D} = 105 \times 10^{-4}$ cm^2/s. Solutions are shown at 1, 2, 4 and 6 min.

The model for the tumbling probability used in the FEM solution and the CD simulations is Equation 3.3 and in the RTBL model is Equation 3.18. This is consistent with the model used in previously reported numerical studies [30, 31]. The first observation is that the FEM solution is completely consistent with the CD simulation as expected on the basis of the equivalence of the models. Second, it is clear that there is a

small but discernible, quantitative difference between the predictions of the RTBL model and the solution of the three-dimensional models (FEM and CD). In the comparison between CD and RTBL presented in Chapter 2, the level of noise in the CD simulations made it difficult to assert with a high degree of certainty that there were differences between the predictions of RTBL and of models (such as CD and Equation 3.1) which take into account the full three-dimensional character of the bacterial motion. These differences are clearly evident in both Figures 3.4 and 3.5, with the RTBL model having a lower peak and a more shallow trough than the three-dimensional models.

The computation times for the FEM solution, CD simulation (using 20,000 bacteria) and the RTBL model (solved by finite differences) are 39, 63 and 1 min respectively of CPU time on an IBM RS/6000 Powerstation 320.

3.4.2 Effect of model selection on the chemotaxis transport coefficient

An important question is to what extent the difference between RTBL and the FEM solution results in significant differences in the transport properties which would be obtained by comparison with experiment. In particular, the value of χ_0 is obtained experimentally by measuring $N(t)$, the number of bacteria entering the upper chamber of the SFDC as a function of time t. For RTBL, it is known that $N(t) \propto \sqrt{t}$ with a slope that increases monotonically with χ_0 [71]. Experimentally, it is also found that $N(t) \propto \sqrt{t}$, so the value of χ_0 obtained from the experimental data is determined by applying the mathematical model to the conditions of the experiment; the value of χ_0 obtained from the experiment is that which yields the same theoretical slope of $N(t) \propto \sqrt{t}$ as that given by a linear least squares regression of the experimental data.

An explicit illustration of the method is presented here using the experimental data shown in Figure 3.6 which contains a plot of $N(t)$ vs. $\sqrt{t}$ for *E. coli* responding to α-methylaspartate in the SFDC [72]. The least squares fitted slope in Figure 3.6 has an error

of 4.7% calculated from the standard deviation based on its relationship to the R^2 correlation coefficient of 0.991 obtained from the linear regression analysis [51]. For χ_0 in the range of our experimental data, χ_0 and the slope in the experimental $N(t)$ vs. $\sqrt{t}$ plot are linearly related, so that when the value of χ_0 is found which has a slope equal to the experimental value (in this case, $\chi_0^{3D} = 1.9 \times 10^{-4}$ cm^2/s, it is assumed that the only source of error in χ_0 is the experimentally determined slope. This linear relationship implies that χ_0 and the slope have the same fractional error. From this it can be concluded that the error in χ_0 is approximately 5%.

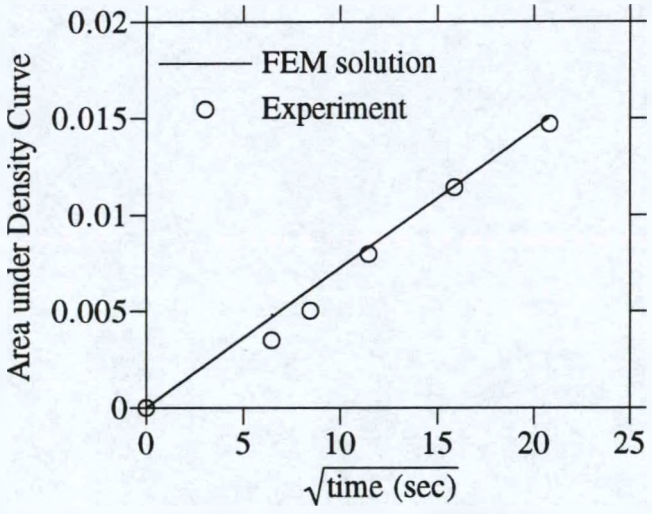

Figure 3.6: The area between the dimensionless bacterial density curve and $c \setminus c_0 = 1$ in the SFDC. The area under the bacterial density curve for the half of the SFDC with a high concentration of attractant is plotted as a function of $\sqrt{t}$ for the case shown in Figure 3.8. The value of χ_0 used to produce the model results is $\chi_0^{3D} = 1.9 \times 10^{-4}$ cm^2/s and yields the same slope as a linear least squares regression of the experimental data. In this comparison the offset time has been included in the simulation solutions [71].

Since the RTBL model has been shown to be a small gradient approximation of Equation 3.1, one can probe the error in χ_0 that might result from the use of RTBL rather than Equation 3.1 by fitting the $N(t)$ vs. $\sqrt{t}$ from RTBL to the corresponding result for Equation 3.1 and then comparing the value of χ_0^{1D} required by RTBL to the value obtained using the balance equation for one-dimensional attractant gradients, Equation 3.1. For

$\chi_0^{3D} = 3.5\times10^{-4}$ cm²/s, Equation 3.1 is solved by FEM and RTBL is fit to the resulting $N(t)$ vs. $\sqrt{t}$ plot. The best fit is given by $\chi_0^{3D} = 1.2\times10^{-4}$ cm²/s which is 31% higher than the expected value of $\chi_0^{3D} = 3.5\times10^{-4}$ cm²/s. For $\chi_0^{3D} = 105\times10^{-4}$ cm²/s, the best fit of RTBL to the $N(t)$ vs. $\sqrt{t}$ plot is given by $\chi_0^{3D} = 0.88\times10^{-4}$ cm²/s which is 230% higher than the value of $\chi_0^{3D} = 26\times10^{-4}$ cm²/s used in the FEM calculation. These two examples are consistent with many other calculations we have performed in which we have found that the value of χ_0 required by RTBL to fit the FEM solution is higher than the value of χ_0 used in the FEM solution. This observation suggests that the values of χ_0 obtained by fitting RTBL calculations to experimental measurements are likely to be overestimates, although the physical basis for this discrepancy is not obvious.

Having established the correctness of the FEM solution to Equation 3.1 by comparison to CD simulation, it is clear that the FEM solution provides a convenient and computationally inexpensive route to calculating the bacterial migration profiles for bacteria subject to one-dimensional attractant gradients. It is thus the appropriate vehicle for comparison with experimental measurements, particularly for obtaining values of transport coefficients.

In the remainder of this chapter however, two questions concerning the model for the tumbling probability will be investigated. The first question is: How do bacterial density profiles calculated using Equation 3.4 for the tumbling probability (corresponding to bacteria returning to the basal tumbling frequency when moving away from an attractant) differ from those obtained using Equation 3.3 (corresponding to bacteria increasing their tumbling frequency when moving away from an attractant) as has been assumed in previously published analyses [29]? This question has important bearing on the interpretation of bacterial density transport coefficients since it is known that *E. coli* obey Equation 3.4 rather than Equation 3.3 [12].

In Figure 3.7, results for the two different tumbling probability models, Equations 3.3 and 3.4, are compared using the Table 3.1 parameters in Equation 3.1. It

is clear that the difference in tumbling probability has a large effect on the bacterial density profile for these cases.

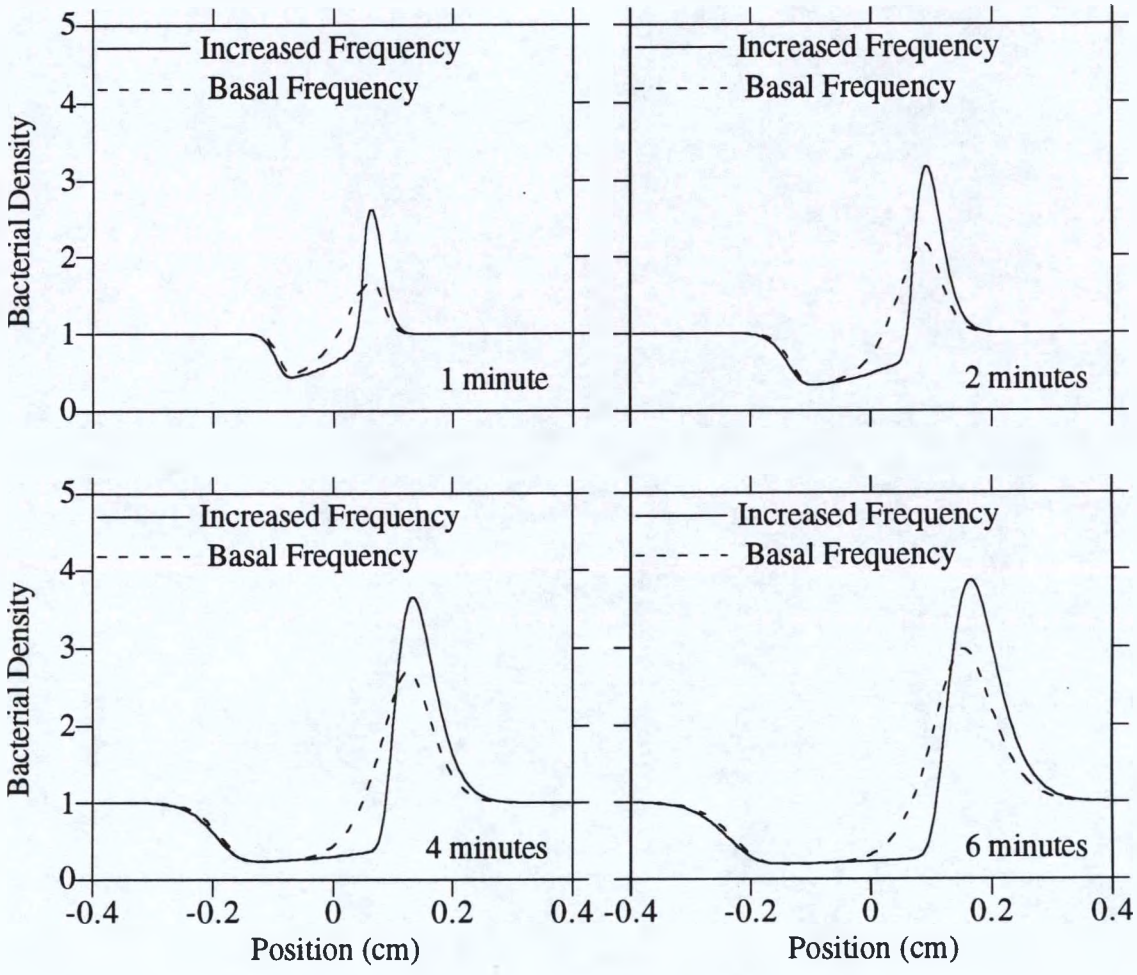

Figure 3.7: Finite element solutions to the balance equation for one-dimensional gradients using $\chi_0^{3D} = 105 \times 10^{-4} \text{cm}^2/\text{s}$. In the first case (solid line), the tumbling frequency β is allowed to increase above its basal level β_0 for populations of bacteria moving against the attractant gradient according to Equation 3.3. In the second case (dashed line), the tumbling frequency is assumed to return to its basal value for bacteria moving against an attractant gradient according to Equation 3.4.

Figure 3.7 shows that the solution obtained using Equation 13 for the tumbling probability would result in lower numbers of bacteria moving into the half of the chamber

where the attractant concentration is highest. Therefore a higher value of χ_0^{3D} would be obtained by fitting solutions obtained using Equation 3.4 to experimental data than would be obtained if Equation 3.3 were used.

The value of χ_0^{3D} used in the solutions shown in Figure 3.7 is at the upper limit of values that one would expect to encounter experimentally [50] and was chosen to emphasize the difference in solutions obtained using the two models for the tumbling probability. Next the effect of the choice of tumbling probability models on the transport coefficient for chemotaxis is examined by comparing FEM solutions to experimental data for *E. coli* responding to α-methylaspartate. The conditions at which the experiment was performed are given in Table 3.2 and are used in the subsequent model calculations.

v (μm/s)	a_0 (mM)	$\mu_0 \times 10^7$ (cm^2/s)	$D \times 10^6$ (cm^2/s)	K_d (mM)
22.	0.01	8.8	7.1	0.125

Table 3.2: Conditions for experimental measurement of the response of *E. coli* to α-methylaspartate [72].

Figure 3.8 compares the solution of the balance equation for one-dimensional gradients using Equation 3.3 and Table 3.2 parameter values to the experimental data of Strauss [72] for *E. coli* responding to an initial step gradient of α-methylaspartate in the SFDC. The model solution shown in Figure 3.9 used Equation 3.4 to calculate the tumbling probability. While the model solutions shown in Figures 3.8 and 3.9 are very similar, the value of χ_0^{3D} used to obtain the solution in Figure 3.9 represents a 100% increase over the value used to obtain the solution in Figure 3.8 which incorporated Equation 3.3. Specifically, if it is assumed that the tumbling probability is given by Equation 3.3 (which states that bacteria moving against the attractant gradient are capable of increasing their tumbling frequency above the basal level), then the value of χ_0 obtained

by fitting to the experimental data is $\chi_0^{3D} = (1.9 \pm 0.1) \times 10^{-4}$ cm²/s. If it is assumed that the tumbling probability is given by Equation 3.4 (bacteria moving against the attractant gradient return to the basal tumbling frequency) and go through the fitting procedure described previously, it is found that $\chi_0^{3D} = (3.8 \pm 0.2) \times 10^{-4}$ cm²/s. Therefore, determination of the chemotactic sensitivity (as reflected in χ_0) from experimental data requires *a priori* knowledge of whether Equation 3.3 or 3.4 applies for the particular bacteria under investigation.

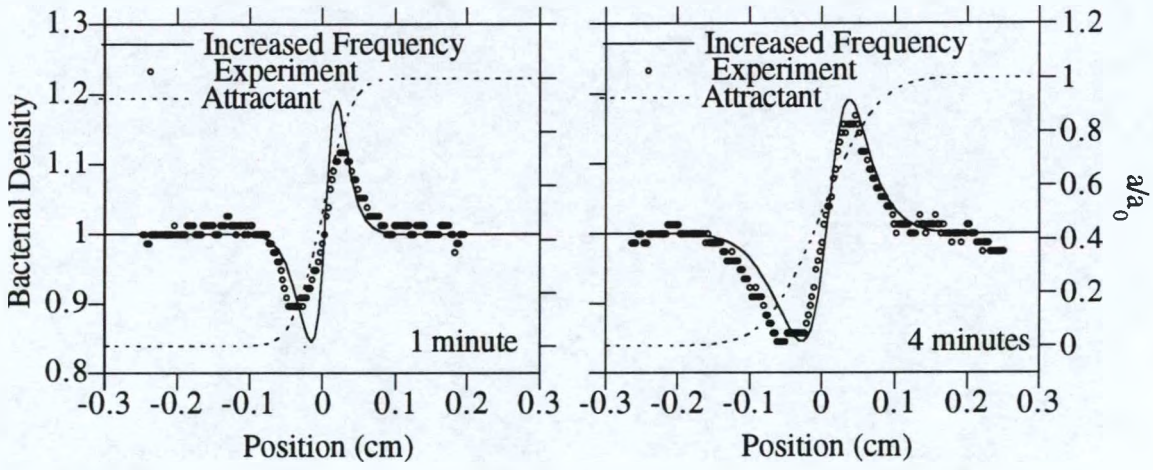

Figure 3.8: Comparison of FEM solutions to experimental data. FEM solutions to the balance equation for one-dimensional gradients (solid line) and experimental data [72] (circles) for the response of *E. coli* to α-methylaspartate in the SFDC with a 0.01 mM initial concentration of α-methylaspartate in the bottom of the SFDC (right side of figure) are shown. Also shown (dashed line) is the dimensionless attractant concentration, a/a_0. In the FEM model solution, the tumbling frequency β is allowed to increase above its basal level β_0 for populations of bacteria moving against the attractant gradient according to Equation 3.3. The value of χ_0^{3D} used in the model solution was 1.9×10^{-4} cm²/s.

The 100% increase in χ_0^{3D} obtained using Equation 3.4 rather than Equation 3.3 is not a general result but is consistent with the small values of χ_0^{3D} involved. It can be shown that in the limit of small ε, in which case the exponentials in Equations 3.4

and 3.3 can be linearized, this factor of two naturally arises by using a small ε perturbative expansion [28].

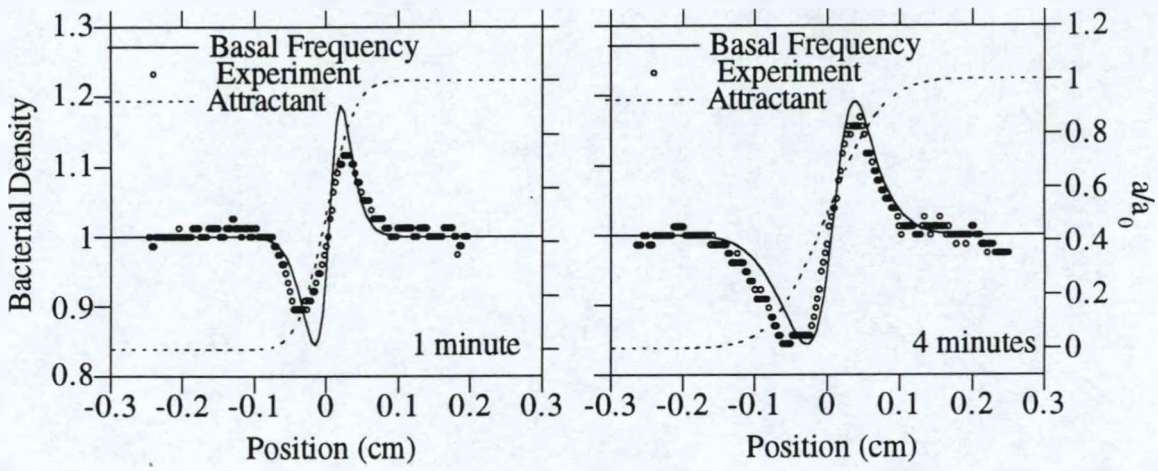

Figure 3.9: Comparison of FEM solutions to experimental data. FEM solutions of the balance equation for one-dimensional gradients (solid line) and experimental data [72] (circles) for the response of *E. coli* to α-methylaspartate in the SFDC are shown. In the FEM model solution, the tumbling frequency β returns to its basal value β_0 for populations of bacteria moving against the attractant gradient according to Equation 3.4. The value of χ_0^{3D} used in the model solution was 3.8×10^{-4} cm^2/s.

The second question is: To what extent is Equation 3.7 a valid approximation for Equation 6 for conditions such as those that exist in the SFDC? At very short times,because the attractant concentration in one half of the chamber is initially zero, it might be expected that the temporal derivative could be quite large, so that Equation 3.7 might not be satisfied. In Figure 3.10, bacterial density profiles are shown both including and neglecting the temporal derivative, and it is clear that there is no practical difference in the density profiles if the temporal derivative is included. Thus, it appears that the neglect of the temporal derivative is a valid assumption.

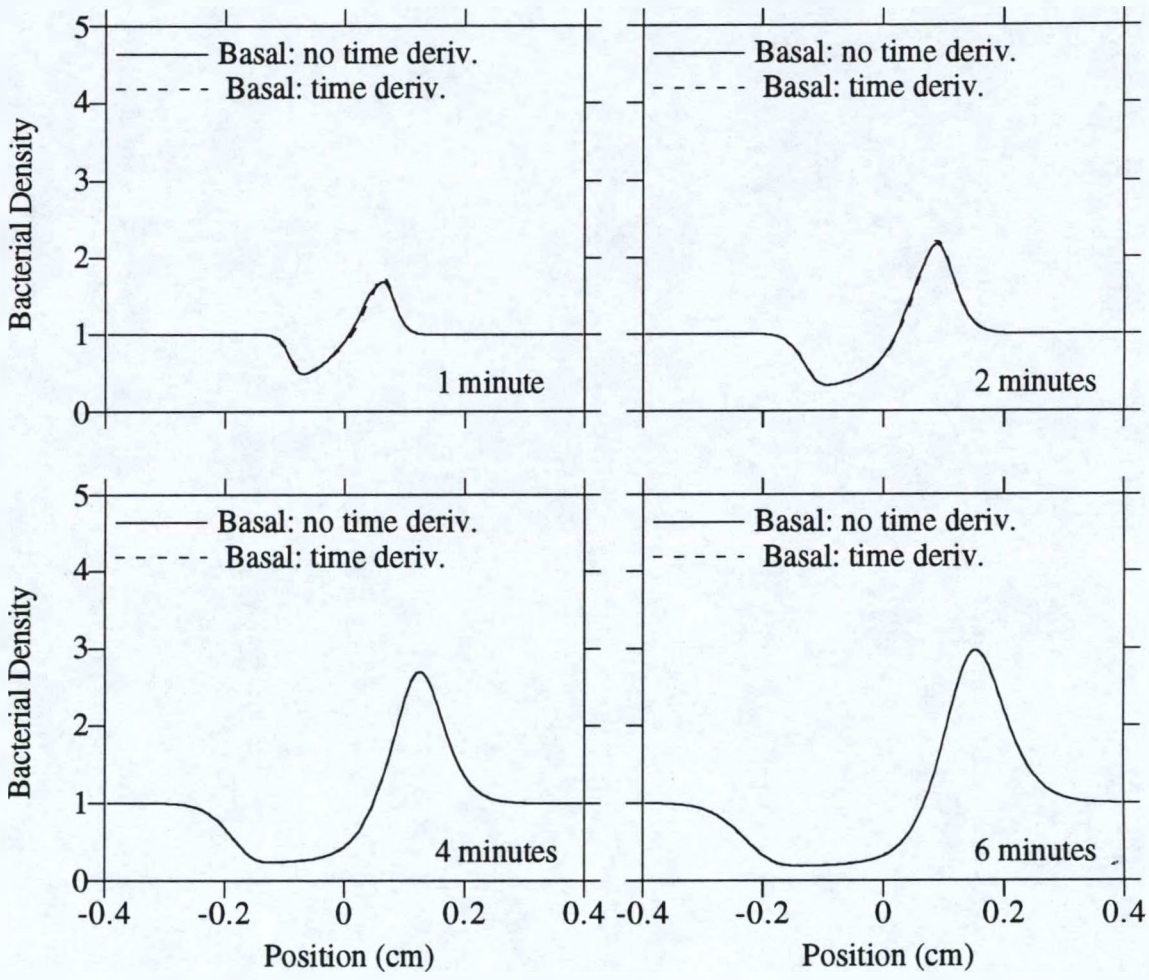

Figure 3.10: Finite element solutions to the balance equation for one-dimensional gradients. In the first case (solid line), the partial derivative with respect to time is included in the substantial derivative of the number of bound receptors (Equation 6). In the second case (dashed line), the partial derivative with respect to time is omitted (Equation 7). Only a slight difference between the solutions is seen at 1 and 2 min and the two solutions are identical at 4 and 6 min on the scale of this graph. Both cases assume that the tumbling frequency returns to its basal value for cells moving in a direction against the attractant gradient.}.

3.5 Conclusion

The reduced cell balance equation for one-dimensional attractant gradients derived by Ford and Cummings [28] were solved in the context of the stopped-flow diffusion chamber assay using a finite element technique. The accuracy of the numerical solution was confirmed by comparison to cellular dynamics simulation which incorporated the same mechanistic model for the chemotactic response used in the cell balance equation. The finite element solution of the balance equation for one-dimensional gradients represents a substantial economy of computational expense over the cellular dynamics simulations.

A summary of the χ_0^{3D} values obtained for the experimental data shown in Figure 3.6 using the different models and tumbling probability expressions considered in this paper is given in Table 3.3. The value of χ_0^{3D} reported for RTBL is the χ_0^{1D} value that gave the same slope as the plot of $N(t)$ vs. $\sqrt{t}$ for the experimental data multiplied by 4 as required by Equation 3.15.

Compared to the solution of the balance equation for one-dimensional attractant gradients, RTBL overpredicts the value of the chemotactic sensitivity coefficient by as much as 230% when $\chi_0^{3D} = 105 \times 10^{-4}$ cm²/s. Values of this magnitude have been reported for conditions under which bacterial growth was limited [50], a situation which is not uncommon in natural environments. It is interesting to note that the use of Equation 3.3 for the tumbling probability of *E. coli* as opposed to Equation 3.4 leads to an underprediction of the correct value of χ_0^{3D} while the use of the RTBL model as opposed to the balance equation for one-dimensional attractant gradients leads to an overprediction of the correct value of χ_0^{3D}. Therefore, analyses of experimental data for the migration of *E. coli* that use the RTBL model and incorporate Equation 3.3 (for example, the studies of Ford and co-workers) contain compensating errors that may result in reasonable values for χ_0^{3D} being obtained from experiment.

Model	Tumbling Probability	Temporal Gradient	$\chi_0^{3D} \times 10^4$ (cm²/s)
RTBL	Eq. 3.3	$\partial a/\partial t=0$	2.6
FEM	Eq. 3.3	$\partial a/\partial t=0$	1.9
FEM	Eq. 3.4	$\partial a/\partial t=0$	3.8
FEM	Eq. 3.4	$\partial a/\partial t\neq 0$	3.8

Table 3.3: Comparison of χ_0^{3D} values for different models. These values of χ_0^{3D} were obtained from fitting to experimental data for various models, tumbling mechanisms and inclusion/exclusion of temporal gradient in tumbling probability.

Two different responses have been reported for bacteria swimming down an attractant gradient. *E. coli* return to a basal tumbling probability corresponding to what is observed in the absence of a chemical gradient [11, 20] while *S. Typhimurium* increase their tumbling frequency over the basal level when moving down an attractant gradient. Solution of the balance equation for one-dimensional gradients revealed a significant difference in the bacterial density profiles depending on the model used for the tumbling probability as shown in Figure 3.7. For bacteria returning to the basal tumbling frequency, the chemotactic response appears less dramatic with respect to the sharpness and intensity of the bands.

Within the SFDC, both a spatial and temporal attractant gradient exist. Prior applications of the RTBL model neglected the temporal gradient arguing that its contribution was small in comparison to the large spatial gradient generated by an initial step change in attractant concentration. Solutions of the balance equation for one-dimensional attractants with and without the temporal gradient showed no significant difference over the range of parameters that were investigated, validating the assumption that the temporal gradient within the material derivative is negligible.

Chapter 4

Bacteria-Surface Interactions

4.1 Introduction

In a homogeneous fluid medium, flagellated motile bacteria such as *E. coli* and *S. typhimurium* execute random walks as they alternate between their two phases of motion: running (motion in essentially straight paths) and tumbling (changes in direction while remaining in place) [9, 12, 46, 70]. In the presence of solid surfaces, this behavior will be modified. Intuition would suggest that long runs initiated close to the surface and in the direction of the surface are not possible because of the presence of the impenetrable solid surface. However, what is not known is the *way* in which bacterial swimming behavior will be modified. Relevant questions are: Will a bacterium swim toward the surface as though the surface is not present until it strikes the surface or will it slow and turn to avoid the surface? If a bacterium strikes the surface, will it rebound from or adhere to the surface? What forces must be considered in determining the swimming behavior of bacteria in the presence of solid surfaces? It is the purpose of this study to answer these questions.

Understanding the mechanisms of bacterial transport in the presence of solid surfaces is essential to being able to model many processes of engineering concern. *In situ*

bioremediation has evolved as a safe and cost effective treatment for the reclamation of soil and groundwater contaminated with hydrocarbons from leaking underground tanks and above ground spills [1, 24, 25, 60, 64, 69]. Research is currently being conducted to extend the use of *in situ* bioremediation to soils contaminated with compounds such as halogenated aliphatics [7, 22, 52, 63, 68]. There is increasing evidence that these recalcitrant compounds can be effectively degraded by naturally-occurring microorganisms. Wastewater treatment relies on the trapping of pathogenic microorganisms in packed beds of sand grains and from groundwater in the aquifer matrix [48, 49]. In the area of the pathogenesis of infection, the most common hospital-acquired infections are catheter-associated. It has been shown that bacterial transport in this situation is enhanced through the presence of a solid surface [35] [54].

A microscopic understanding of bacterial motion near solid surfaces is necessary to predict the macroscopic behavior of populations of bacteria for the systems described above. While bacterial transport has frequently been studied by analogy to similar non-living systems, such studies have met with varied success. An effective mathematical model for one experimental system is often a poor model for another, seemingly similar system. These inconsistencies are often the result of a fundamental misunderstanding or oversimplification of the nature of bacterial motion and bacteria-surface interactions.

In this study, a specially designed microscope is used to follow the paths of individual bacteria swimming in the fluid adjacent to a solid surface. The near-surface traces of the bacteria are analyzed to determine differences in the swimming behavior of the bacteria compared to motion in the bulk fluid phase. The variation in the swimming speed as a function of the surface-to-cell distance is compared to two theoretical solutions: one that treats the bacterium as a sphere being propelled against a constant resistive force and another that treats the bacterium as a sphere with a single attached flagellum rotating at a constant angular speed. The zeta potentials for the system are determined and used to calculate the DLVO (Derjaguin-Landau and Verwey-Overbeek) interaction potential as a

function of the separation distance to offer an explanation of the tendency of cells to swim along a solid surface tracing out circular paths.

4.2 Background

That a motile bacterium must modify its swimming behavior in the presence of a solid surface is obvious since, clearly, it cannot penetrate the wall. Lubrication theory suggests that the presence of a solid surface would influence the swimming speed of the bacterium through a viscous medium well before it makes physical contact with the surface [6]. In addition, one might expect that interactions between the surface and cell arising from surface charges and the distribution of ions in the surrounding medium would influence the motion of a bacterium very near the surface. To characterize the motion of a bacterium near a surface by its response to these external forces, two issues must be considered: 1) At what distance is the bacterium considered to be "near" the wall and at which, the presence of the wall must be taken into account to determine the motion of the bacterium, and 2) What forces or interactions must be considered in these regions?

Two distinct surface-to-cell distance regions can be identified in which changes in bacterial motion should be anticipated. The interactions that need to be considered in these two regions are different; in the first region, interactions are dominated by the surface chemistry of the system and the medium composition, while in the second region, hydrodynamic interactions are dominant.

The region in which the surface chemistry of the system is important is confined to, roughly, the 100 nm nearest to the surface. In the study of these interactions, the DLVO theory of colloid stability is often employed [65, 74-76]. This theory accounts for the long range (on a molecular scale) van der Waals and electrostatic interactions between the bacteria and the surface as a function of the separation distance and the medium composition. In addition to these interactions, there are very short-ranged forces that are

thought to be important in the irreversible adhesion of bacteria to a solid surface. These interactions are not addressed in this study since for all the cases studied under our experimental system, no irreversible adhesion was observed.

According to DLVO theory, the total interaction potential between a solid surface and a colloid particle or bacterium is given by

$$G_T(h) = G_A(h) + G_E(h) \tag{4.1}$$

where h is the separation distance, $G_A(h)$ is the contribution of the van der Waals interaction and $G_E(h)$ is the contribution resulting from the overlap of the electrical double layers of the bacterium and the solid surface in the suspension medium. Letting the flat solid surface be (1), the particle/bacterium of radius b be (2) and the suspension medium be (3), Norde and Lyklema [55] give the following approximation for G_A:

$$G_A = -\frac{A_{123}}{6}\left[\frac{2b(h+b)}{h(h+2b)} - \ln\left(\frac{h+2b}{h}\right)\right] \tag{4.2}$$

where A_{123} is the Hamaker constant for the system and can be written in terms of the individual components as:

$$A_{123} = \left(\sqrt{A_1} - \sqrt{A_3}\right)\left(\sqrt{A_2} - \sqrt{A_3}\right) \tag{4.3}$$

For bacteria and natural surfaces in aqueous media, A_{123} is usually positive so G_A is negative and attractive. The interactions resulting from double layer overlap may be expressed as [55]:

$$G_E(h) = \pi\varepsilon_r\varepsilon_0 b\left(\phi_{13}^2 + \phi_{23}^2\right)\left\{\frac{2\phi_{13}\phi_{23}}{\phi_{13}^2 + \phi_{23}^2}\ln\left[\frac{1+\exp(-\kappa h)}{1-\exp(-\kappa h)}\right] + \ln\left[1-\exp(-2\kappa h)\right]\right\} \tag{4.4}$$

where $\varepsilon_r\varepsilon_0$ is the dielectric permittivity of the medium and κ is the reciprocal Debye length. The surface potential ϕ is usually approximated by the zeta potential ζ. For the system studied here, both ϕ_{13} and ϕ_{23} are negative and so G_E is positive and repulsive.

The reciprocal Debye length is a function of the medium composition and is given by [37]:

$$\kappa^2 = \left[\frac{1000e^2 \mathrm{N_A}}{\varepsilon_r\varepsilon_0 k_B T}\sum_i z_i^2 M_i\right] \tag{4.5}$$

where e is the charge on an electron, k_B is Boltzmann's constant, T is the absolute temperature, z_i is the charge on ion i in the medium, M_i is the concentration of ion i in mol/l, and $\mathrm{N_A}$ is Avagadro's number.

The second region of surface-cell interactions extends out to about 10 μm from the solid surface. In this region, hydrodynamic interactions between the cell and the surface become important. For a slow moving spherical particle moving in an unbounded viscous fluid, the force of drag resisting the motion of the sphere can be calculated from the solution to Stokes' equation for creeping flow around a sphere, which is [19]:

$$F_{\text{resistance}} = 6\pi\mu bU \tag{4.6}$$

where μ is the fluid viscosity, U is the speed of the sphere and b is the radius of the sphere. If the shape of a bacterium can be approximated by a sphere and if it is swimming at a constant speed, the force provided by the flagella is equal to the resistance from the fluid and can be calculated by Equation 4.6.

Now, consider the case of a sphere moving toward a solid surface with speed U and whose center is a distance h from the solid surface, as pictured in Figure 4.1. The

force on a sphere moving at a constant velocity U toward the solid wall will no longer remain constant but will increase as the separation distance decreases.

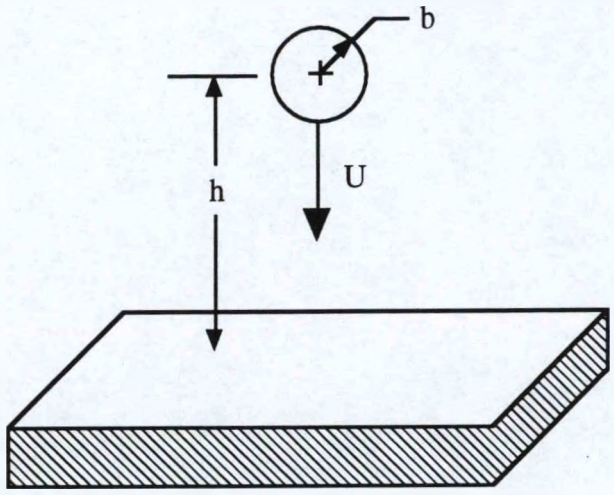

Figure 4.1: Perpendicular motion of a sphere toward a plane surface. A sphere of radius b moves perpendicularly toward a solid surface with speed U at a separation distance of $h-b$.

Brenner [19] gives the solution to the creeping flow equation for the force resisting the motion of the sphere as it approaches the solid surface perpendicularly as:

$$F(h/b)_{\text{resistance}} = 6\pi\mu bU\lambda(h/b) \tag{4.7}$$

where h is the distance from the center of the sphere to the solid surface and λ is given by:

$$\lambda = \frac{4}{3}\sinh\alpha\sum_{n=1}^{\infty}\frac{n(n+1)}{(2n-1)(2n+3)}\left[\frac{2\sinh(2n+1)\alpha+(2n+1)\sinh 2\alpha}{4\sinh^2\left(n+\frac{1}{2}\right)\alpha-(2n+1)^2\sinh^2\alpha}-1\right] \tag{4.8}$$

and:

$$\alpha = \cosh^{-1}\left(\frac{h}{b}\right) = \ln\left\{\frac{h}{b} + \sqrt{\left[\left(\frac{h}{b}\right)^2 - 1\right]}\right\} \tag{4.9}$$

By comparing Equations 4.6 and 4.7, it can be seen that λ represents the increase in the force resisting the motion of the sphere due to the presence of the solid surface. If the sphere approaches the wall such that the force resisting its motion remains equal to its value in an unbounded fluid (i.e.; at a separation distance of ∞), then its speed can be calculated by equating Equations 4.6 and 4.7:

$$F_\infty = 6\pi\mu b U_\infty = 6\pi\mu b U\lambda = F(h/b) \tag{4.10}$$

or:

$$\frac{U}{U_\infty} = \lambda^{-1} \tag{4.11}$$

The conditions under which this expression is valid for use in determining the speed of a bacterium as it approaches a solid surface are: 1) a flagellar bundle which produces a constant force and 2) an insignificant change in momentum relative to the forces acting on the bacterium. For Reynolds numbers relevant to the motion of bacteria through water ($O(10^{-5})$), this later condition is valid [19].

There are other more sophisticated models for bacterial motion toward a plane surface than that of a sphere moving with a constant propulsive force. Ramia [59] solved Stokes' creeping flow equation for an arbitrarily shaped body and an associated single helical flagellum rotating at a constant angular speed. The equations were solved using a boundary element numerical method (BEM). General descriptions of the boundary element method can be found in Brebbia *et al.* [18] and Kane [38]. This solution method allows for arbitrary incident angles to the solid surface. Shown in Figure 4.2 is the solution given by

Ramia *et al.* [59] for cell orientations of 90° (parallel to the surface), 135°, and 180° (perpendicular to and toward the surface) from the surface normal and assuming a spherical cell body. The dependence of the speed of a sphere moving perpendicular to the surface as given by Equation 4.11 is shown superimposed on the BEM solutions. The definition of the orientation angles is illustrated in Figure 4.3.

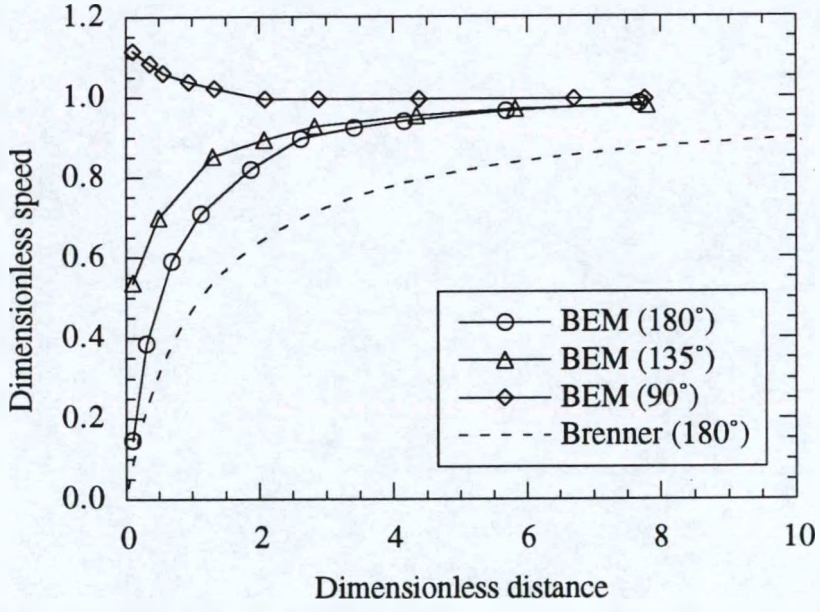

Figure 4.2: Solution of Stokes' equation by Ramia *et. al.* The boundary element method (BEM) is used to solve Stokes' equation for a sphere with a flagellum rotating at constant rate moving toward a solid surface at 3 different orientation angles. Also shown is the solution to Equation 4.11, based on Brenner's solution for the force on a sphere perpendicularly approaching a solid surface. The dimensionless speed is the instantaneous speed divided by the speed in an unbounded fluid. The dimensionless distance is $(h-b)/b$.

One interesting result of the analysis of Ramia *et al.* is that bacteria swimming close and parallel to the surface derive a propulsive advantage from the surface and swim at a speed 10% higher than in the bulk. Also, the velocity changes more quickly for bacteria moving at 180° from the surface normal than for cells moving at 135° from the surface normal. Compared to the solution of Equation 4.11 for a sphere moving perpendicular to the

surface opposed by a constant force, the swimming speed is higher at a given separation distance for cell orientation angles of either 135° or 180°. One reason for the higher velocity predicted by the BEM solutions is that these solutions assume the flagellum rotates at a constant rate, while Equation 4.11 assumes that the force produced by the flagella is constant. A flagellum rotating at a constant speed would produce more thrust near a solid surface due to hydrodynamic interactions between the flagellum and the surface [59], resulting in higher swimming speeds for a given separation distance.

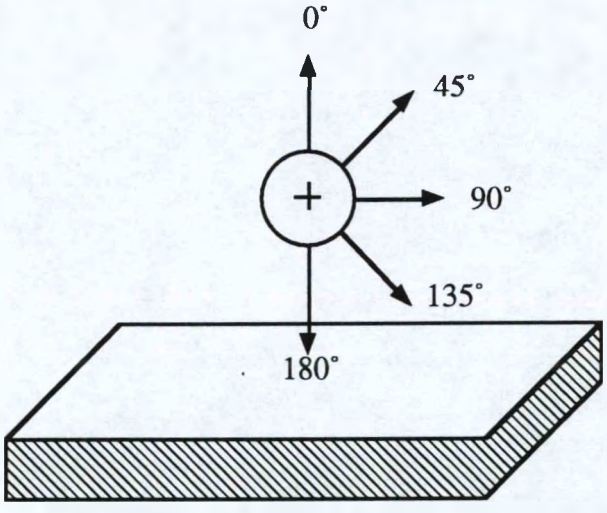

Figure 4.3: Orientation angle definitions. This diagram illustrates the orientation angles referred to in the text. The orientation angle is defined such that 0° is coincident with the surface normal, 90° is parallel to the surface, and 180° is perpendicular to the surface and opposite in direction to the surface normal.

4.3 Methods and Materials

Two strains of *E. coli* bacteria were used in this study: NR50 and HCB437. Both of these strains swim by the rotation of flagella located around the periphery of the cell body. The strain NR50 is a wild type cell with a rod-shaped body 1 μm by 2 μm in size. The swimming behavior of NR50 in an isotropic fluid medium is characterized by a series of runs interrupted at intervals by tumbles (see Section 2.2). These cells were originally obtained from Judy Pile in the Microbiology Department at the University of Pennsylvania.

The strain HCB437 is a smooth swimming (non-tumbling) mutant. Smooth swimming behavior is the result of the deletion of the gene responsible for the production of CheY, a protein known to be necessary for bacteria to exhibit tumbling. The HCB437 cells are rod-shaped but are somewhat larger and longer than the wild type cells with body dimensions of approximately 2 by 4 μm, judged from a visual comparison to NR50 using transmitted light microscopy. These cells were obtained from Howard Berg in the Department of Cell and Developmental Biology at Harvard University and the Rowland Institute in Cambridge, Massachusetts. The differences in the genotype of this strain and wild type cells can be found in Appendix D.

4.3.1 Preparation of samples

The wild type cells were cultured from frozen stock stored in 300 μl aliquots before each experiment. Cultures were made by thawing an aliquot of stock and by pipetting 100 μl of the stock into a 250 ml shaker flask with 50 ml of a sterile growth medium containing buffering agents and minimal nutrients [2] (see Appendix E for the medium composition). This was amended with 0.5 ml each of galactose (0.55 M) and thiamine (1.5 mM) solutions. The flask of nutrients and bacteria was incubated on a temperature controlled rotary shaker (150 rpm) at 30° C for 11-12 hours. This yielded cultures with cell densities of between 10^8 and 10^9 cells/ml in the mid-exponential growth phase. Just prior to an experiment, the final sample was obtained by dilution of the culture stock with motility buffer solution [36] (see Appendix E for the buffer composition) containing the same concentration of buffering compounds found in the growth medium but without nutrients. The smooth swimming cells were also prepared from stock frozen in 300μl aliquots. These cells were cultured by the addition of 200 μl of the frozen stock to 50 ml of sterile Tryptone broth in a 250 ml shaker flask (see Appendix E for the medium composition). The inoculated flasks were incubated on a rotary shaker at 30° C for 5

hours yielding cultures with densities between 10^8 and 10^9 cells/ml. Tryptone broth was used as a growth medium for the smooth swimming cells because HCB437 is unable to synthesize certain amino acids necessary for growth, and the Tryptone broth supplies them directly.

Just before an experiment, the final sample was prepared by diluting an appropriate amount of the culture solution with 1000 µl of motility buffer solution to obtain a sample with a density of approximately 10^6-10^7 cells/ml. This usually required approximately 5 µl of the culture stock resulting in a typical dilution of 1:200.

4.3.2 Measurement of electrophoretic mobility

In this study, the interactions between *E. coli* and glass microscope cover slips in a aqueous medium of phosphate buffers were examined. Two quantities required by DLVO theory to characterize the electrostatic interactions between a colloid/bacterium and a solid surface are the surface potentials of the colloid/bacterium and the solid surface in the suspension medium (see Equation 4.4). The surface potential is typically assumed to be approximately equal to the zeta potential. The zeta potential is the potential at the edge of the shearing plane, or the effective boundary between the solution associated with the solid surface and the bulk liquid phase [43]. The electrophoretic mobility μ_E of a particle in the suspension medium is related to the zeta potential by [37]:

$$\zeta = \mu_E \mu \varepsilon, \varepsilon_0 \tag{4.12}$$

In order to determine the zeta potential for the glass, microscope cover slips were washed with distilled water and pulverized with an agate mortar and pestle. The ground glass was suspended in the phosphate buffer solution (see Appendix E for the buffer composition). The ionic strength of the phosphate buffer was 0.19 M. This procedure was used by Litton

and Olson [42] to determine electrophoretic mobilities for solid material that could be ground into fine particles as an alternative to measuring streaming potentials. Some of the glass particle settle quickly, but the solutions prepared this way remained turbid for periods longer than 24 hr. In making a measurement, the solution of glass particles was allowed to settle for an hour and then a sample of the supernatant was taken. The sample was inserted into the analysis chamber of a Doppler Electrophoretic Light Scattering Analyzer (Coulter Delsa 440, Coulter Electronics, Amherst, MA) and the electrophoretic mobility was measured at 30° C. The Coulter Delsa 440 calculates the zeta potential from the electrophoretic mobility using Equation 4.12. For the bacteria, cells were taken from the culture flask and washed by filtering with buffer solution according to the procedure used by Berg and Turner [14]. Cells were resuspended in buffer and a sample was inserted into the analysis chamber.

The values of the electrophoretic mobility and zeta potentials measured for the bacteria and the ground glass are given in Table 4.1.

Material	Electrophoretic mobility (μm-cm/V-s)	Zeta potential (mV)
Cover slip glass	-2.51	-32.21
E. coli NR50	-1.49	-19.09

Table 4.1: Electrostatic parameters for the wild type bacteria and finely crushed microscope cover slip glass.

4.3.3 Tracking microscope

The microscope used to acquire the tracking data was designed and built by Howard Berg [8]. The body of the instrument is a standard Nikon transmitted light microscope. It is fitted with a special stage connected by a strut to three electromagnetic

coils, arranged so that their axes are mutually orthogonal to represent the three coordinate directions. A schematic of the equipment is shown in Figures 4.4 and 4.5.

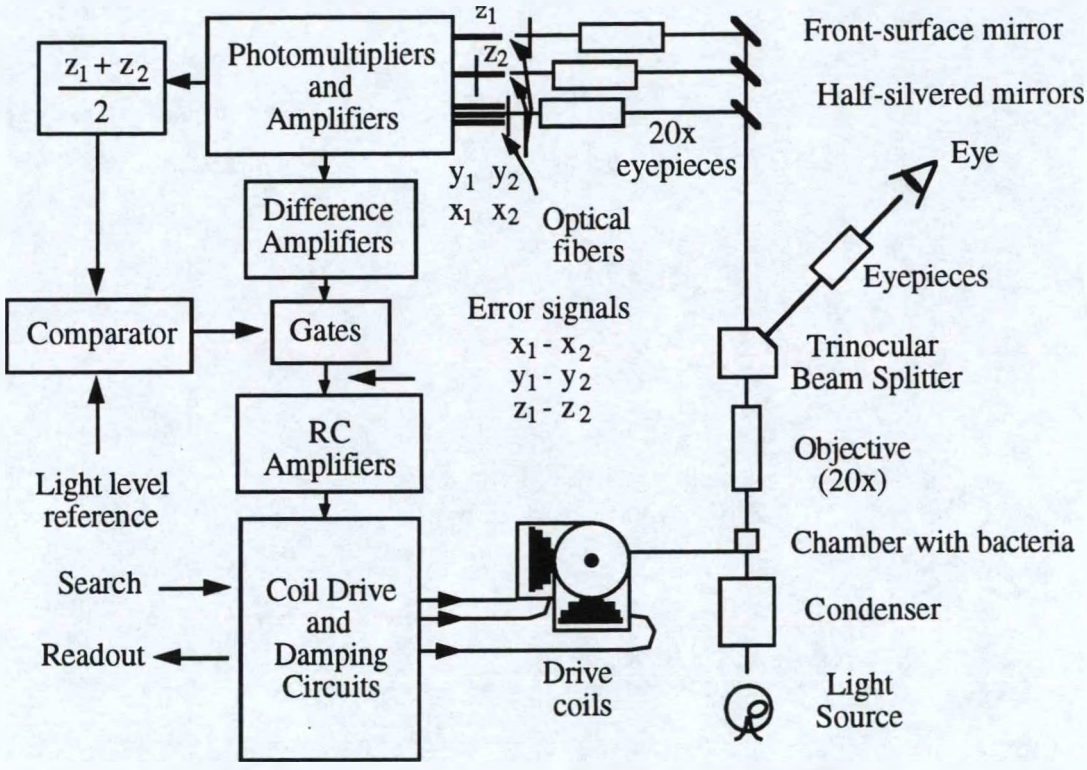

Figure 4.4: Schematic of the tracking microscope used in this study. Adapted from Berg [8].

The stage is moved by varying the current in the coils shown in Figure 4.5. A sample of bacteria diluted with buffer solution is placed in a small "box" or chamber with glass windows on the top and bottom on the stage. Light from the light source passes through the chamber and the objective to a trinocular beam splitter. Part of the light is transmitted to the viewer while part is allowed to pass through the splitter and is projected on the end of an array of six optical fibers.

The microscope is configured with a phase contrast condenser and a 20× inverse phase objective so that the focused image appears brighter than the background. In this

configuration, bacteria in focus appear as bright spots on a dim background while those out of focus appear as dim fuzzy images. The portion of the image focused on the optical fiber array is approximately equal to the diameter of a bacterium (about 1 μm). The optical fibers transmit the light from the image to photomultiplier tubes which produce a voltage signal proportional to the amount of light falling on the ends of the optical fibers. Four of the optical fibers are arranged in an array as shown in Figure 4.6.

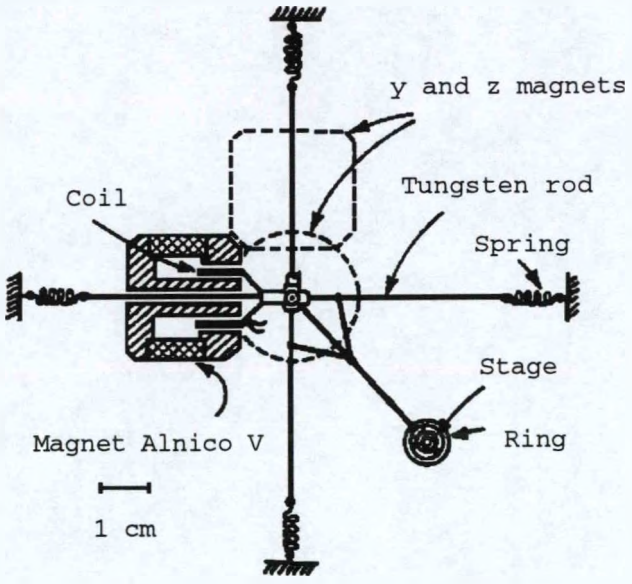

Figure 4.5: Close-up of the stage and coil arrangement on the microscope. Adapted from Berg [8].

When the image is in focus and positioned on the end of the x_1 optical fiber, more light is passed through that fiber compared to the x_2 fiber and a larger signal is produced by the photomultiplier tube connected to the x_1 fiber. Therefore, if the image of a bacterium is focused somewhere on the end of the array of optical fibers, the light level in each of the fibers indicates the position of the image of the bacterium relative to the fibers. The configuration of the z_1 and z_2 optical fibers is somewhat different. The position of the ends of the z_1 and z_2 optical fibers is such that when the image is perfectly focused on the end of the array of x and y optical fibers, it is focused slightly in front of the end of the z_1

optical fiber and slightly behind the end of the z_2 optical fiber. Since an image in focus will appear brighter than an out of focus image, the relative voltage signal from the z_1 and z_2 photomultiplier tubes indicates the end of the fiber on which the image is most nearly in focus.

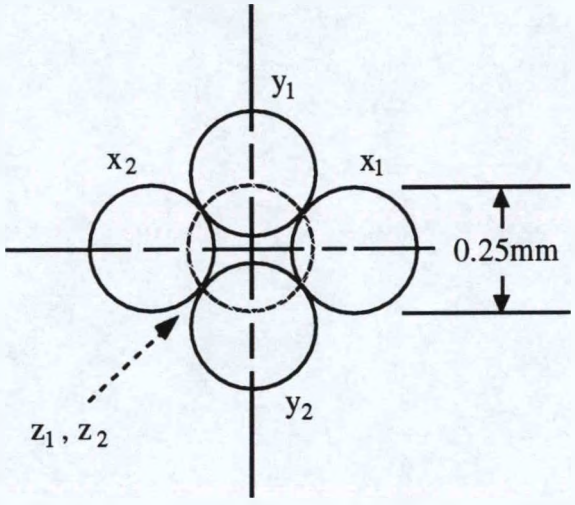

Figure 4.6: Alignment of the ends of the optical fibers. This is the alignment of the ends of the optical fibers as the would appear viewed from the chamber along the light path to the three mirrors in Figure 4.4. Adapted from Berg [8]. The z_1 and z_2 fibers appear superimposed on the center of the array viewed from this perspective.

The microscope is equipped with a feedback control circuit that senses the voltage in each of the photomultiplier tubes and changes the current in the stage control coils to move the stage. If the image of a bacterium falls on the ends of the optical fibers, a circuit senses an increase in the voltage signal from the photomultiplier tubes attached to the z_1 and z_2 optical fibers. When the light level increases above the background level, a circuit is closed that allows the position of the stage to be controlled automatically by varying the current in the coils in proportion to the voltage signal from the photomultiplier tubes. If the image of the bacterium is positioned over the x_1 optical fiber, the current in the stage coils is varied to bring the image back toward the x_2 optical fiber. If the image is focused more

toward the z_1 optical fiber, this fiber is receiving more light and the coils adjust the stage position so that the image focus is moved toward the z_2 optical fiber. If the bacterium itself is in motion, the stage will be moved opposite to the motion of the bacterium in order to keep its image in focus on the ends of the optical fibers.

A low concentration of cells (10^6-10^7 cells/ml) is necessary to suppress extraneous diffracted light from nearby cells which would interfere with the light from the cell being tracked. At this concentration, the occasion of a cell moving into the approximately 2 μm sphere in which its image will appear sufficiently in focus on the optical fibers by chance is rare. The microscope is therefore provided with a three-axis joystick controller that allows the user to move the stage as he/she views the dilute sample of bacteria. When a bacterium is found in a nearby region, the user maneuvers the stage with the joystick so that the focal region of the optical fiber array encloses the bacterium. When this occurs, the control circuit of the microscope closes and tracking begins. As the stage and chamber move in synchronization with the motion of the bacterium, the current in the coils generates a voltage signal that is proportional to the chamber position and therefore the position of the bacterium in the chamber.

A 16 bit A/D converter was used to digitize the voltage signal from the coils (National Instruments model NB-MIO-16XH). The data acquisition board was controlled by software written using the LabView 3.0 software package (National Instruments). The voltage in each of the three stage control coil circuits was digitized at the rate of 12 samples/s.

Two types of chambers were used in these experiments and differ in the way in which the top windows were mounted on the chambers and the type of top window that is was used. The body of the first type, shown in Figure 4.7 is machined from tantalum. The bottom window of the chamber is a disk of glass cut from a microscope cover slip and sealed in place with silicone adhesive. When an experiment was performed, a drop of the

sample of bacteria in buffer solution was placed in the chamber. The top window was then sealed in place with vacuum grease.

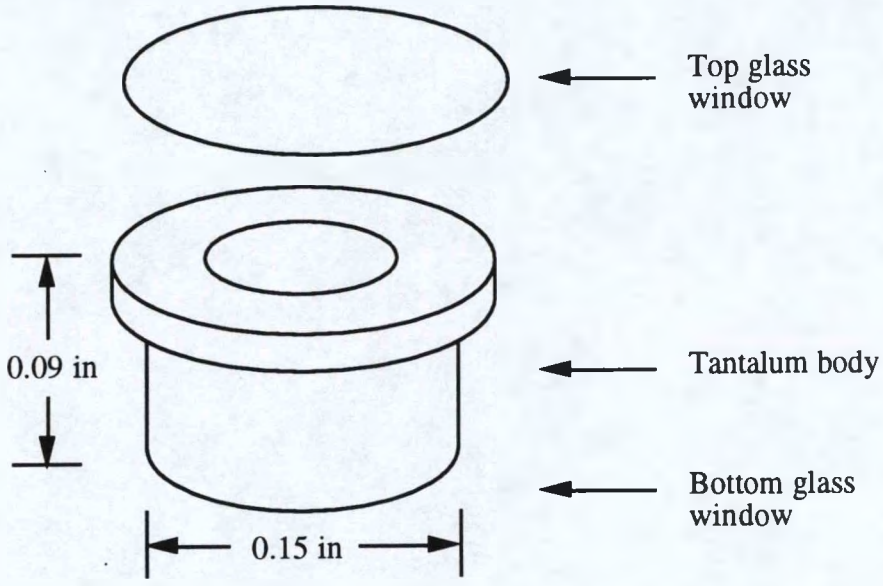

Figure 4.7: Chamber type 1. This is a diagram of the type of chamber used in tracking experiments performed on bacteria in the bulk fluid.

For experiments in which the position of the inside surface of the top window needed to be determined, the grease seal for the top window did not hold the window sufficiently still and the window would shift significantly in the grease. For this reason, a second type of chamber was designed in which the top window could be sealed between the body of the chamber and a threaded cap. The bottom half of the second type of chamber, shown in Figure 4.8, has a body machined from tantalum with machine threads cut on the outside of the body.

A glass disk was sealed on the bottom of the tantalum body using silicone adhesive. The upper half of the chamber is machined from brass and is threaded on the inside. To prepare the chamber for an experiment, a drop of the sample solution was placed in the bottom half of the chamber. A latex gasket and top window were secured in place by screwing the top half of the chamber onto the bottom half. The top windows are disks cut

from microscope cover slips and are printed with an array of dots on the fluid side as shown in Figure 4.9. The dot array was printed on the glass using chromium metal deposition (Klarman Rulings, Manchester, New Hampshire). Each dot is 10 μm in diameter and has a thickness of less than 2 μm.

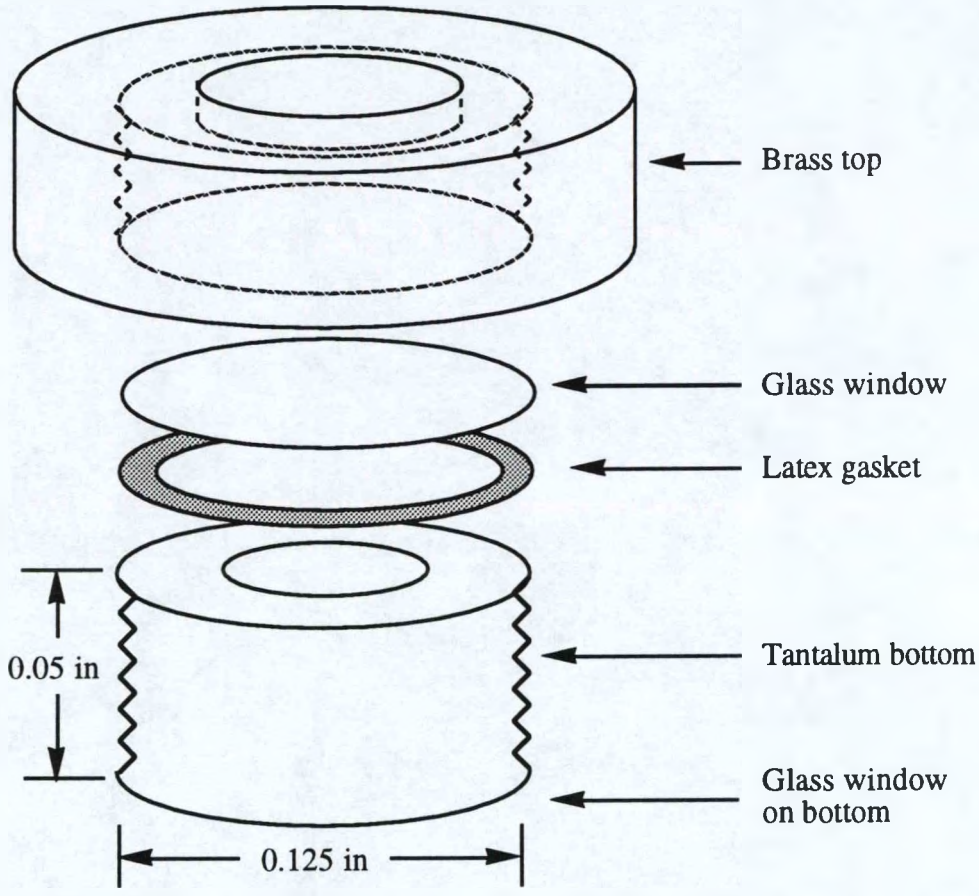

Figure 4.8: Chamber type 2. The type of chamber was used in tracking experiments performed on bacteria near the surface is shown above (not to scale).

In an experiment in which the distance between the tracked bacterium and the surface was needed, the windows were sealed onto the top of the bottom half of the chamber with the grid of dots on the side of the top window glass facing the interior of the chamber. The chamber was then placed on the stage with the dotted window glass on top. The position of the surface exposed to the bacteria was determined by maneuvering the

stage and chamber so that a dot was positioned in the region in which a bacterium would be tracked and in sharp focus.

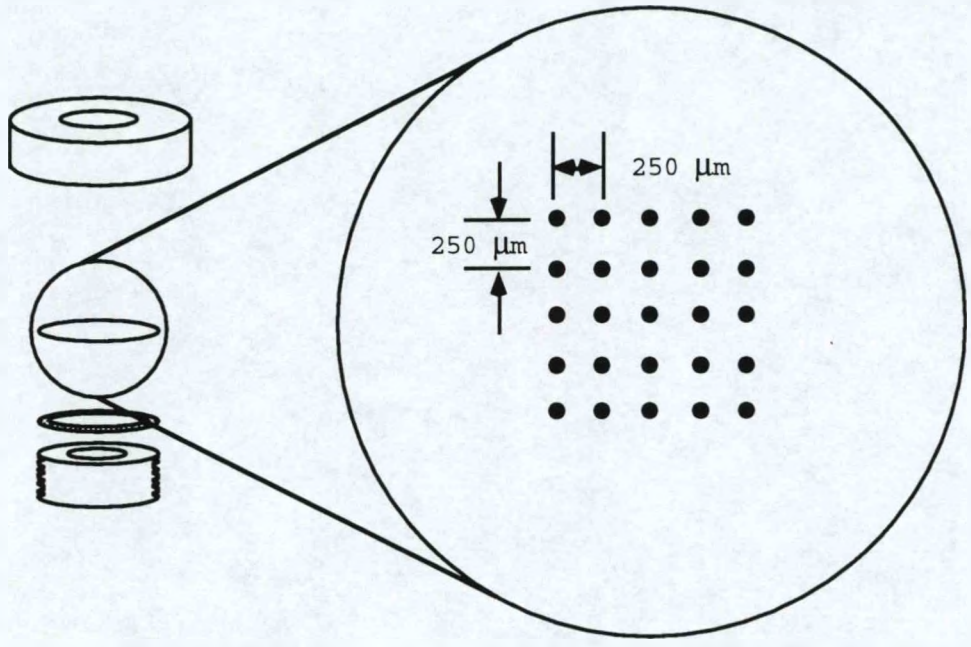

Figure 4.9: Dot array on top window of chamber type 2. Shown is an exploded view of the underside of the top window used in tracking experiments near the surface of the glass window. An array of dots was printed on the underside of the window to allow the position of the surface of the glass to be determined (not to scale).

The voltage signals from the three coils were then recorded. This procedure was repeated until the coordinates of three of the calibration dots on the interior surface of the top window glass were recorded. The glass surface was assumed to be planar and the three coordinates were used to calculate the surface normal for the top window. If the top window glass were perfectly parallel to the x-y plane, it would be necessary to record the coordinates of only one surface point to determine the distance to the surface. However, since a slight misalignment would cause substantial errors on the length scale relevant to the experiment, an accurate determination of the position of the surface was necessary.

In the tracking experiments originally performed by Berg and Brown [11], it was found that the swimming motion of bacteria in pure buffer solution is frequently not smooth, but that bacteria often wobble substantially as they swim. The researchers found that the addition of 0.18% (w/v) hydroxypropyl methylcellulose decreased the wobbling motion of the swimming bacteria and they felt that this lead to a more accurate analysis of the data. For this reason it was decided that these experiments performed in this study would be performed in a buffer solution to which 0.18% (w/v) hydroxypropyl methylcellulose was added (Biochemika Methocel 90 HG). The stage of the tracking microscope is equipped with a heating coil and was maintained at 30°C for all the tracking experiments. An initial set of experiments on bacteria moving in the bulk liquid to determine the effects of Methocel on the swimming behavior of *E. coli*.

4.3.4 Data analysis algorithm

In order to determine the phase of motion for each bacterium at each sample point, the data analysis method of Berg and Brown [12] was used. The x component of a bacterium's velocity at time t_j (the time at which sample j was taken) was determined from the position data using the following 5 point differencing scheme:

$$\left(\frac{dx}{dt}\right)_j = \frac{2}{3\Delta t}\left[x_{j+1} - x_{j-1}\right] - \frac{1}{12\Delta t}\left[x_{j+2} - x_{j-2}\right] \tag{4.13}$$

where x_j is the x position of the bacteria at time t_j and Δt is the sample interval (1/12 s, in this case). The velocity of the bacterium in the y and z directions was similarly calculated. A bacterium's direction was determined using the velocity components derived from Equation 4.13. The rate at which a bacterium was changing its direction was called the angular speed and was defined by:

$$\dot{\theta} = \text{acos}\left(\frac{\mathbf{a} \bullet \mathbf{b}}{|\mathbf{a}||\mathbf{b}|}\right) / \text{sample interval} \tag{4.14}$$

where

$$\mathbf{a} = \left[(v_x)_j, (v_y)_j, (v_z)_j\right] \quad , \quad \mathbf{b} = \left[(v_x)_{j+1}, (v_y)_{j+1}, (v_z)_{j+1}\right]$$

The angular speed was used as a criteria for determining the phase of motion of a bacterium. A bacterium was taken to be in a tumbling phase of motion when tracking began. The beginning of a run was scored at data point i when the angular speed was less than 35° per sample point (at 12 samples/s this is 420° /s) for points i, $i+1$ and $i+2$. A run was said to end at point j when either of two criteria were met: 1) the angular speed was greater than 35° /sample for samples j and $j+1$, or 2) the angular speed was greater than 35° /sample for sample j and the difference angle Φ for point j was greater than 35° where the difference angle at j was defined as:

$$\Phi_j = \text{acos}\left(\frac{\mathbf{c} \bullet \mathbf{d}}{|\mathbf{c}||\mathbf{d}|}\right) \tag{4.15}$$

where:

$$\mathbf{c} = \left[\left\{(v_x)_{j-1} + (v_x)_j\right\}, \left\{(v_y)_{j-1} + (v_y)_j\right\}, \left\{(v_z)_{j-1} + (v_z)_j\right\}, \right]$$

and:

$$\mathbf{d} = \left[\left\{(v_x)_{j+1} + (v_x)_{j+2}\right\}, \left\{(v_y)_{j+1} + (v_y)_{j+2}\right\}, \left\{(v_z)_{j+1} + (v_z)_{j+2}\right\}, \right]$$

The criteria for distinguishing between the two phases of motion and the use of the angle 35° as the criterion to which the angular speed and the difference angle are compared were first used in the study by Berg and Brown [12]. By this algorithm, the minimum run length was three data points but a tumble could be of any length that is an integer multiple of the sample interval of 1/12 s, including zero. These criteria were developed by viewing stereo plots of the tracking data and the results of the analysis by representing tumble points

in the data as bright dots and run points as dim dots. Various analysis algorithms and criteria were tested by Berg and Brown with the success of a particular algorithm or criterion being judged by the degree to which the analysis results agreed with a visual examination of the data for apparent tumble locations. The algorithm and criteria outlined here gave the best agreement with a visual inspection of the stereo plots. For this work, a test of various criteria was also performed and it was determined that the algorithm developed by Berg and Brown was satisfactory for this study. However, it might be useful to make a systematic study of the effect of various criteria and analysis algorithms on the results of the analysis.

The angle through which a bacterium was reoriented as result of a tumble was designated the turn angle. For a run which ends at point k and was followed by a run which begins at point l, the change in direction from point k to l is called the turn angle φ and is defined by:

$$\varphi = \operatorname{acos}\left(\frac{\mathbf{e} \bullet \mathbf{f}}{|\mathbf{e}||\mathbf{f}|}\right) \tag{4.16}$$

where:

$$\mathbf{e} = \left[\left\{(v_x)_{k-2} + (v_x)_{k-1} + (v_x)_k\right\}, \left\{(v_y)_{k-2} + (v_y)_{k-1} + (v_y)_k\right\}\left\{(v_z)_{k-2} + (v_z)_{k-1} + (v_z)_k\right\}\right]$$

and:

$$\mathbf{f} = \left[\left\{(v_x)_l + (v_x)_{l+1} + (v_x)_{l+2}\right\}, \left\{(v_y)_l + (v_y)_{l+1} + (v_y)_{l+2}\right\}\left\{(v_z)_l + (v_z)_{l+1} + (v_z)_{l+2}\right\}\right]$$

4.4 Results

4.4.1 Bulk tracking experiments

First, a set of experiments were performed in which bacteria were tracked at distances far from the walls and windows of the chamber (approximately 400 μm) in buffer solutions to which 0.18% (w/v) Methocel was added and to which it was not added to determine the effect of the compound on the swimming behavior of the bacteria in the bulk before experiments were performed near a surface.

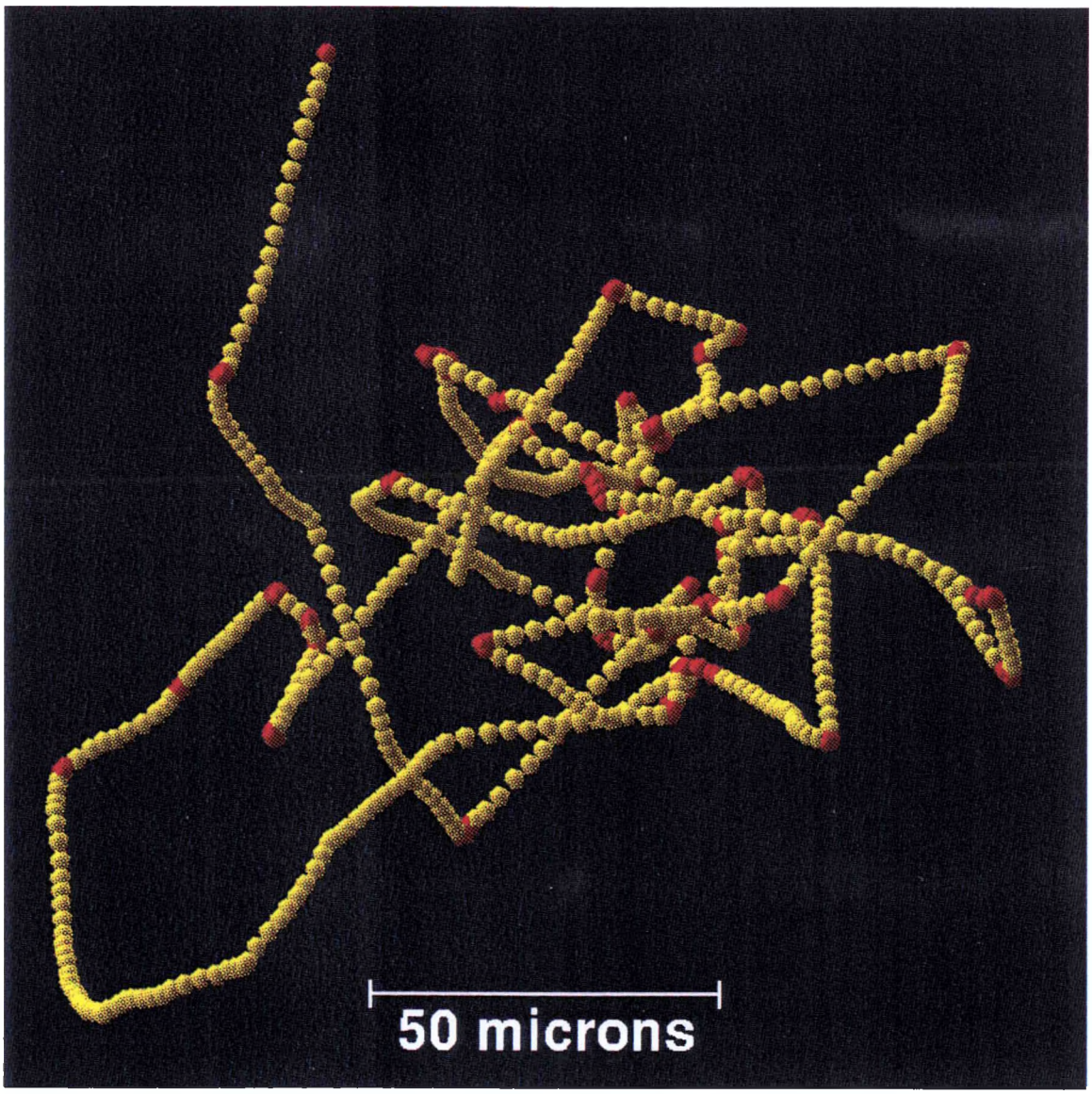

Figure 4.10: Wild type bacterium in bulk. Shown is the trace of a bacterium tracked in the bulk fluid. Each sample point is represented by a sphere. Yellow spheres represent sample points for which the analysis determined the bacterium was executing a run. Tumbles are indicated by purple spheres.

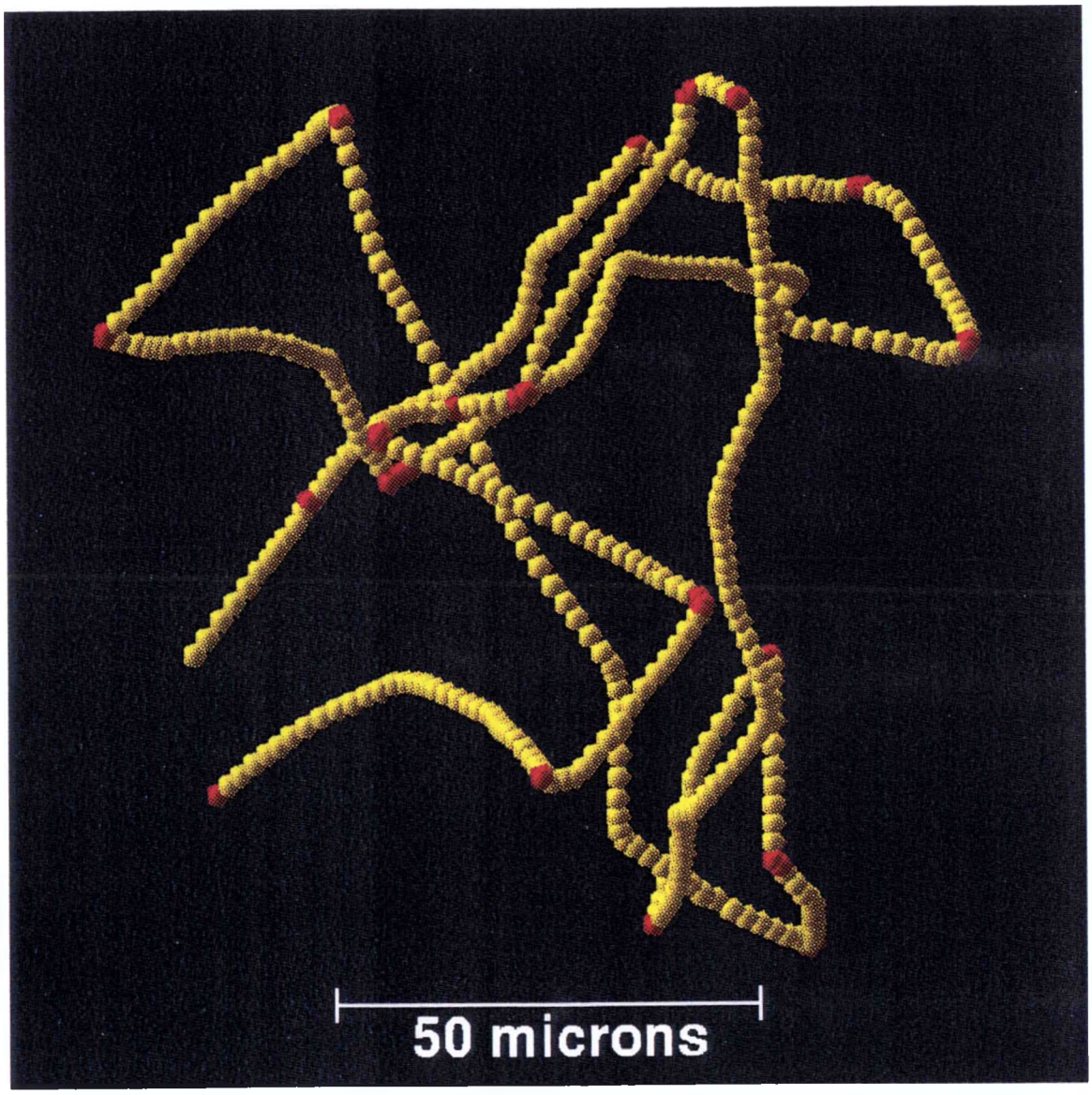

Figure 4.11: Wild type bacterium in bulk. This is another example of a trace from a bacterium tracked in the bulk fluid.

Figures 4.10 and 4.11 show the traces of two individual bacteria from the sample to which Methocel was added. Tracking chambers of the type shown in Figure 4.7 with plain glass top windows were used in the experiments that examined bacterial motion far from solid surfaces. The position of the bacteria at each sample point is shown as a sphere. The spheres are assigned different colors based on the phase of bacterial motion; yellow spheres represent data points at which it was determined the bacteria was in the running phase while purple points indicate positions where the bacteria were in the tumbling phase of bacterial motion.

Shown in Figure 4.12 is the variation of the cell swimming speed as a function of the tracking time for the bacterial trace shown in Figure 4.10.

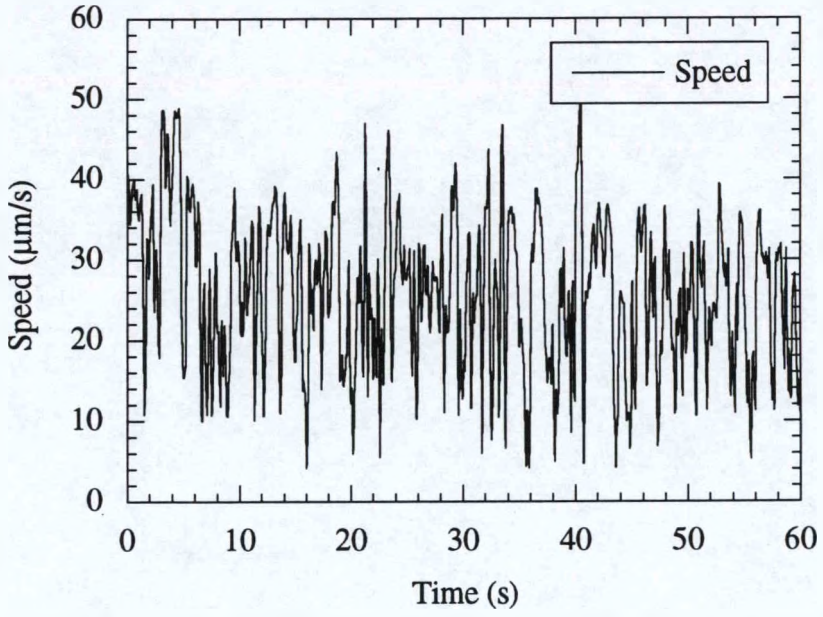

Figure 4.12: Speed of a wild type bacterium in the bulk fluid. Shown is the speed of the bacterium in Figure 4.10 as a function of time.

It can be seen that the cell swimming speed varies substantially (between 4 and 50 μm/s). Part of this variation is due to the decrease in swimming speed as cells tumble since they tumble in place, however there is still considerable variation during the running phase of motion. Figure 4.13 is a close-up of the region of Figure 4.12 between 20 and 30 s. The

solid dots in this figure represent sample points at which tumbles occurred according to the analysis. In this figure, the swimming speed during running can be seen to vary between 15 μm/s and 47 μm/s.

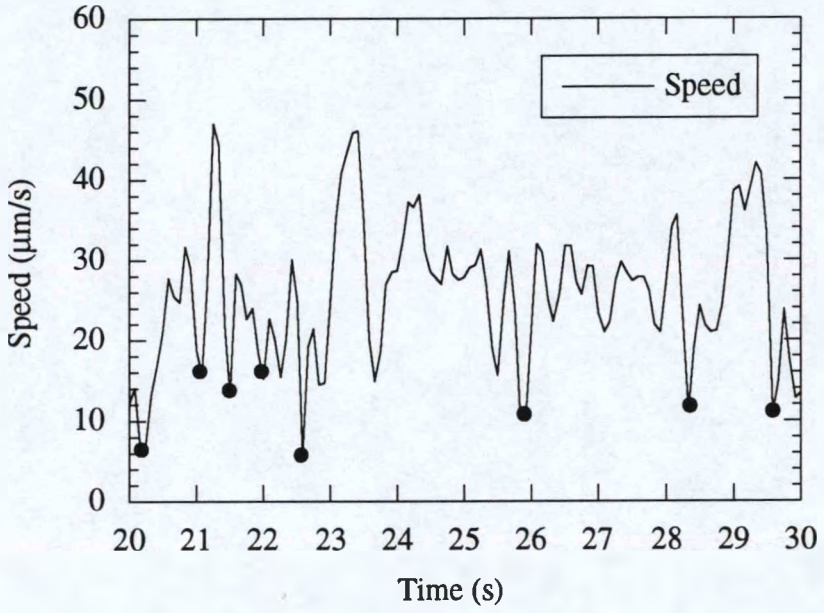

Figure 4.13: Close-up of bacterial swimming speed. Shown above is the region from 20 s to 30 s in Figure 4.12 above to illustrate the variation in swimming speed. Points where the analysis determined that tumbles occurred are shown as solid dots on the speed trace.

The properties that characterize the transport of a population of bacteria in an isotropic fluid medium are the mean run time, the mean cosine of the turn angle and the swimming speed of the population (see Equation 2.28). Shown in Figures 4.14, 4.15, and 4.16 are the distributions of run times, turn angles and run speeds for a population of 100 bacteria from a single tracking experiment in which 100 cells were tracked. The run time and turn angle distributions count each run or turn angle as one value in the distribution. The run speed distribution counts the mean run speed for each bacterium as one value since reporting each run as an event would over represent slower run speeds (the microscope is able to track slower cells longer).

The mean run time for the distribution shown in Figure 4.14 is 0.85±1.12 s (reported as the mean ± the standard deviation). The solid line in the figure is the Poisson interval distribution whose mean is equal to the population mean and is given by:

$$f(t) = \frac{1}{\langle \tau \rangle} \exp\left[\frac{\Delta t - t}{\langle \tau \rangle}\right] \tag{4.17}$$

where Δt is the minimum observable interval and $\langle \tau \rangle$ is the experimentally measured run time for the population[12].

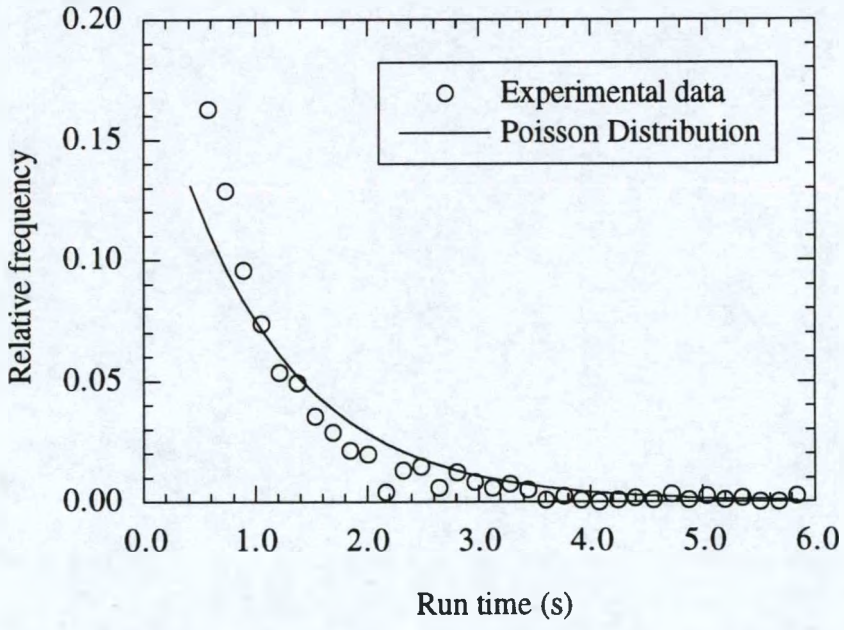

Figure 4.14: Run time distribution with methylcellulose. The distribution of run times from a tracking experiment is shown in which 0.18% (w/v) Methocel was added to the motility buffer. In this experiment 100 bacteria were tracked. The solid line is the Poisson interval distribution whose mean is the same as the experimental mean.

In this analysis, the minimum run length is 3 sample intervals or 3/12 s. This interval distribution is obtained for events which occur at random; that is, the probability of the event occurring during an observation interval is the same irrespective of when the observation is made. The fact that the experimental data agrees well with the Poisson

distribution indicates that the tumbling event occurs at random. This observation confirms those of Berg and Brown [12] made by tracking *E. coli* AW405, another wild type cell. Berg and Brown reported a mean run time of 0.86±1.18 s.

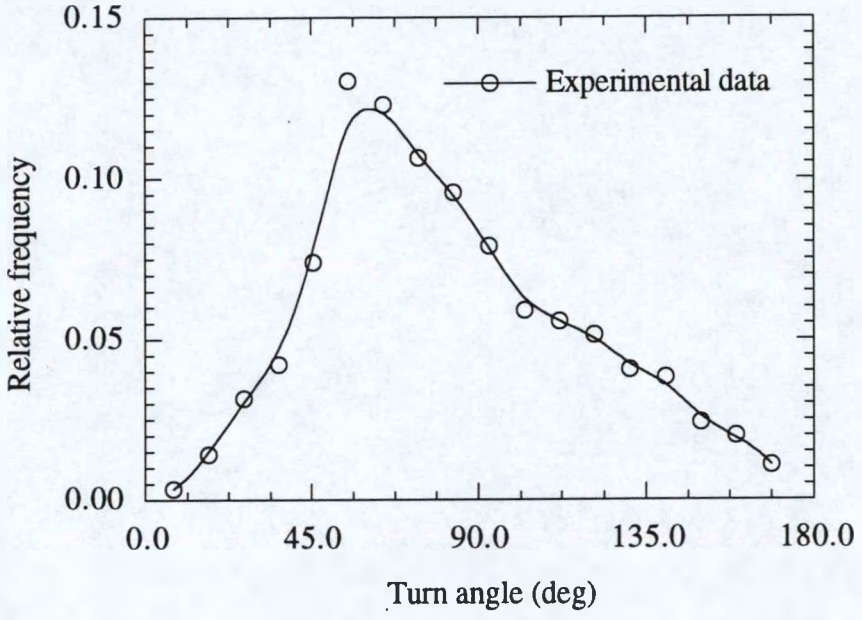

Figure 4.15: Turn angle distribution with Methocel. This figure shows the distribution of turn angles for the same experiment shown in Figure 4.14. The solid line is a curve fit to the data.

The mean turn angle is 82°±35° and the mean cosine of the turn angle is 0.13. In the tracking experiments performed by Berg and Brown, the cells showed a more significant bias toward smaller turn angles with a mean turn angle of 68°±36°. The mean run speed is 28.7±5.7 μm/s which is significantly higher than that reported by Berg and Brown of 14.2±3.4 μm/s. The NR50 is most likely a more motile strain, however direct comparison of AW405 and NR50 were not made in this study. Also, the growth media are different. The media used by Berg and Brown Berg and Brown contained glycerol as a carbon source and also included threonine, leucine, and histidine [12].

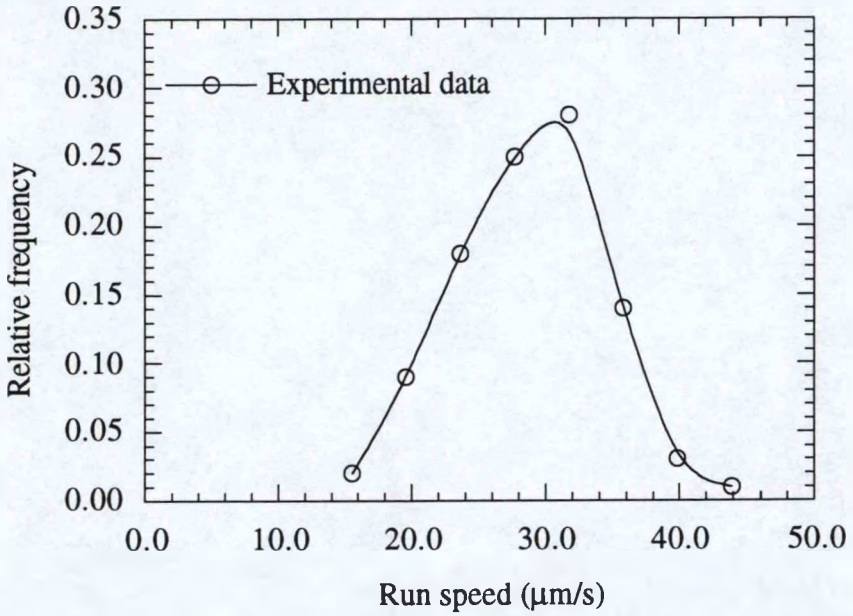

Figure 4.16: Run speed distribution with Methocel. This figure shows the distribution of run speeds for the same experiment shown in Figure 4.14. The solid line is a curve fit to the data.

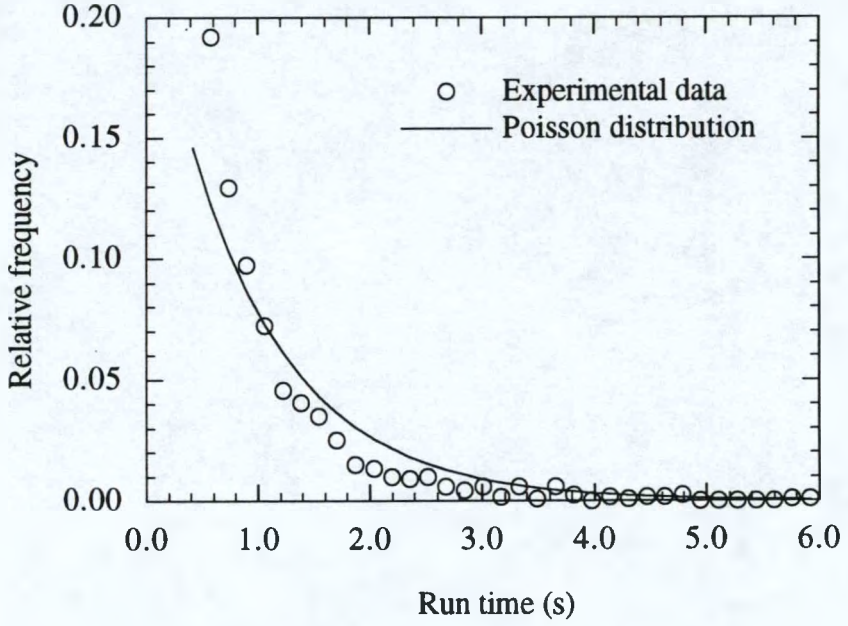

Figure 4.17: Run time distribution without Methocel. This figure shows the distribution of run times from a tracking experiment in which no Methocel was added to the motility buffer. In this experiment 130 bacteria were tracked. The solid line is the Poisson interval distribution whose mean is the same as the experimental mean.

Shown in Figures 4.17, 4.18, and 4.19 are the run time, turn angle, and run speed distributions for the NR50 bacteria tracked while swimming in buffer solution without the addition of Methocel. The mean run time for the distribution shown is 0.69±0.78 s which is slightly lower than the mean of 0.85 s recorded for the same strain swimming in a solution that contained methyl cellulose. The mean turn angle is 80°±36° and the mean cosine of the turn angle is 0.15, which shows a slightly greater bias to smaller turn angles than those recorded for the cells in methyl cellulose. The turn angle distribution for the cells tracked in the buffer solution with methyl cellulose exhibits a sharp peak around 55° while the distribution for cells tracked in buffer without Methocel shows a gradual rise to the maximum frequency at around 55° and then a gradual decrease.

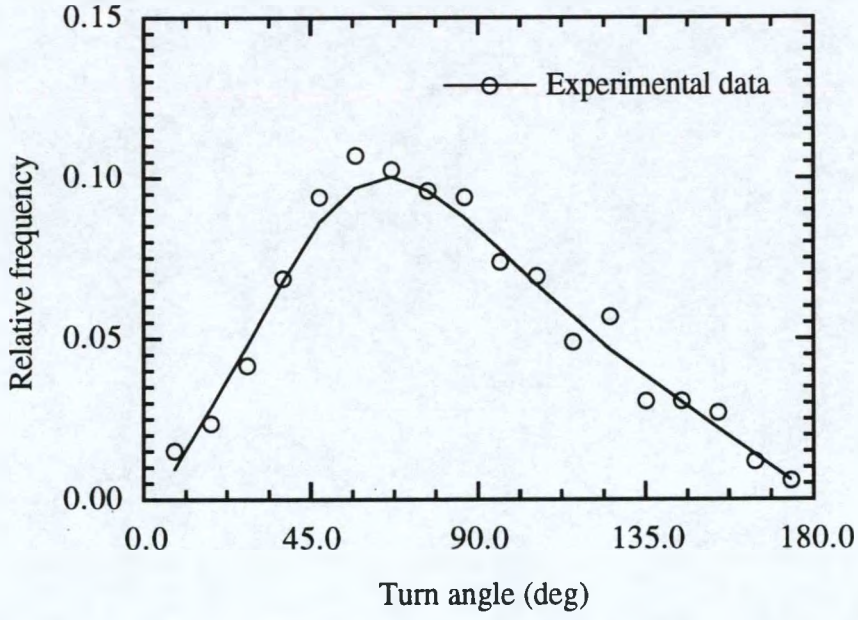

Figure 4.18: Turn angle distribution without Methocel. This figure shows the distribution of turn angles for the same experiment shown in Figure 4.17. The solid line is a curve fit to the data.

The mean run speed of 24.2±5.0 μm/s is slightly lower than that recorded for the cells in Methocel. This is consistent with observations by other researchers that the swimming speed of some bacteria increases with the addition of viscosity enhancing agents

[32]. This is due to an increase in the efficiency of the flagellar propulsion at higher viscosities [13]. The decrease in mean run time and mean turn angle could be explained by slightly increased cell wobble in the absence of Methocel. This would lead to more spurious tumbles being scored by the data analysis algorithm which would decrease the mean run time. Tumbles generated by the analysis as a result of cell wobble would be recorded as having small turn angles which would lead to a corresponding decrease in the mean turn angle.

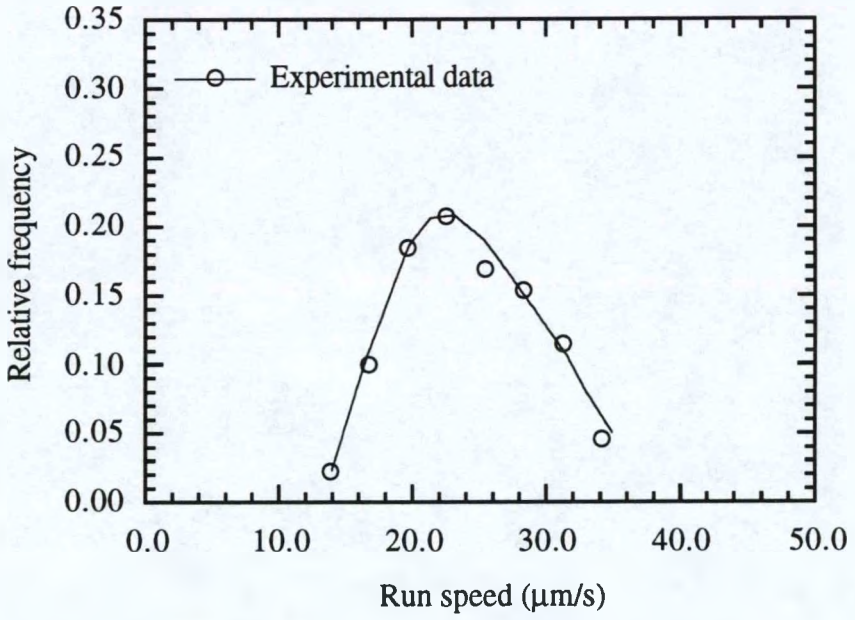

Figure 4.19: Run speed distribution without Methocel. Shown is the distribution of run speeds for the same experiment shown in Figure 4.17. The solid line is a curve fit to the data.

4.4.2 Near surface tracking experiments

In the next series of experiments, the chamber and windows were used that allowed the surface position to be determined by focusing on the dot array on the inside surface of the upper chamber window. The chamber and windows used are shown in Figures 4.8 and 4.9. After the position of the surface was determined the chamber position was

adjusted with the joystick so that the microscope was focused on the region of the fluid from 10 to 40 μm beneath the glass surface. The chamber was maneuvered within this region in order to track bacteria moving close to the glass surface. Bacteria at distances greater than 20 μm from the surface were observed to exhibit behavior similar to that found in the bulk fluid. However, bacteria moving very close to the surface exhibited a variety of behaviors.

Shown in Figure 4.20 is an example of a trace for the wild type bacteria from a cell moving near the glass surface. In this figure, the red plane surrounded by the white border is the position of the interior surface of the top window as determined by the calibration of the surface position described above. The single white line is the surface normal. As in the two previous diagrams of traces from cells far from the surface, the yellow spheres indicate points where the analysis indicated the bacterium was in the running phase while the purple spheres represent points where the analysis determined the bacterium was executing a tumble. For this and all following cases, the buffer solution contained 0.18% (w/v) Methocel to increase cell swimming speed and to reduce cell wobble.

In Figure 4.20, tracking begins with the cell in a tumble near the surface at the left edge of the figure. After two short runs away from the surface, it begins to move toward the surface. While close to the surface, it executes a tumble and continues to move along the surface. Executing another tumble, it moves away from the surface, tumbles again, returns to the surface and moves along it continuing its characteristic run-tumble swimming behavior adjacent to the surface before tumbling and moving away again. Finally, it returns to the surface as the trace ends.

Figures 4.21 and 4.22 plot the surface-to-cell distance, swimming speed and orientation as a function of time. The solid circles along the distance line are points where a tumble occurred. The orientation of the cell is the angle between the cell's direction vector and the surface normal as shown previously in Figure 4.3. The bacterium moves approximately parallel to the surface between 2 and 4 s, 6 and 10 s and from 13 s to the end

of the trace as indicated by the nearly constant surface-to-cell distance of 5 μm and the orientation angle of approximately 90° shown in Figure 4.22.

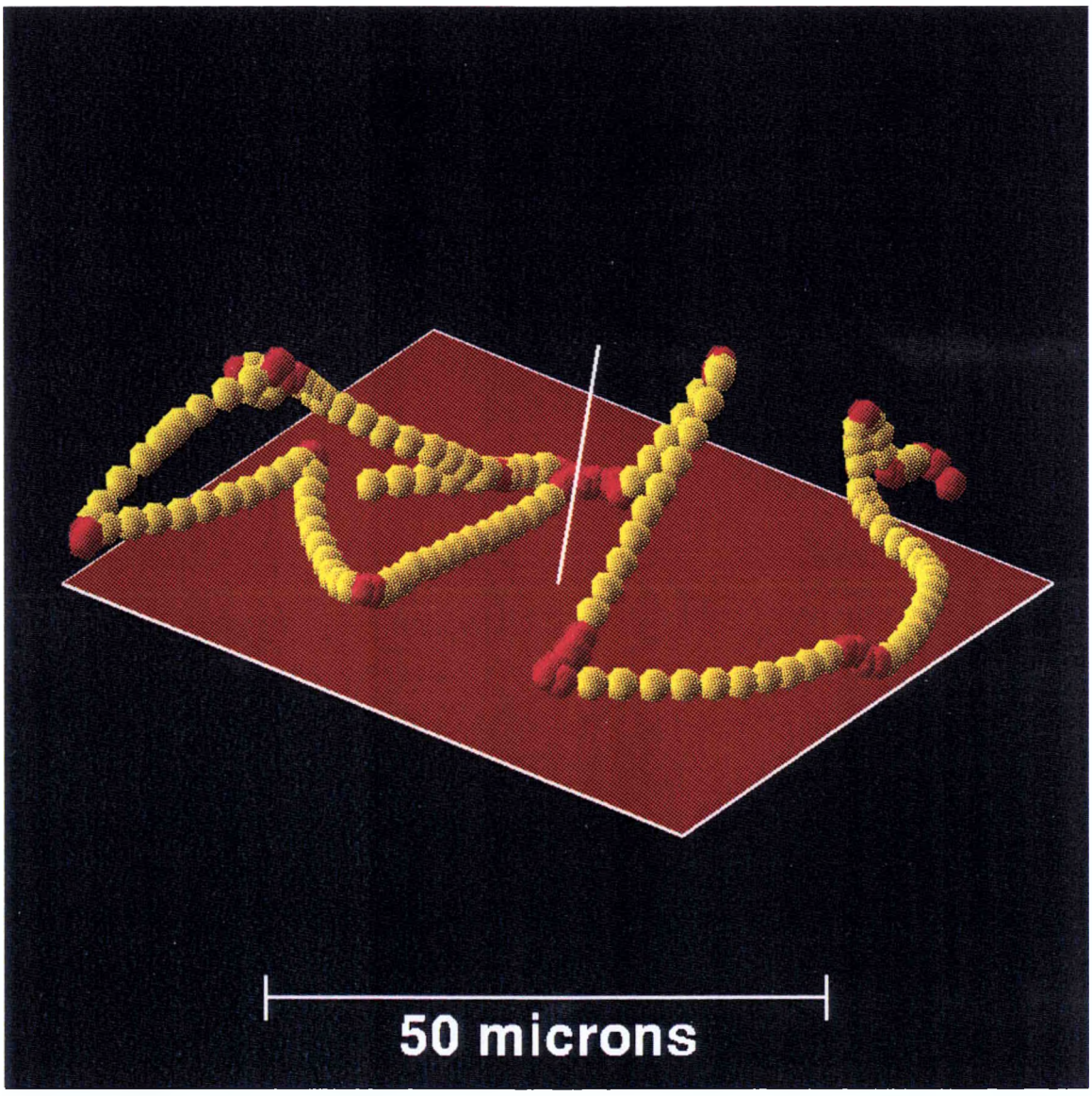

Figure 4.20: Wild type bacterial trace 1. In this figure is shown the trace of a wild type bacterium that was tracked near the surface of the upper window of the tracking chamber. The red plane with a white border represents the position of the glass surface as determined by the position of the array of calibration dots as discussed in the text. The normal to the surface is shown as a white line. Yellow spheres represent sample points that are part of a run, while purple points represent points where the analysis algorithm indicated a tumble occurred.

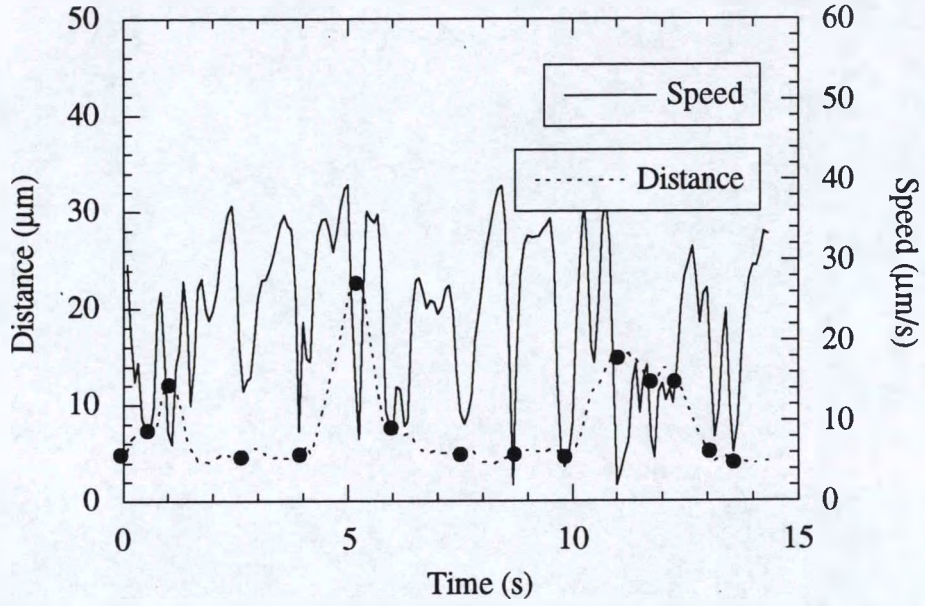

Figure 4.21: Distance and speed for wild type bacterium 1. The swimming speed and the surface-to-cell distance as a function of time are plotted for the bacterium shown in Figure 4.20. The solid circles along the distance line indicate points where the bacterium tumbled.

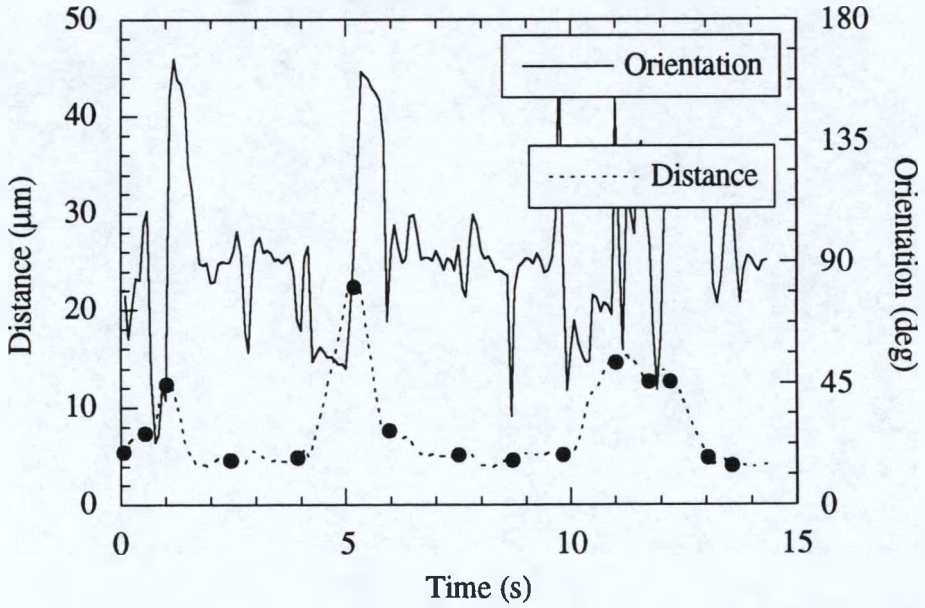

Figure 4.22: Distance and orientation for wild type bacterium 1. The orientation and surface-to-cell distance are plotted as a function of time for the bacterium shown in Figure 4.20. The solid circles along the distance line indicate points where the bacterium tumbled.

The periods of surface motion end with tumbles for this trace, although the initiation of a tumble does not necessarily terminate surface motion. This is illustrated by the solid dots at 2.5 s, 7.5 s, and 8.5 s in Figure 4.22. The orientation angle drops significantly near the tumbles at 2.5 and 8.5 s indicating that the bacterium was pointed away from the surface, but the cell continues to swim along the surface after tumbling. Also note that in Figure 4.21, tumbles are associated with a sudden decrease in the swimming speed.

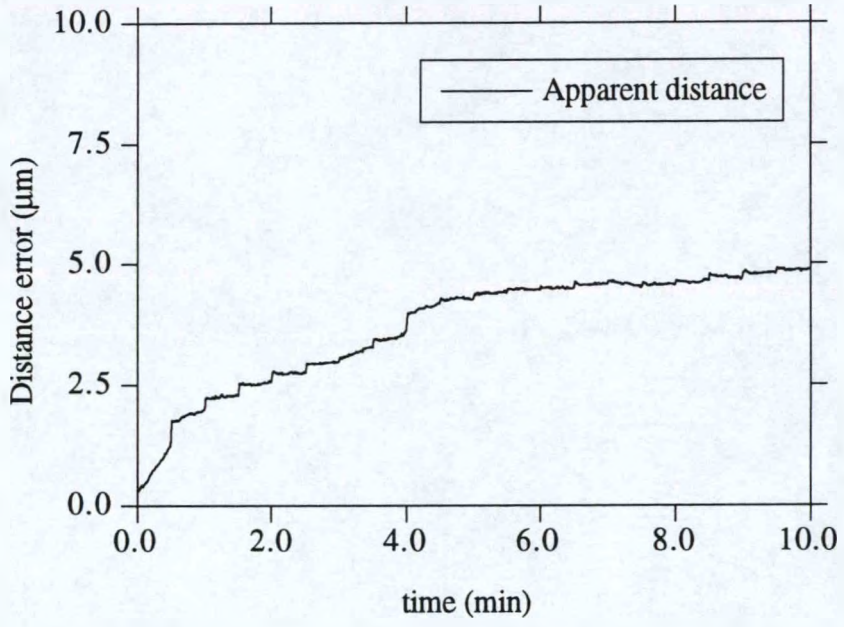

Figure 4.23: Time variation in the apparent distance from the surface to a point known to be on the surface. The initial error of about 0.3 μm at the start of the trial is due to the error in obtaining the position of the surface by focusing on the array of dots as discussed in the text.

An interesting point to consider is the distance between the bacterium and the glass surface when the bacterium is moving parallel and close to the surface in Figure 4.22. The present configuration of the tracking microscope and the method used to locate the surface position does not allow the direct determination of the distance from a cell to the surface with adequate accuracy. There is some slight error incurred during the calibration of the

glass surface position. This is typically on the order of 1-2 μm. However, the accuracy of the calculated surface-to-cell distance tends to drift with time. A measure of the expected error was obtained by tracking a stationary particle adhered to the glass surface and monitoring its apparent movement as a function of time. Figure 4.23 shows an example of this type of experiment.

In this trial, a micron-sized particle was found adhered to the glass surface and tracking was begun. After every thirty seconds of tracking, the automatic stage control circuit was opened so that the stage could be manipulated manually. The joystick was maneuvered through its full range of motion in the x, y and z directions. This was done in order to simulate the motion of the stage during an actual tracking experiment. After manipulating the joystick, the original stationary particle was again tracked while its apparent position was monitored. The apparent surface-to-cell distance of the stationary particle is seen to drift away from its location at the beginning of the experiment until after approximately 10 min of tracking time (which is similar to the tracking time of a typical experiment), the error in the particle's distance is approximately 5 μm. This indicates that the error in the measurement of the position of the surface slowly increases with time but is relatively constant for times on the order of a few seconds.

During cell tracking experiments, it was observed that runs parallel to the surface such as those in Figure 4.20 occurred when the calibration dots were in clear focus. It was observed by focusing on the dots immediately after calibration and recording the indicated distance to the surface that the actual surface-to-cell distances were 0±2 μm (or less than 2 μm from the surface) when the calibration dots were in clear focus as opposed to the value of 4-5 μm indicated by Figure 4.21.

Another interesting feature of the trace of the bacterium shown in Figure 4.20 is its path when moving close to and parallel to the surface. The cell path appears to be slightly curved during these runs. The curvature of these paths is clockwise. A clearer example of

this circling behavior for runs adjacent to the surface can be seen in the trace of another bacterium shown in Figure 4.24.

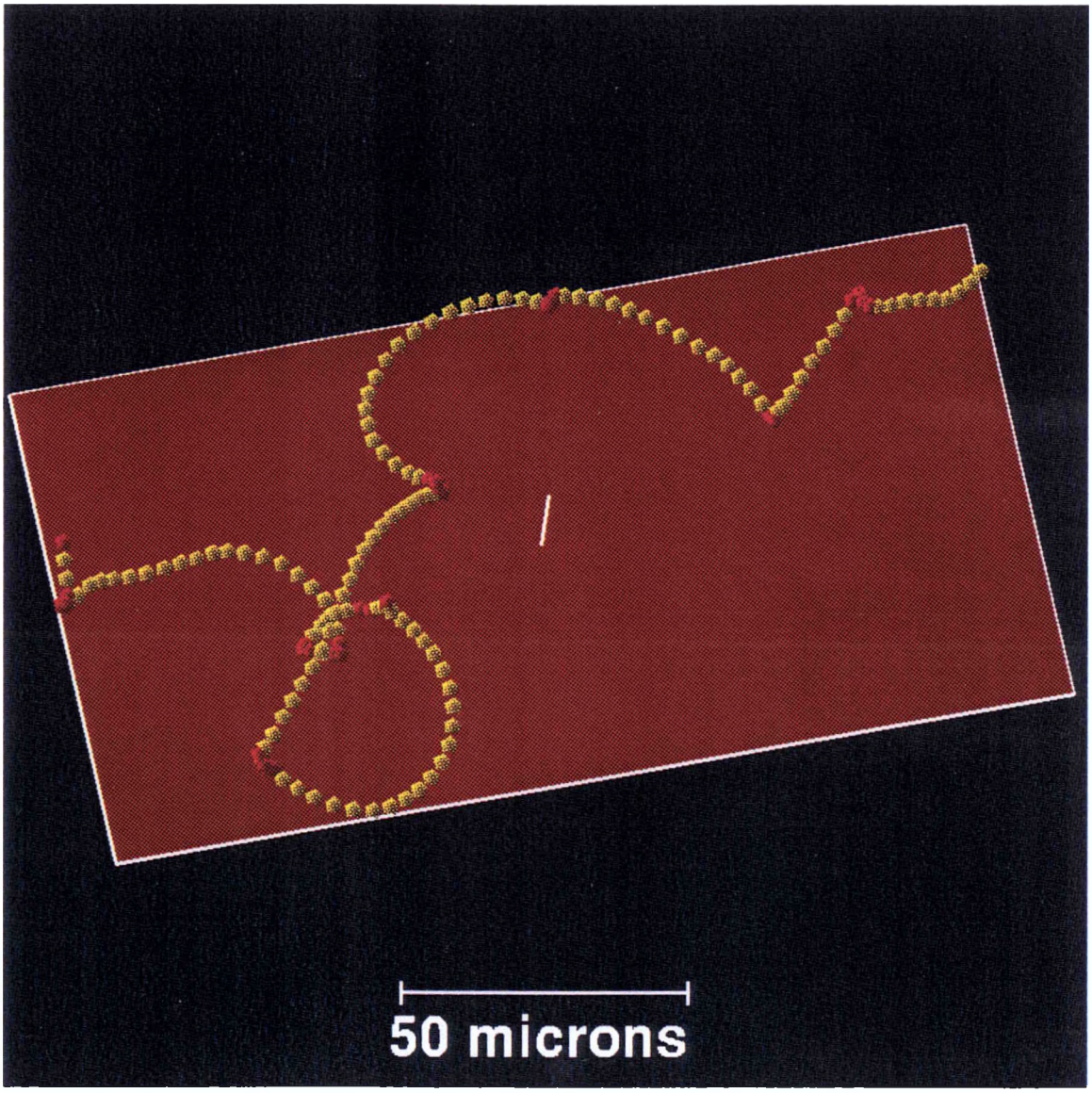

Figure 4.24: Wild type bacterial trace 2. Shown is the trace of a wild type bacterium moving near the surface. The circular portions of the cell's path occurred when the cell was closest to the glass surface.

Tracking began at the left edge of the figure. The trace has been rotated so that the surface normal is nearly perpendicular to the plane of the page. Comparison of the three-dimensional cell trace and the distance of the bacterium as a function of time in Figure 4.25

shows that periods in which the cell moves at a constant small distance from the glass surface correlate with periods in which the cell exhibits a circular swimming pattern.

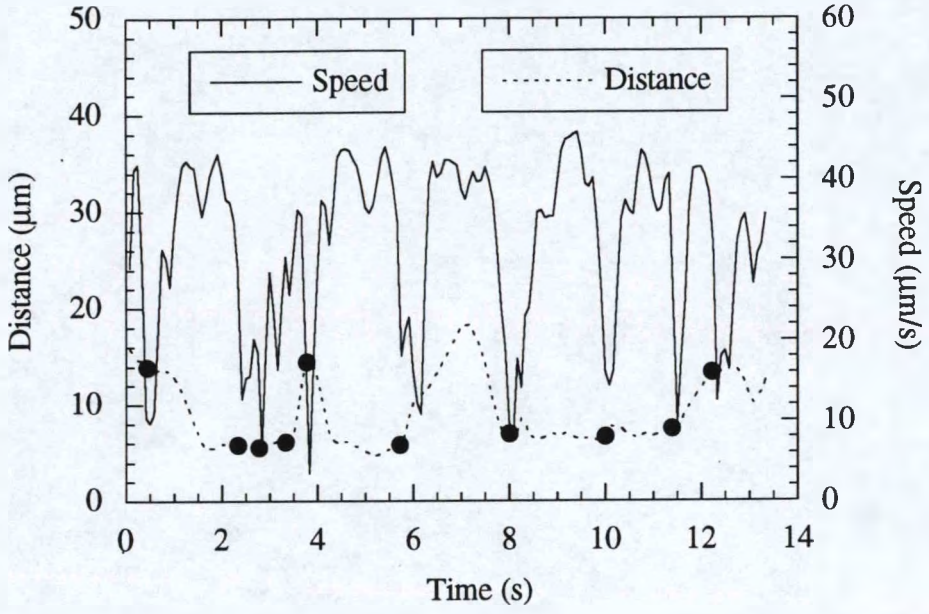

Figure 4.25: Distance and speed for wild type bacterium 2. The surface-to-cell distance and swimming speed are plotted for the bacterium shown in Figure 4.24.

Similar to the previous trace, periods of circular motion near the surface end with a tumble.

Figure 4.26 shows an example of a wild type cell swimming in a circular pattern when moving close to the surface while executing one long, continuous run. At the end of this run, the bacterium turns away from the surface and swims off into the bulk. Figures 4.27 and 4.28 show the variation of the cell swimming speed and orientation angle while swimming. Since this cell did not execute a tumble, its swimming speed remained relatively constant compared to the two previous bacteria, varying between 17 μm/s and 31 μm/s. The direction of the circling is always the same for each of the bacterial traces shown; that is, the bacteria always make clockwise circles on the glass surface. Other researchers have also documented bacterial circling when cells swim very close to a solid surface [14]and have observed that the rotational direction of the circles is also

clockwise. Examples of runs adjacent to the surface were observed in which there was not significant curvature in the cell path, however this behavior was not as common as the circling pattern. More examples of wild type cell traces can be found in Appendix F.

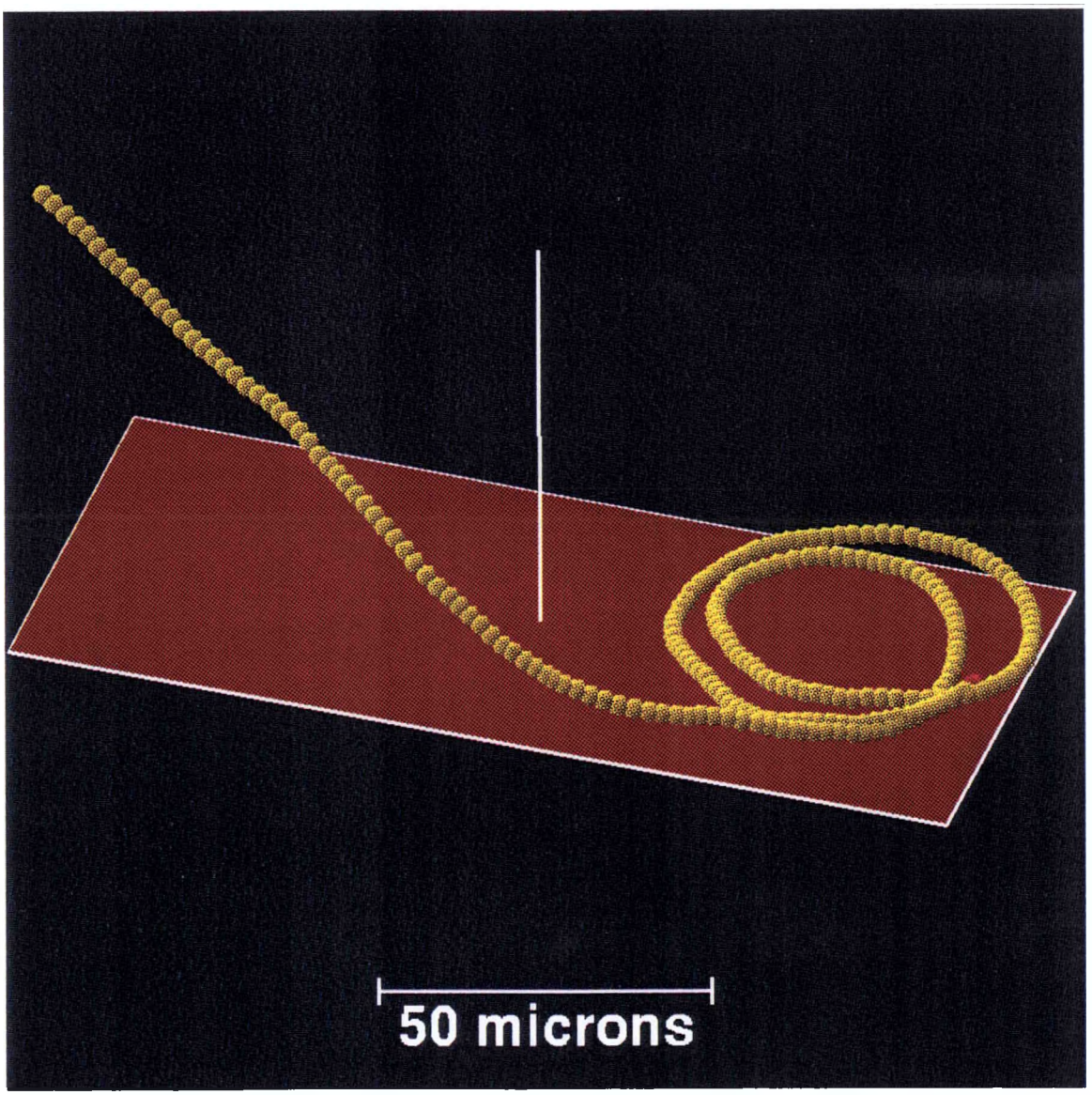

Figure 4.26: Wild type bacterial trace 3. Shown is a cell trace from a wild type cell tracked near the glass surface.

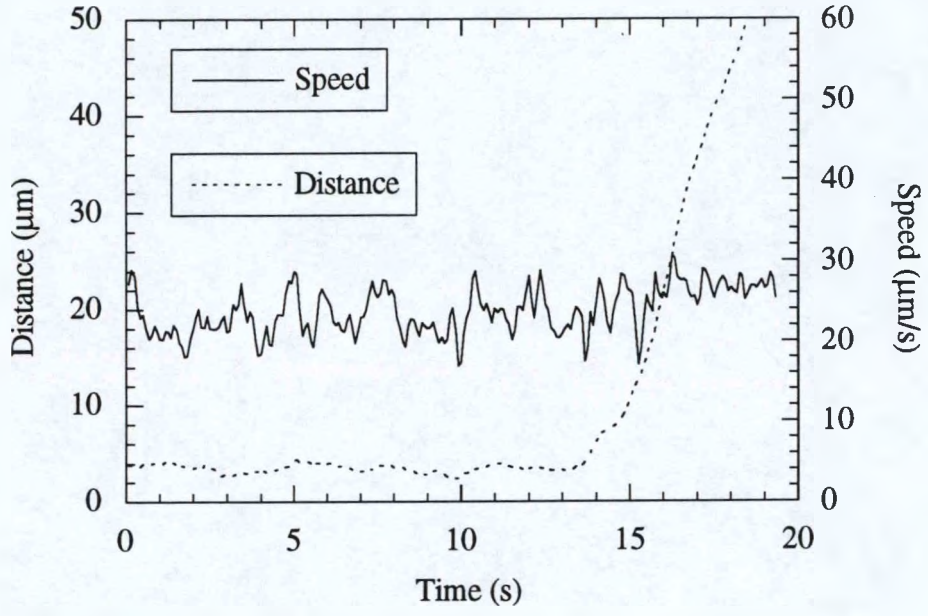

Figure 4.27: Distance and speed for wild type bacterium 3. Note that the data analysis algorithm identified this trail as a single continuous run.

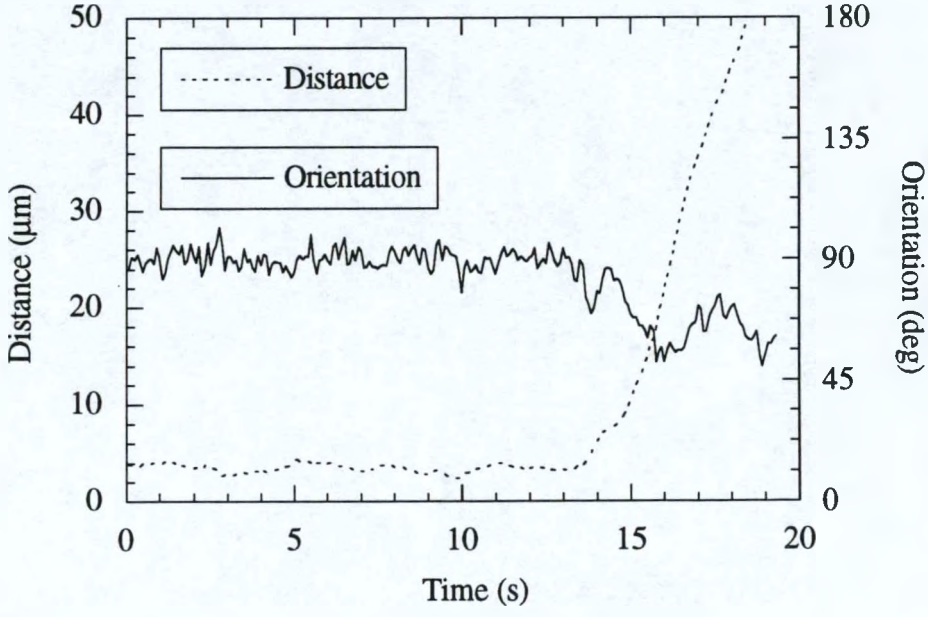

Figure 4.28: Distance and orientation for wild type bacterium 3.

4.4.3 Effect of the solid surface on the swimming speed

The individual cell traces shown previously were taken from several tracking experiments performed to collect data for wild type cells moving near a solid surface in a buffer solution containing 0.18% (w/v) Methocel. A total of 90 cells were tracked in these experiments. The tracking data were analyzed to determine if a dependence of the swimming speed on the surface-to-cell distance and cell orientation could be observed. If a swimming bacterium can be approximated as a sphere with a single flagellum rotating at a constant speed as in the theoretical work of [59], or as a sphere moving against a constant force as in Equation 4.11, then the work of Ramia *et al.* and Brenner suggest that hydrodynamic interactions would result in lower swimming speeds for cells moving toward a solid surface and within 10 μm of the surface.

The data were analyzed by dividing the fluid adjacent to the surface into four distance regions and four directional regions. The four distance regions were 0-10 μm, 10-20 μm, 20-30 μm, and >30 μm from the surface. The four orientation regions were defined relative to the normal to the glass surface and were 0°-45° (away from the surface), 45°-90°, 90°-135° and 135°-180° (toward the surface). The mean speed during running was generated for each bacterium that occupied each of the possible 16 regions of the distribution (four possible orientations and four possible cell-to-surface distances). The means for each bacterium were used to form the distributions. For example, a bacterium's trace was analyzed to determine the number of sample points and the swimming speed at each of these sample points for each of the 16 distance-orientation ranges (0-10 μm at 0°-45°, 10-20 μm at 0°-45°, etc.). The mean swimming speed for each of the 16 ranges for which samples existed were calculated by dividing the sum of the swimming speeds at each sample point by the number of samples in the distance-orientation range. The mean swimming speed for each bacterium in each region calculated in this way was used to form

the population distributions so that each bacterium was represented once in each range it occupied.

Figure 4.29 shows the dependence of the mean swimming speed on the cell orientation for each distance range. The orientations plotted are the midpoints of the four regions. For cells moving in the distance range 0-10 μm, the highest swimming speeds were recorded for cells moving in the two orientation ranges the most parallel to the solid surface, while the lowest mean swimming speed was recorded for cells moving between 135° and 180° from the surface normal (toward the surface) and within 10 μm of the surface.

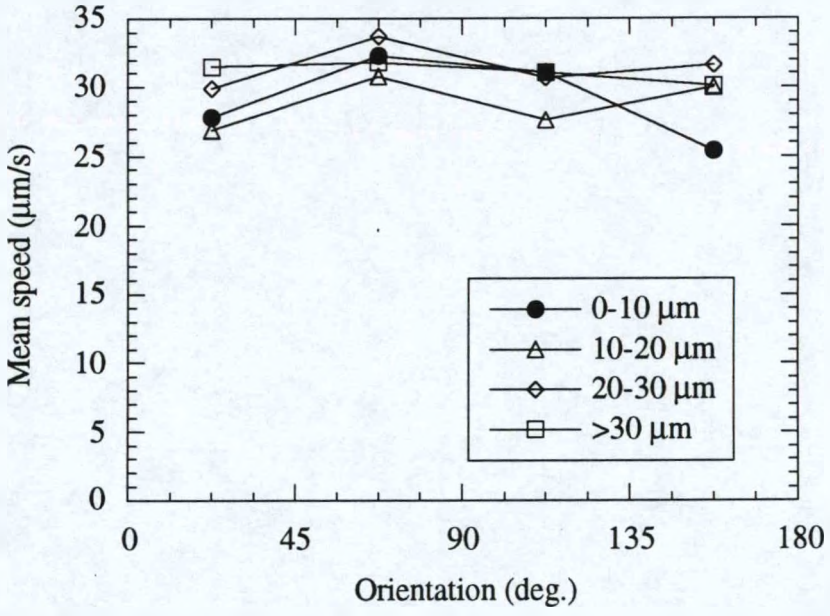

Figure 4.29: Mean swimming speed as a function of orientation. The four distance values plotted in the figure are the midpoints of the regions identified in the legend.

Figure 4.30 shows the same data plotted to show the variation of the swimming speed as a function of distance for each of the four orientation ranges. The distances plotted are the midpoints of the ranges and the range 30-∞ μm is omitted. In this figure, it is seen that bacteria swimming with directions in the 135°-180° orientation range

(swimming toward the surface) shows the greatest variation, with the mean swimming speed decreasing as the distance to the surface decreases.

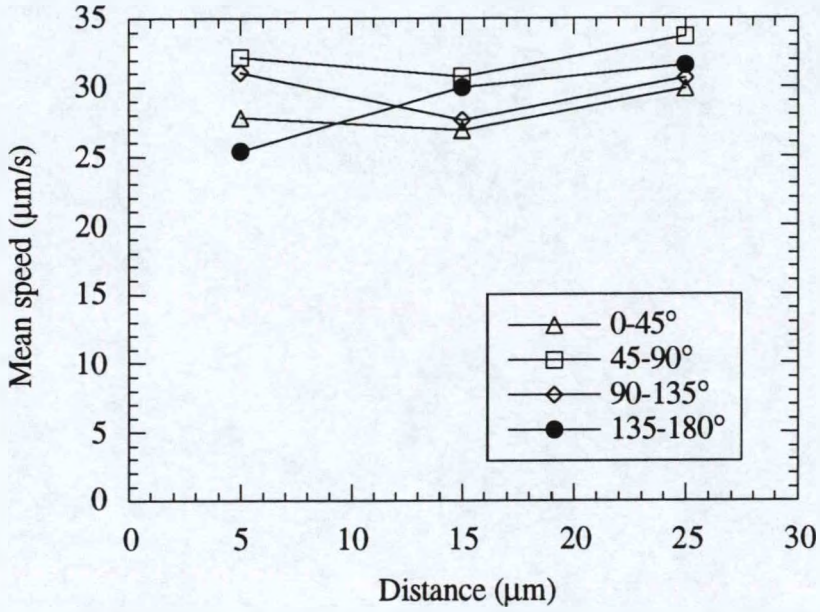

Figure 4.30: Mean swimming speed as a function of orientation. The data shown in Figure 4.29 is plotted as a function of distance. Data for distances greater than 30 μm is omitted.

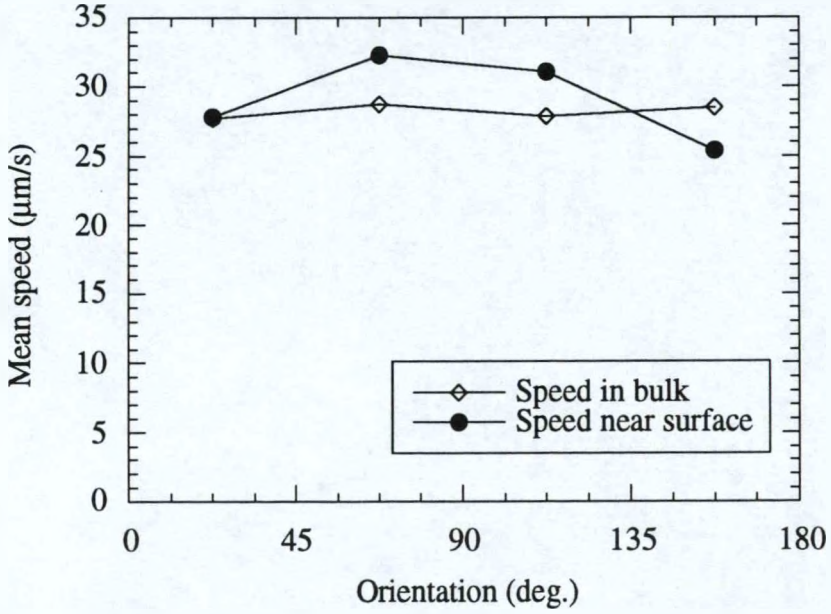

Figure 4.31: Mean swimming speed in bulk versus orientation. The data in the distance range 0-10 μm for the surface tracking experiments is also shown for comparison.

For comparison, the tracking data that generated the distributions shown in Figures 4.14, 4.15, and 4.16 was analyzed to show the variation of the mean swimming speed with the orientation angle for cell swimming very far from the surface (approximately 400 μm). The results of the analysis are shown in Figure 4.31 along with the data for 0-10 μm. As discussed in Section 4.3, the tracking chamber used for experiments in the bulk fluid did not have top windows printed with an array of dots for determining the plane of the surface. The surface plane for this data was determined by locating and recording the position of surface defects on the top window glass so the calibration to the surface in this case is only approximate but is included here to show that the mean swimming speed is relatively constant with respect to direction for cells moving far from the surface.

The data for the bacteria near the surface were also analyzed by considering the four orientation ranges and dividing the distance into two regions: 0-10 μm and >10 μm. The rationale for using these distance ranges is based on the dependence of the swimming speed on the separation distance in Equation 4.11 and illustrated in Figure 4.2, since the decrease in the speed of a sphere moving with constant propulsive force toward a plane wall is less than approximately 12% of the value in the bulk for surface-to-cell distances of greater than 10 times the radius of the sphere. The $100(1-\alpha)\%$ confidence interval on $(\mu_1 - \mu_2)$ (the difference in the population means for a given orientation) was calculated by [51]:

$$\text{conf. int.} = \left(\langle X_1 \rangle - \langle X_2 \rangle\right) \pm t_{\alpha/2}\sqrt{S_1^2 / n_1 + S_2^2 / n_2} \tag{4.18}$$

where $\langle X_1 \rangle$ and $\langle X_2 \rangle$ are the mean run speeds for the sample at >10 μm and <10 μm respectively, S_1 and S_2 are the associated variances, n_1 and n_2 are the number of samples, and $t_{\alpha/2}$ is the value of the Student t with $\alpha = 0.5$. Shown in Figure 4.32 are the 95% confidence intervals for this analysis. In this figure, μ_1 is the population mean for the distance range 10-∞ μm and μ_2 is the population mean for the 0-10 μm distance range.

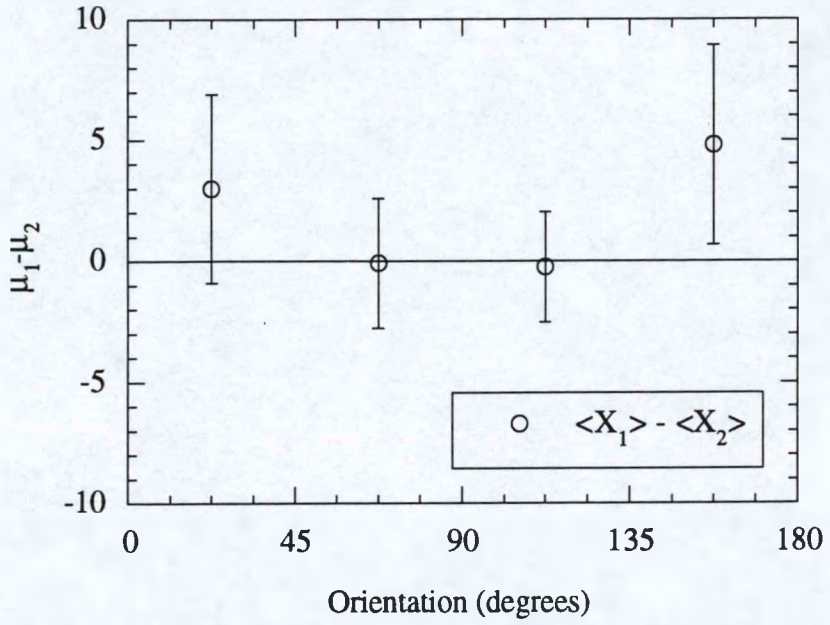

Figure 4.32: 95% confidence intervals on the difference in mean swimming speeds. The difference in the values of the mean swimming speeds are plotted with brackets to indicate the 95% confidence interval on the population parameter, $\mu_1 - \mu_2$.

This figure shows that one can assert with 95% confidence that for bacteria moving toward the solid surface at an orientation angle greater than 135° relative to the surface normal, the mean swimming speed for bacteria at less than 10 μm from the solid surface is significantly less than the mean swimming speed at greater than 10 μm from the surface. This assertion cannot be made for any of the other orientations since their confidence intervals bracket $(\mu_1 - \mu_2) = 0$.

4.4.4 Comparison of cell traces to solutions of theory for spheres: Wild type cells

As discussed in Section 4.2, Brenner [19] considered the hydrodynamic interactions between a solid plane surface and a spherical particle as the particle moved perpendicularly toward the surface. Ramia [59] considered the hydrodynamic interactions

between a spherical body with a flagellum and a plane surface for cells with different orientation angles to the surface normal. These two theoretical solutions suggest another manner in which the data can be analyzed. Individual cell traces could be isolated in which the cells swam nearly perpendicular to the solid surface and their speed could be analyzed as a function of the separation distance.

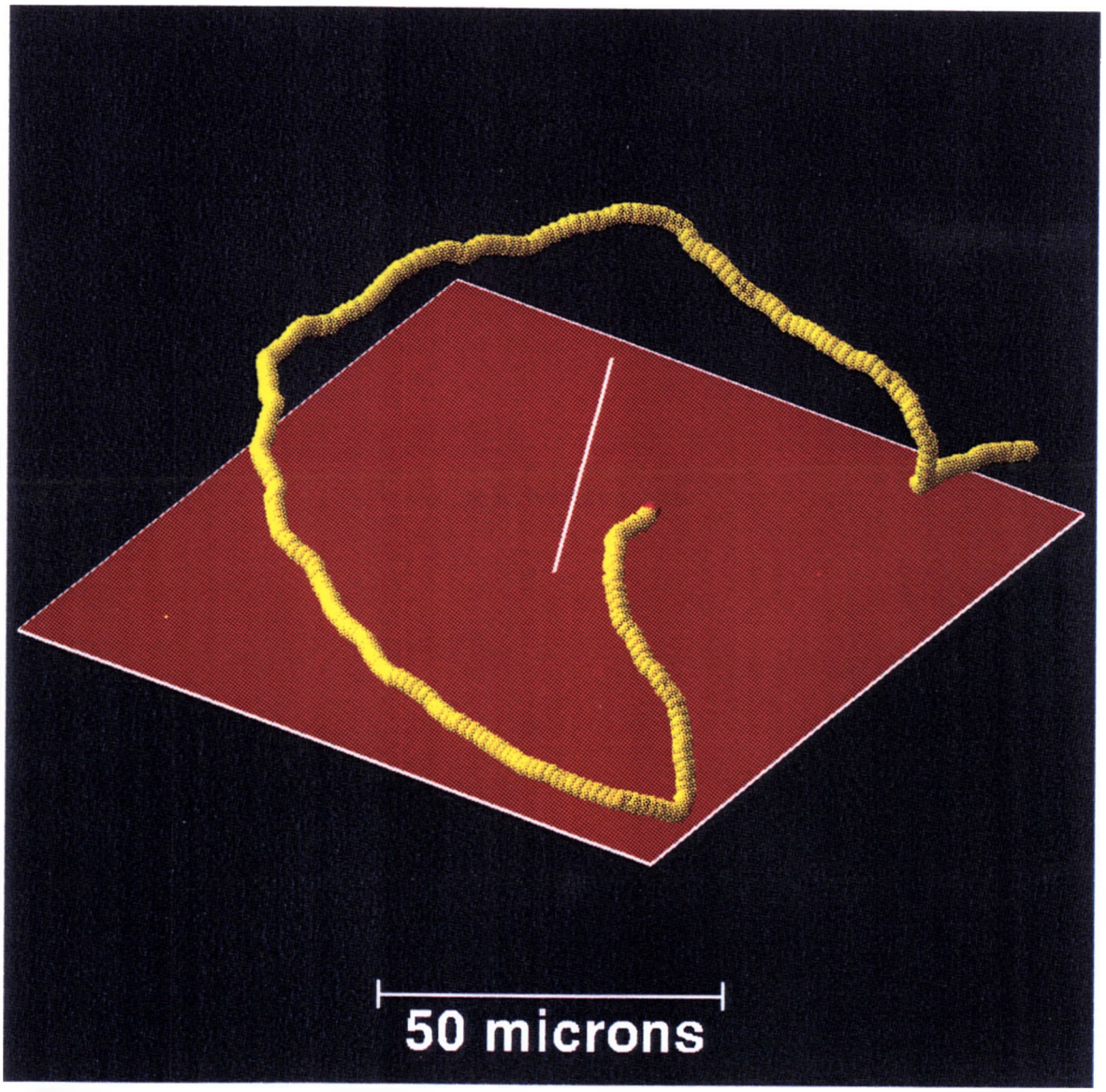

Figure 4.33: Wild type bacterial trace 4. This bacterium executes a single tumble, shown as a purple sphere at the lower center of the figure.

Figure 4.33 is the trace of a bacterium that was tracked while executing two long runs with one tumble. Tracking began with the cell moving toward the surface from about the center of the figure. At two points during the trace, the cell approaches the surface at an orientation angle between 135° and 180° as can be seen in Figure 4.34. Figures 4.35 and 4.36 show the experimentally measured speed as a function of the separation distance plotted along with the solutions of Ramia *et al.* [59] for approach angles of 135° and 180° and the solution of Equation 4.11 for the two portions of the trace where the cell approaches the surface at a large orientation angle.

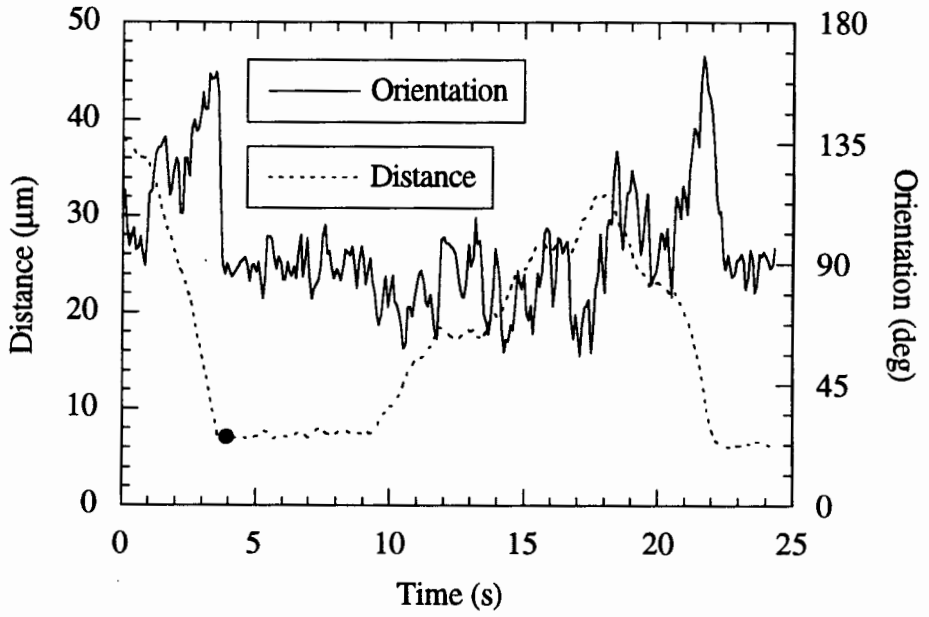

Figure 4.34: Distance and orientation for wild type bacterium 4. The single tumble is indicated by the solid dot at approximately 4 s. The bacterium can be seen to approach the surface at an orientation of between 135° and 180° at approximately 4 s and again at approximately 22 s.

The values of the distances plotted in this figure are the experimentally determined distances minus the closest approach distance of the bacterium shown in Figure 4.33. The closest approach distance was determined to be 6.8 μm by examining the data in Figure 4.37. It was felt that this was a more accurate representation of the true surface-to-

cell distance for the reasons previously discussed. In order to compare to the theoretical solutions, the experimentally measured speeds were normalized by dividing by the speed of the bacterium at the separation distance $(h-b)/b$ closest to 10.

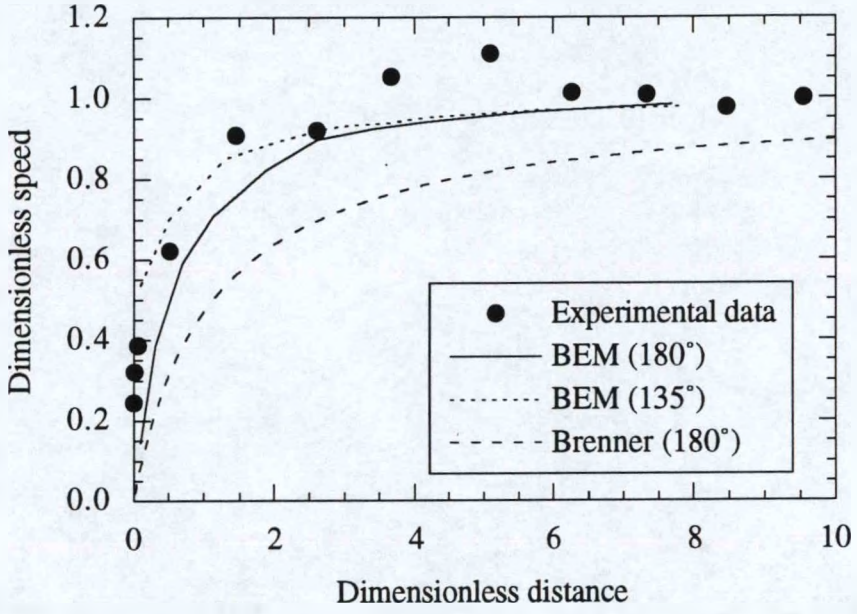

Figure 4.35: Speed versus separation distance for wild type bacterium 4, first run. The experimental data (•) is plotted with the BEM solutions of Ramia *et al.* at 180° and 135° and the solution of Equation 4.11. The dimensionless distance is $(h-b)/b$ where b is the radius of the cell body and h is the distance from the center of the cell to the surface. The dimensionless speed is the instantaneous speed divided by the speed in an unbounded fluid, U_∞. For the experimental data, the velocity closest to 10 μm was used as U_∞. The dimensionless distance for the experimental data was calculated assuming a representative cell radius of 1 μm.

Due to the variability in the bacterial swimming speed (see Figure 4.37), this normalization scheme resulted in some experimentally-determined dimensionless swimming speeds shown in Figures 4.35 and 4.36 that are greater than one. For the two cases shown, the BEM solution provides a better representation of the experimental data than the solution of Equation 4.11.

Figure 4.38 shows the trace of another wild-type cell that executed a run at a large orientation angle at a distance less than 10 μm from the surface. Figures 4.39 and 4.40

show the variation of the surface-to-cell distance, the speed and the orientation of the cell as a function of time.

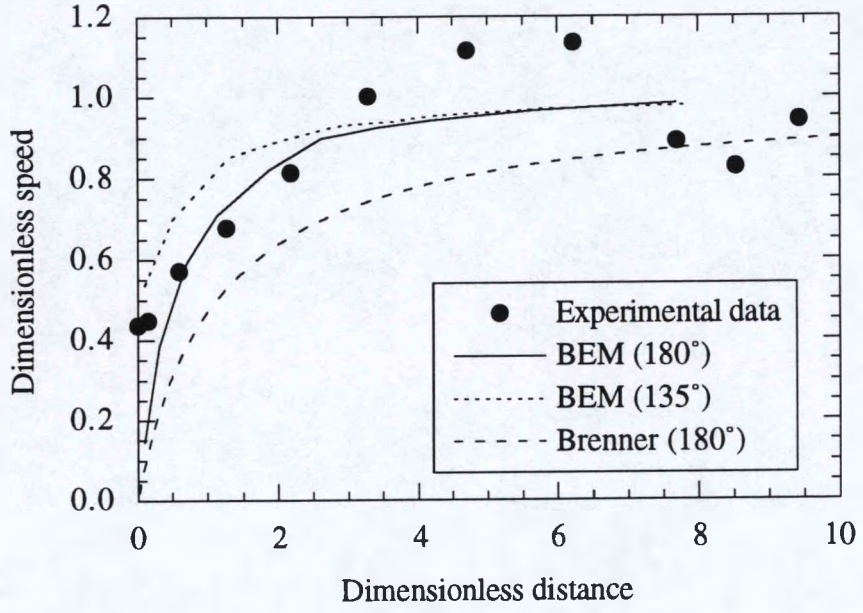

Figure 4.36: Speed versus separation distance for wild type bacterium 4, second run. The experimental data (•) is plotted with the BEM solutions of Ramia *et al.* and the solution of Equation 4.11.

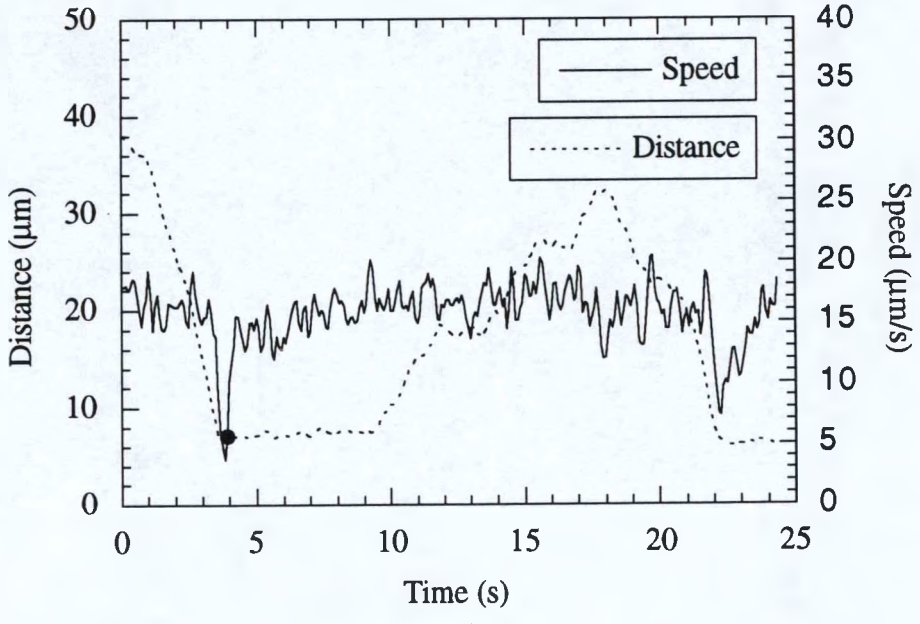

Figure 4.37: Distance and speed for wild type bacterium 4. The single tumble is indicated by the solid dot at approximately 4 s.

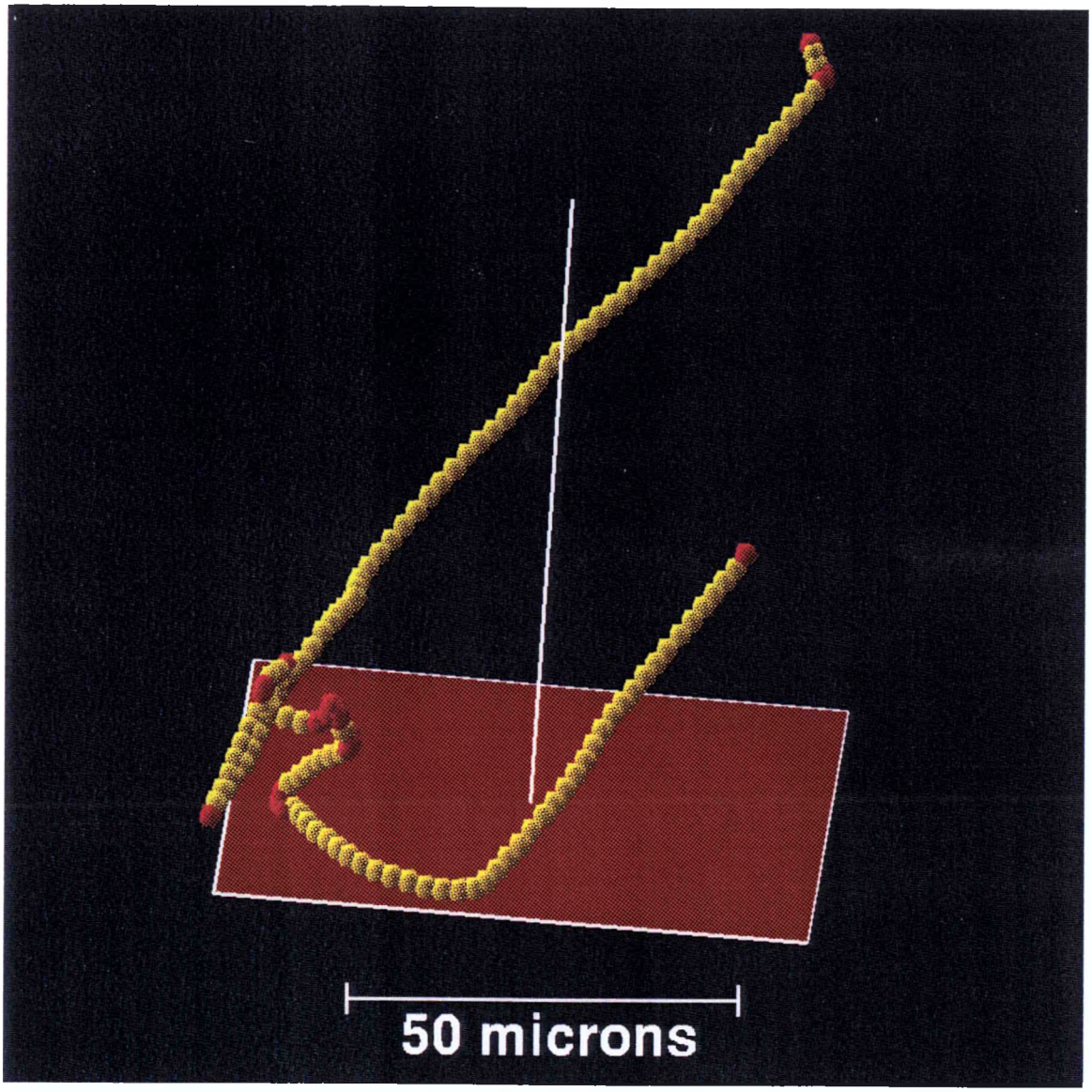

Figure 4.38: Wild type bacterial trace 5. Shown is the trace of a wild type bacterium moving near the surface. The circular portions of the cell's path occurred when the cell was closest to the glass surface.

Figure 4.41 compares the speed of the cell as it approaches the solid surface an average orientation angle of 135° to the BEM solution of Ramia *et al.*. As in the previous case, the surface-to-cell distance has been adjusted for error in the measurement by subtracting the closest approach distance. The experimental data agreeing most closely with the BEM solution for a cell orientation of 135°. In Figure 4.40, the orientation of the cell as it swam toward the surface (near 2 s) was approximately 135°.

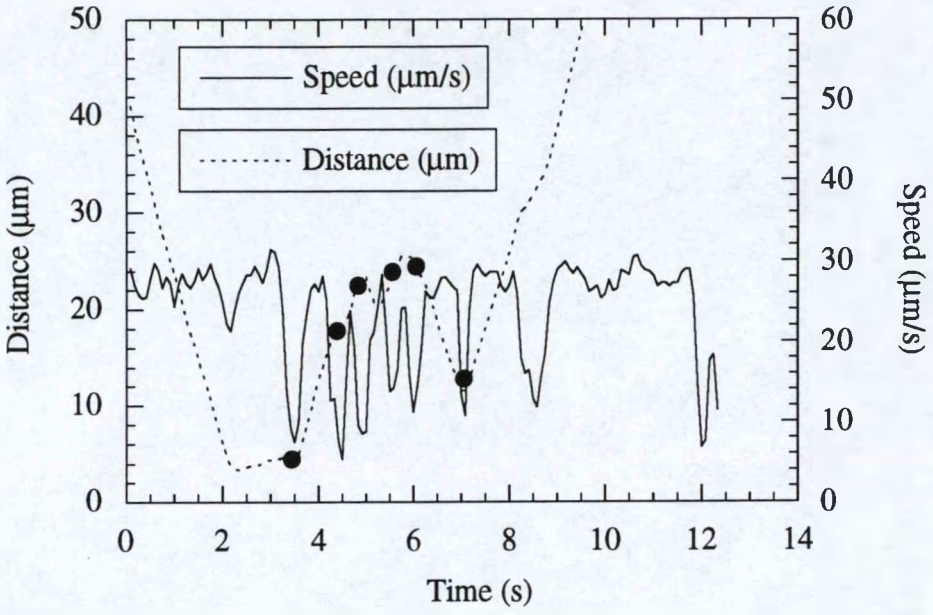

Figure 4.39: Distance and speed for wild type bacterium 5.

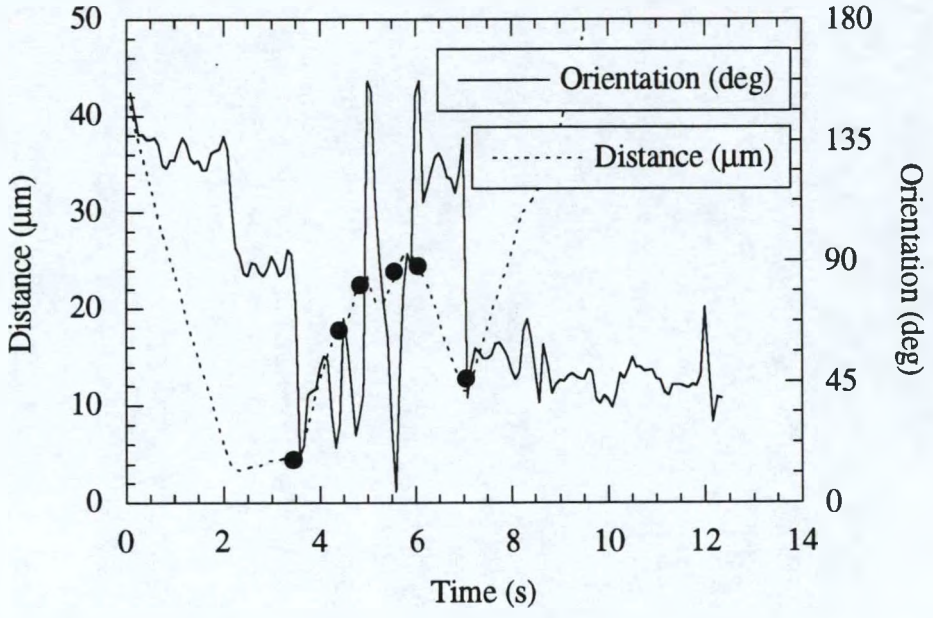

Figure 4.40: Distance and orientation for wild type bacterium 5.

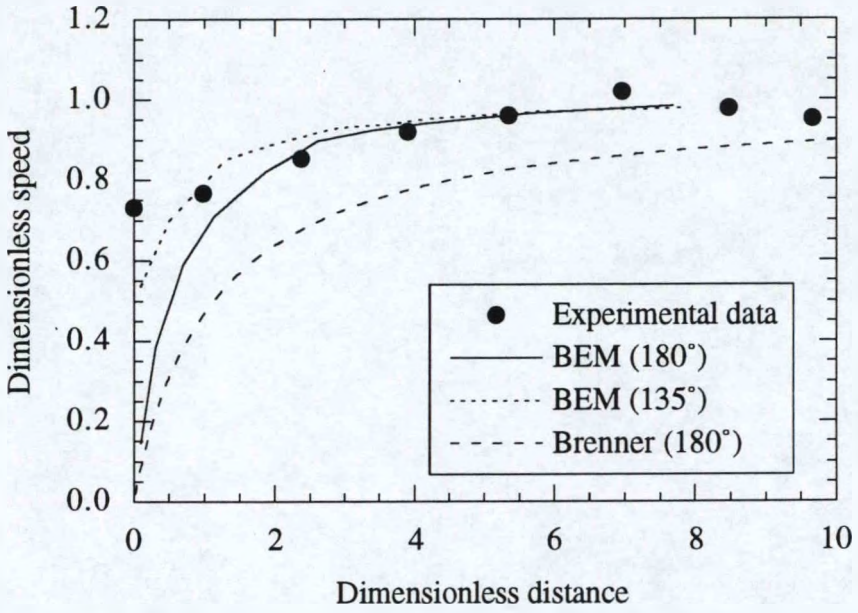

Figure 4.41: Speed versus separation distance for wild type bacterium 5. The experimental data is plotted for the region in Figure 4.39 just prior to 2 s.

4.4.5 Comparison of experimental data to solutions of theories for spheres: Smooth swimming cells

One complicating factor in these comparisons is the tumbling behavior of the bacteria. The initial run toward the surface in the trace shown in Figure 4.33 terminates in a tumble near the surface. Since bacterial swimming speeds slow as the bacterium enters a tumble, it cannot be determined if the reduction in swimming speed as the separation distance decreases is a result of hydrodynamic interactions between the cell and the surface or if it is because the cell is about to execute a tumble. It is difficult to determine how the cell becomes aligned with the surface: by striking the surface or by turning until its path is aligned with the surface. If the cell strikes the surface and begins swimming parallel to it, then the analysis would record the action as a tumble. For the bacterial trace shown in Figure 4.33 the cell appears to undergo a tumble the first time it reaches the surface, as seen in Figure 4.37 near 4 s.

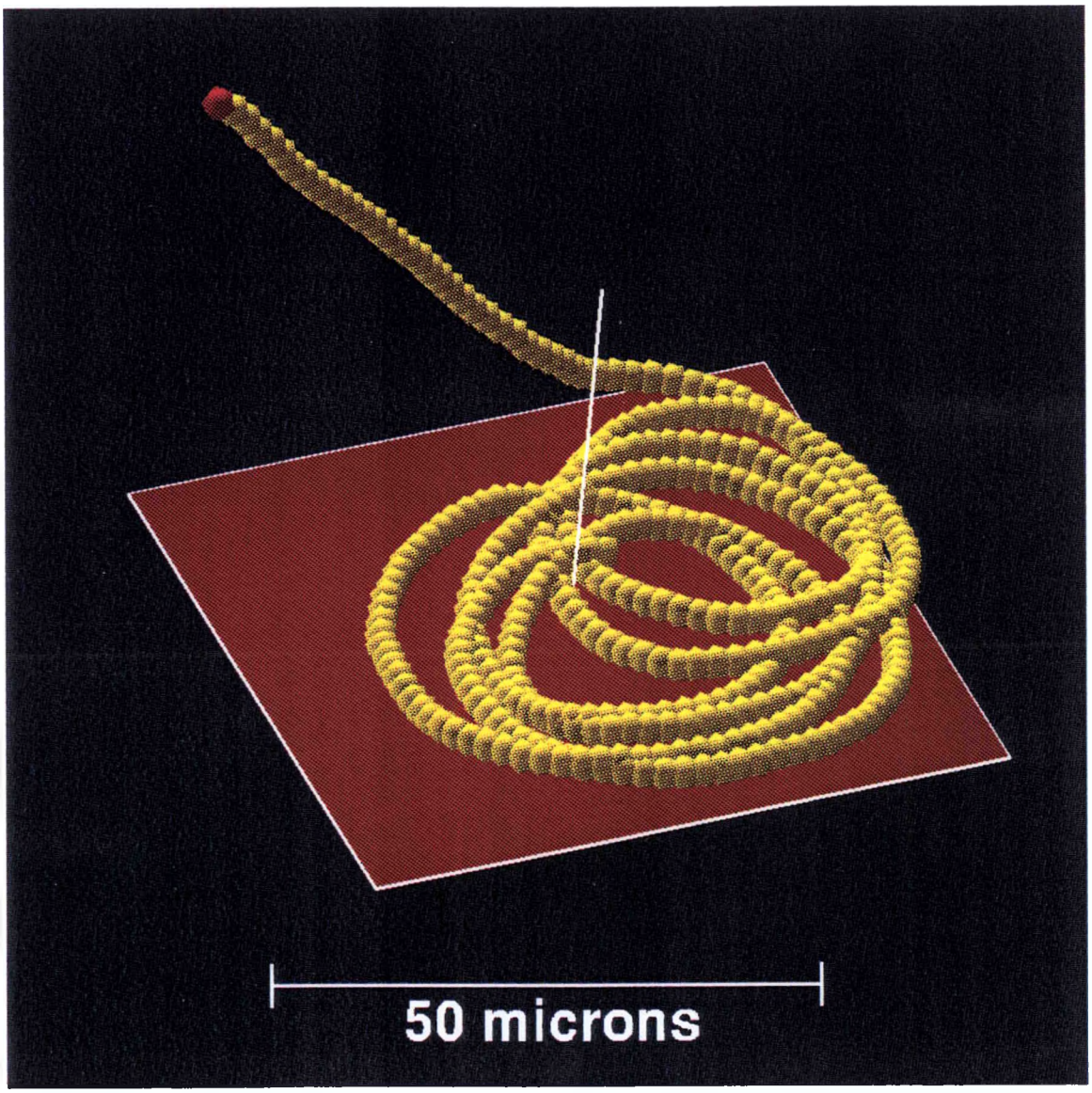

Figures 4.42: Smooth swimming bacterial trace 1, view 1. The smooth swimming bacteria have a deletion in the gene responsible for the tumbling behavior in *E. coli.* As expected, the data analysis does not predict tumbles in the traces of these bacteria.

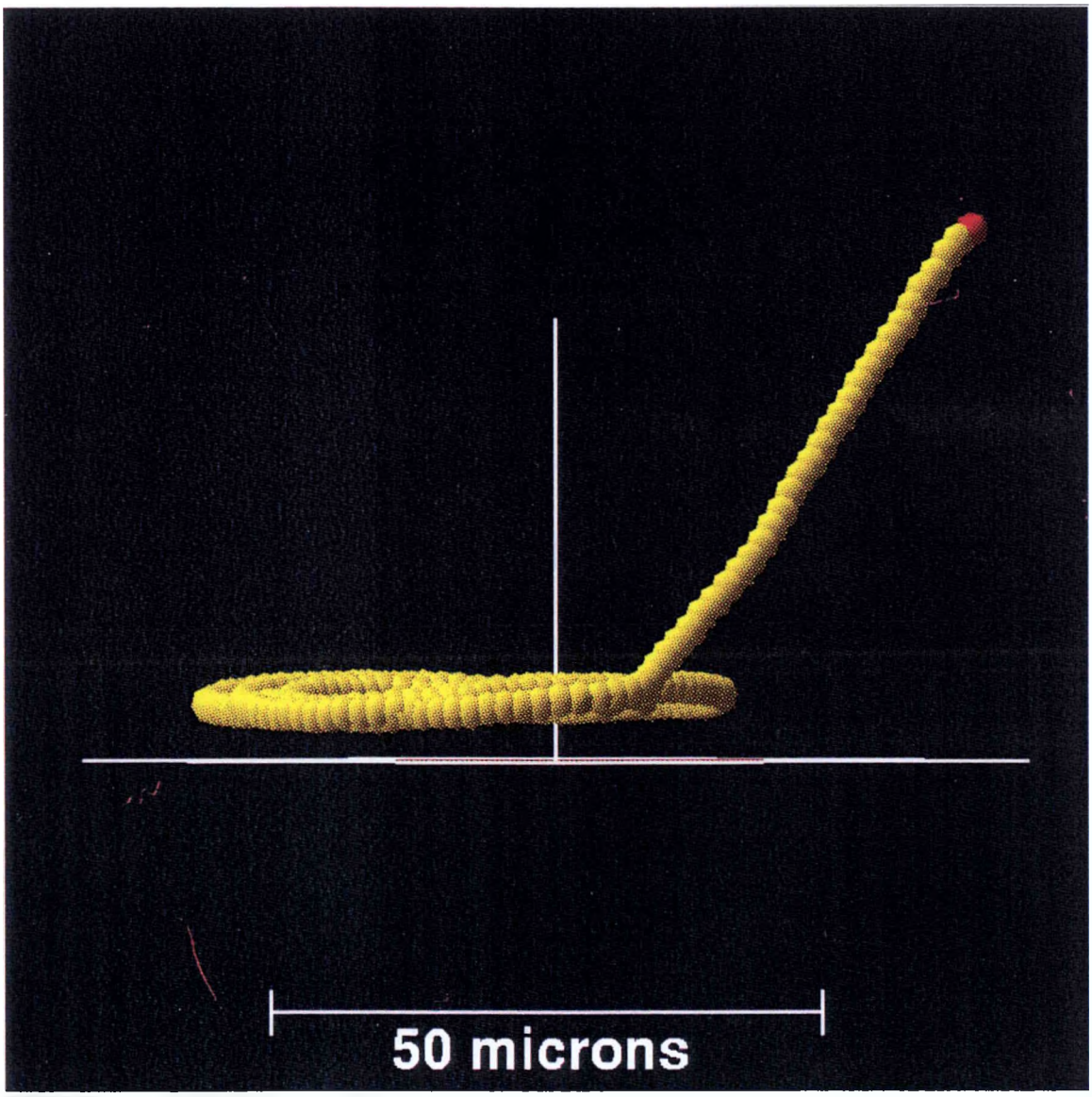

Figure 4.43: Smooth swimming bacterial trace 1, view 2. The bacterium whose trace is shown here is the same as that shown in Figure 4.42. The drift in the distance measurement causes error in the distance measurement which makes the bacteria in this trace appear to be a significant distance above the surface. Since it was observed that the calibration dots were in clear focus while bacteria were circling on the surface, the actual surface-to-cell distance for cells moving along the surface was less than 2 μm as discussed in the text.

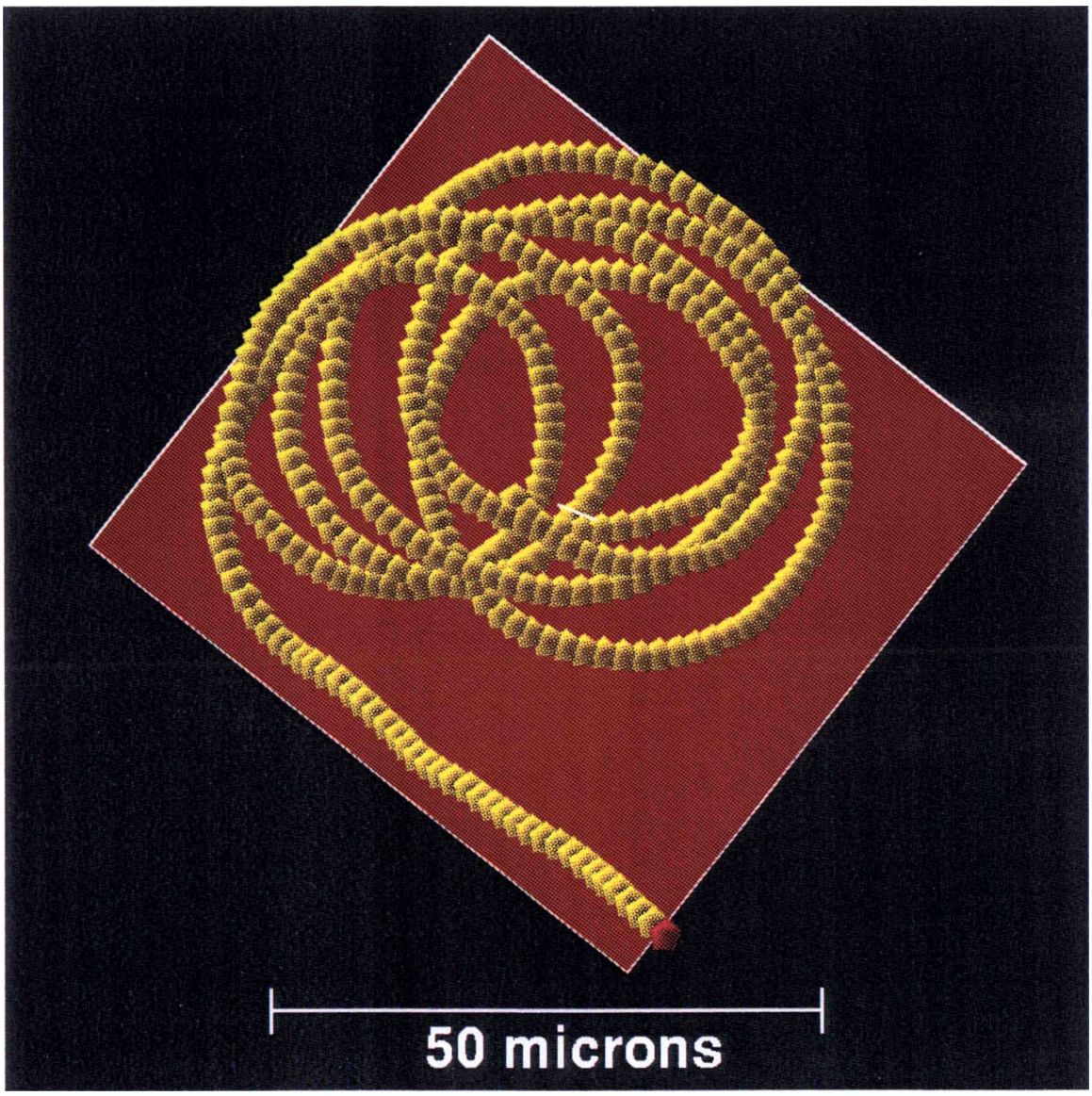

Figure 4.44: Smooth swimming bacterial trace 1, view 3. The same trace as in Figures 4.42 and 4.43 is shown, viewed from the along the normal. The nearly perfect circles that bacteria often make when swimming along a solid surface can be seen plainly here.

However, the second time the cell approaches the surface (near 22 s), the cell does not tumble when it reaches the surface. Another illustration of this behavior can be seen in Figure 4.39 near 2 s for the cell shown in Figure 4.38.

For these reasons, experiments were performed using the smooth swimming mutant bacteria HCB437. For these experiments, the region approximately 100 μm above the surface was scanned with the tracking microscope to attempt to track cells that were swimming toward the glass surface. Since the cells are long and cylindrical, cells moving toward the surface appear foreshortened. Figures 4.42, 4.43, and 4.44 show three different views of the trace of a smooth swimming bacterium. Figure 4.43 shows the trace on edge.

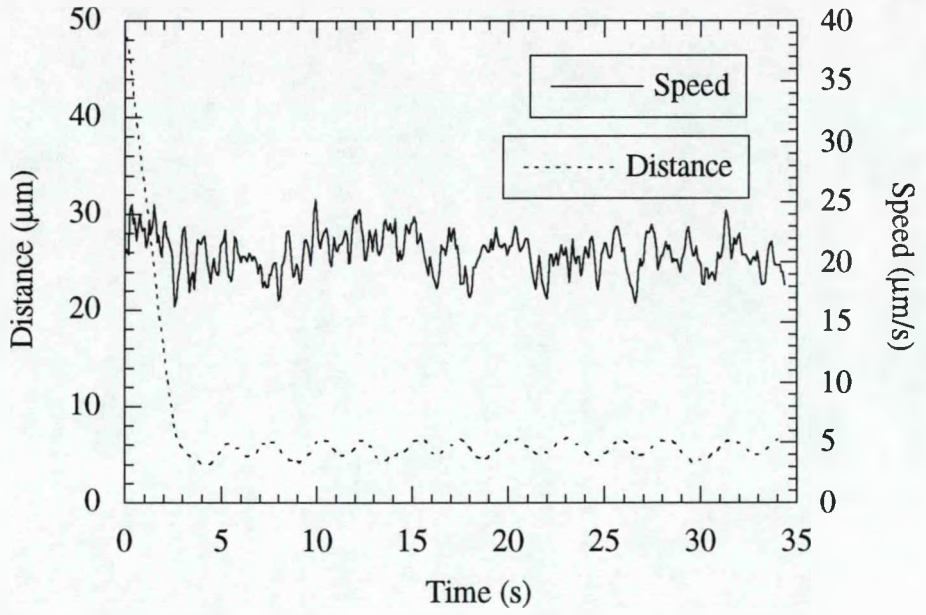

Figure 4.45: Distance and speed for smooth swimming bacterium 1. The line indicating the distance to the surface oscillates between 5 s and 35 s, when the bacterium was observed to move along the surface in circles. The oscillations in the surface distance are the result of a nonuniform surface calibration. As the cell circles in this figure, its surface-to-cell distance appears to oscillate between approximately 4 and 5 μm.

The trace appears to be a significant distance above the surface due to the error in the surface-to-cell distance caused by the drift in the measurement as discussed previously. For cells circling in this manner, it was always observed that the array of calibration dots on the glass surface were in clear focus, indicating that the actual cell to surface distance was less than 2 μm. Figure 4.44 shows the trace from above. This illustrates the nearly perfect 30-50 μm diameter circles that the cell forms as it moves on the surface. The surface-to-cell distance, speed, and orientation of the bacterium are shown as a function of time in Figures 4.45 and 4.46.

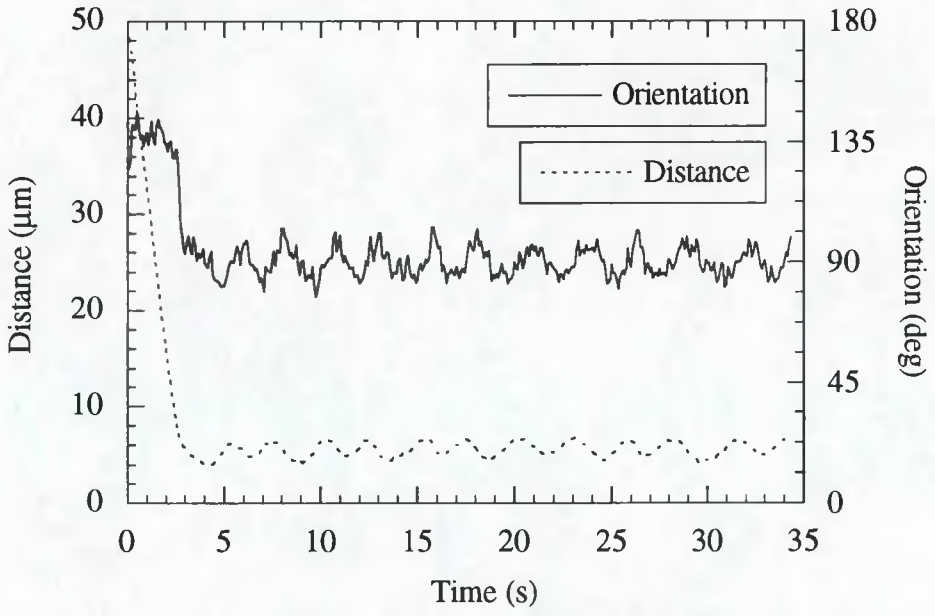

Figure 4.46: Distance and orientation for smooth swimming bacterium 1. The bacterium begins to swim toward the surface at approximately 135°.

Notice that in Figure 4.45, the swimming speed is more constant than for the wild type (non-mutant) cells, although there is still a significant amount of variation (from 16 μm/s to 25 μm/s). The speed is plotted as a function of the separation distance in Figure 4.47 for the initial surface-oriented portion of the run. The experimentally-determined bacterial swimming speed begins to drop more quickly and does not reach as low a value as the BEM solution.

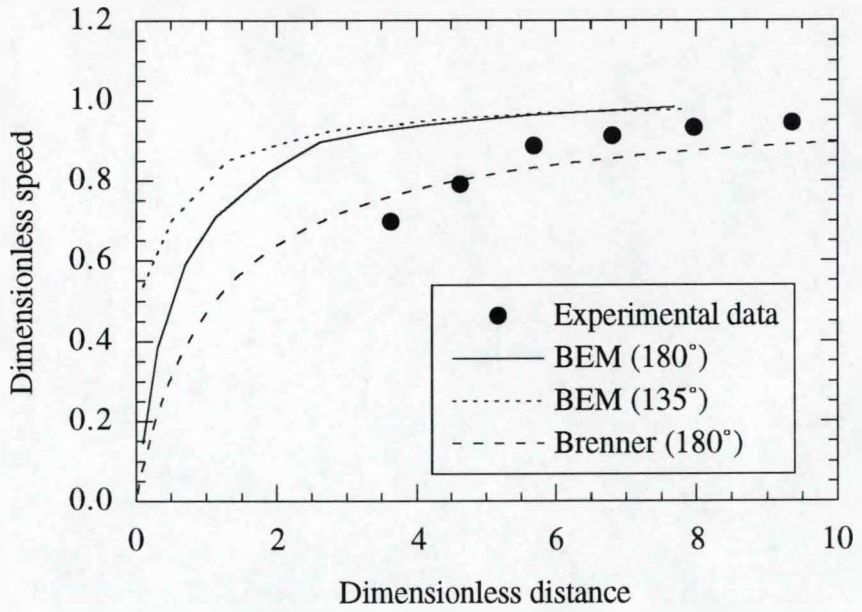

Figure 4.47: Speed versus distance for smooth swimming bacterium 1.

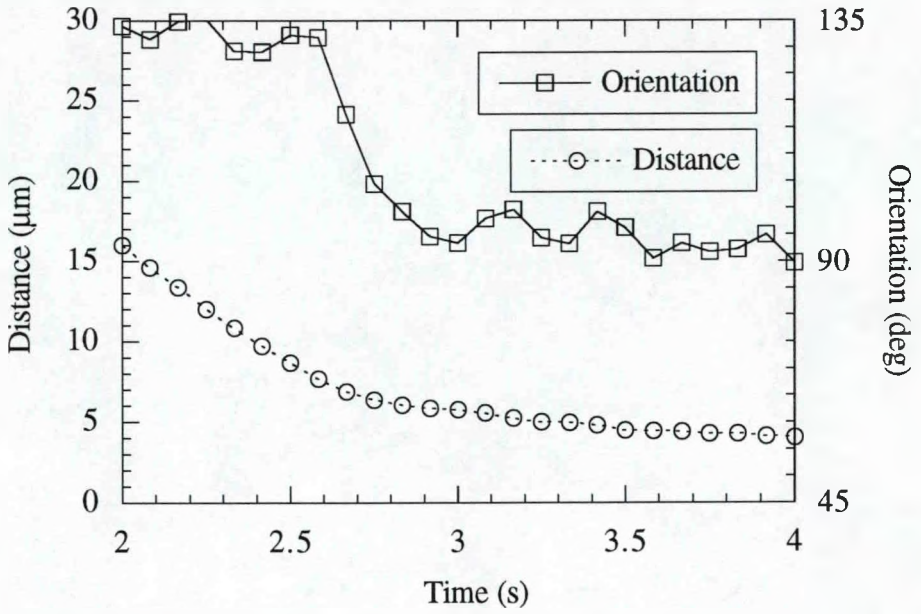

Figure 4.48: Close-up of orientation for smooth swimming bacterium 1. Here, data for each sample point is shown as a circle (on the distance curve) or as a square (on the orientation curve).

The experimental swimming speed in the figure is only shown while it decreased. For closer separations, the swimming speed begins to increase back to its value away from

the surface. The reason for this can be seen by examining Figures 4.42 and 4.43 and also in Figure 4.48. As the cell approaches the solid surface, it begins to turn away from the surface as evidenced by the decrease in its orientation angle between 2.5 s and 3.0 s in Figure 4.48. The cell turns gradually until it is parallel to the solid surface and as it turns, the hydrodynamic force due to the interaction between the cell and the surface decreases and the swimming speed increases. The experimentally determined velocity also begins to decrease further from the solid surface than the BEM solution predicts. A possible cause for this is the length of the smooth swimming cells of approximately 4 μm. The exact position on the cell body that the microscope is tracking is not known and probably shifts along the length of the cell. If the microscope is tracking at the back end of the cell as the forward end nears the surface, then the cell will appear to decrease its swimming speed while the point tracked is up to 4 μm further away from the surface than the end of the cell closest to the solid surface.

Figure 4.49 is the trace of another smooth swimming cell for which tracking began as the cell moved toward the surface. As in the previous case, the cell begins swimming in circles adjacent to the glass surface. The surface-to-cell distance and the orientation angle as a function of time for this cell are shown in Figure 4.50. Figure 4.51 shows the velocity as a function of the separation distance as the cell approaches the surface. The agreement between the experimental data and the BEM method is very good.

Figure 4.52 shows the cell trace for a bacterium that approaches the surface nearly perpendicularly, turns until parallel to the surface and then executes a straight run across the surface. Although curved runs are the most frequently observed, some bacteria move in nearly straight paths across the glass surface. The speed and surface-to-cell distance is plotted as a function of time in Figure 4.53. Figure 4.52 shows the cell trace for a bacterium that approaches the surface nearly perpendicularly, turns until parallel to the surface and then executes a straight run across the surface. Although curved runs are the most frequently observed, some bacteria move in nearly straight paths across the glass

surface. The speed and surface-to-cell distance is plotted as a function of time in Figure 4.53.

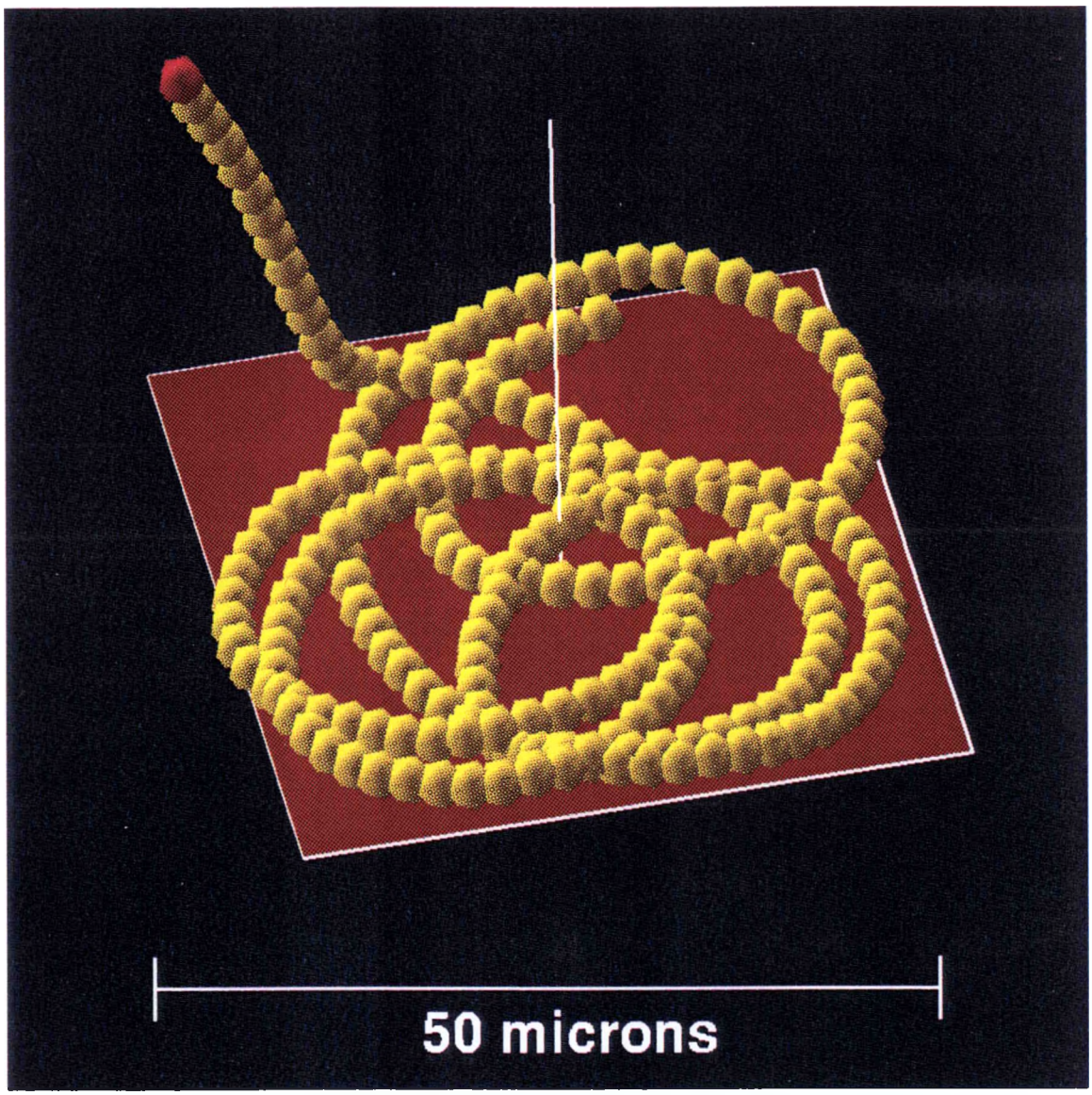

Figure 4.49: Smooth swimming bacterial trace 2. Tracking began for the bacterium whose trace is shown here at approximately 35 μm from the surface. The bacterium approached the surface and then began swimming in circles on the surface.

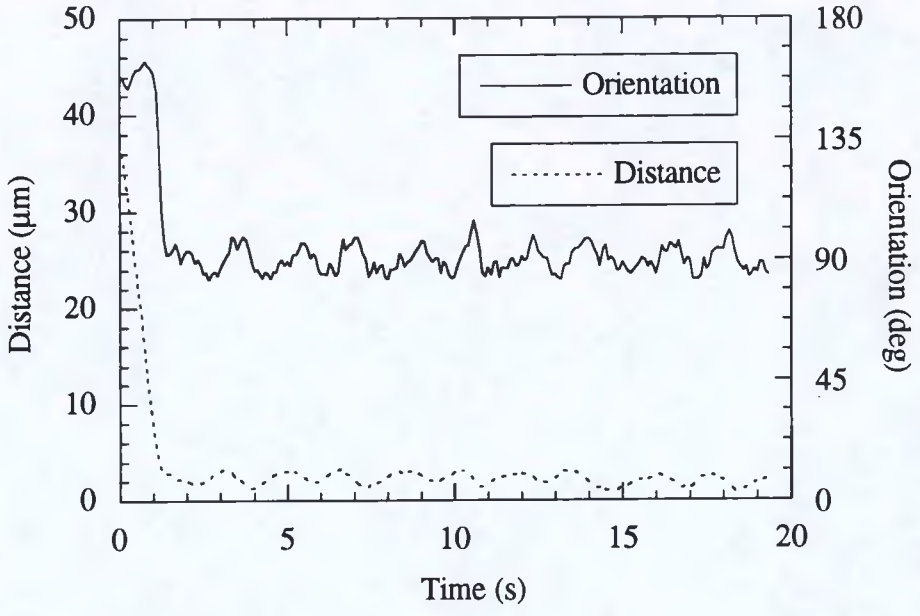

Figure 4.50: Speed versus orientation for smooth swimming bacterium 2.

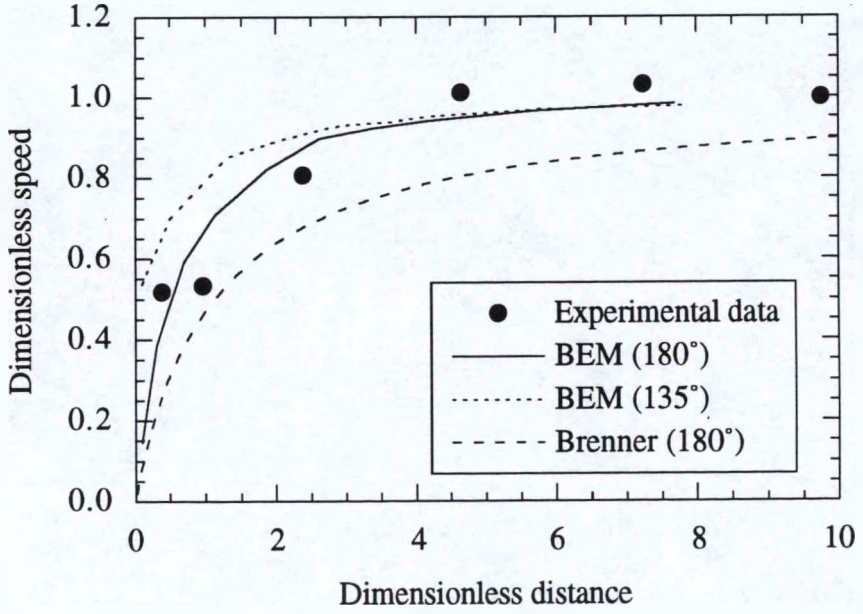

Figure 4.51: Speed versus distance for smooth swimming bacterium 2.

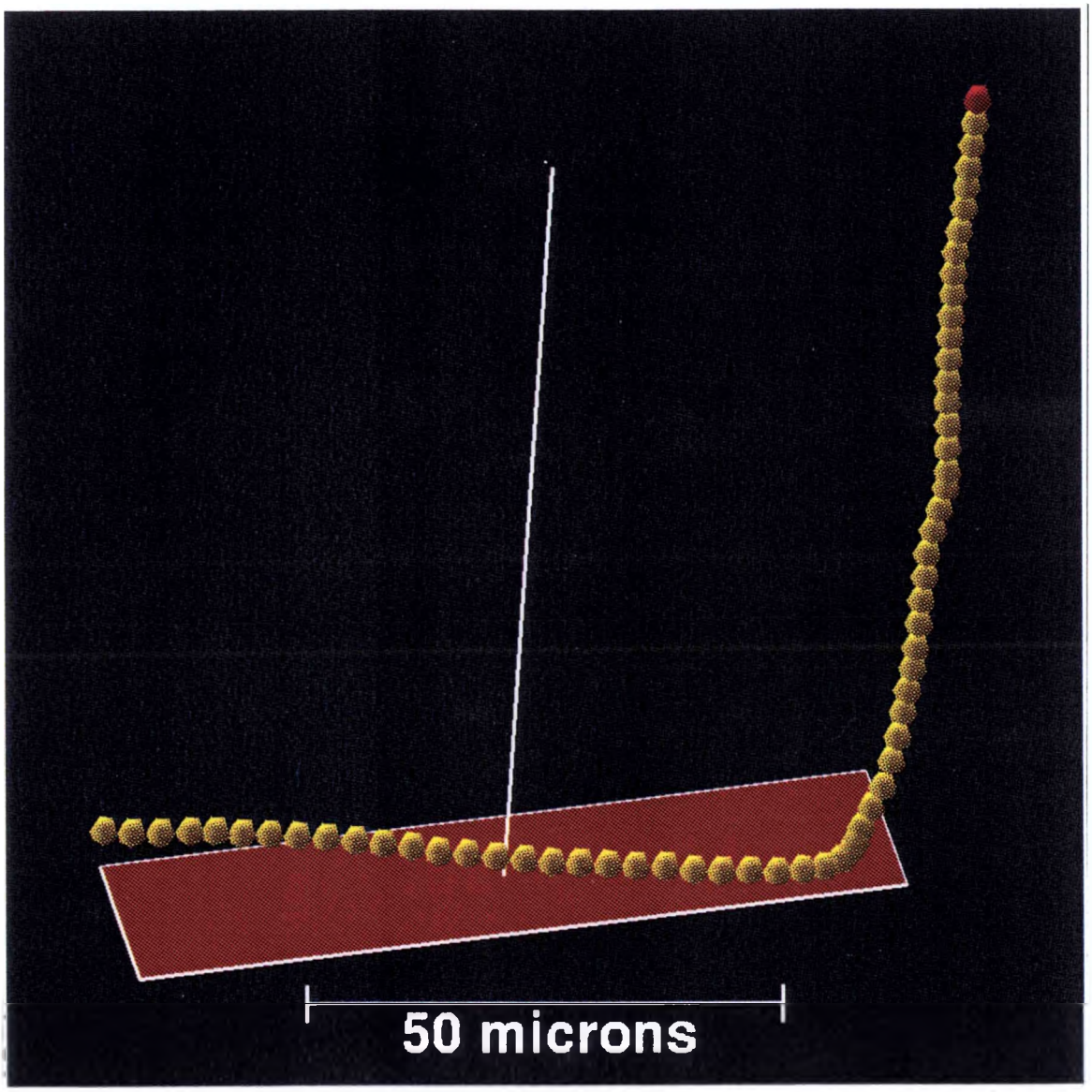

Figure 4.52: Smooth swimming bacterial trace 3. The bacterium whose trace is shown here, approached the surface and began swimming along it, without showing significant curvature in its path. Essentially straight bacterial paths across the surface were observed, although not as frequently as circular paths.

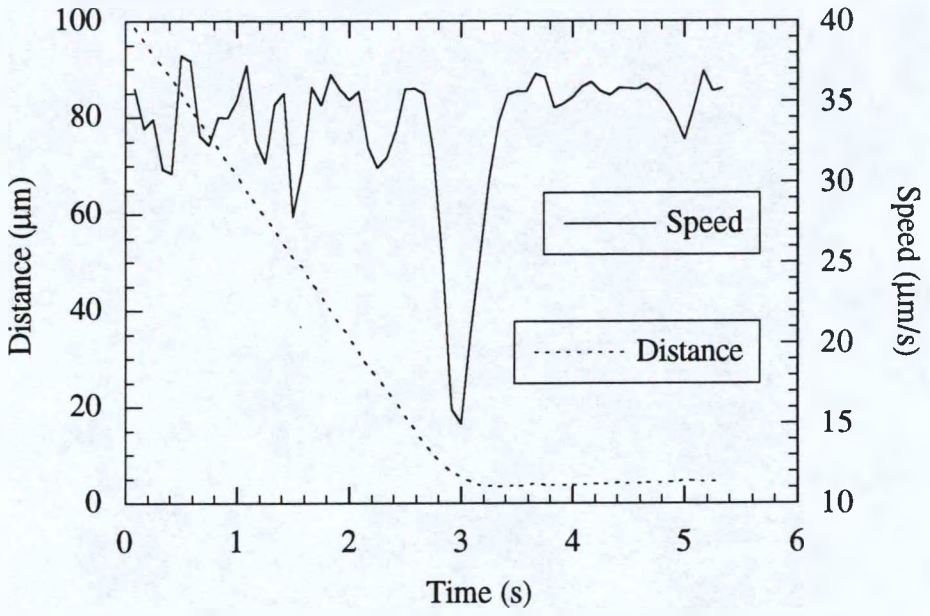

Figure 4.53: Distance and speed for smooth swimming bacterium 3.

The mean swimming speed for the data shown in Figure 4.53 is slightly higher while the bacterium is swimming adjacent to the surface (35.4 μm/s) than in the bulk (33.9 μm/s). For most of the bacterial traces that had significant runs both on the surface and in the bulk fluid, it was observed that the mean run speed near the surface was either essentially the same as the bulk value or slightly higher that the bulk value.

Figure 4.54 compares the BEM solution to the experimental data for this bacterium. As in Figure 4.47, the speed decreases more quickly in the experimental data than in the BEM solution, likely a result of the variation of the exact position of tracking along the cell body as discussed previously. Similar to the bacteria shown in Figure 4.43, the cell begins to turn away from the surface as it gets near and then runs parallel to the surface.

Four more traces from tracking experiments performed on smooth swimming bacteria are found in Appendix F. They exhibit the same features as those shown here. Perpendicular runs near the surface show a decrease in the cell swimming speed as the cell

nears the surface. Cells turn out parallel to the surface as they approach it. They frequently move in a circular path when swimming adjacent to a solid surface, but do not always do so.

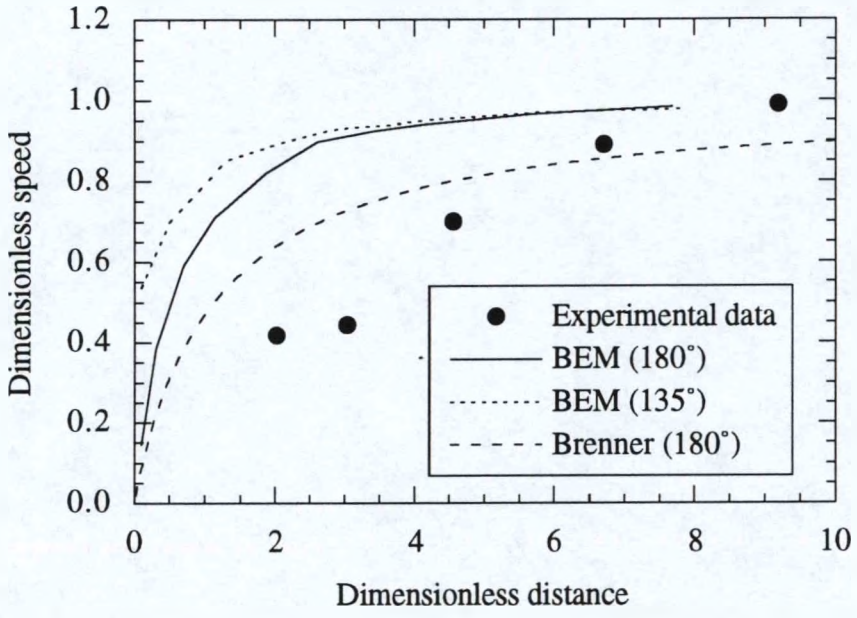

Figure 4.54: Speed versus distance for smooth swimming bacterium 3.

4.5 Discussion

Both the statistical data collected by tracking 100 individual bacteria moving near a solid surface and the analysis of the swimming speed of individual bacteria approaching a solid surface indicate that for distances less than 10 μm and orientation angles between 135° and 180°, the swimming speed is significantly less than at distances greater than 10 μm or for orientation angles less than 135°. The experimental data for the change in swimming speed as a function of the separation distance agrees well with the solutions of Ramia *et al.* using the BEM method and the solution of Equation 4.11. Comparison of bacterial swimming speeds adjacent to the surface to speeds in the bulk for individual cells shows that mean swimming speeds adjacent to the surface are equal to or slightly higher

than swimming speeds in the bulk. This phenomenon has been shown to be a result of an increase in flagellar propulsive advantage above increases in the translational and rotational drag on the cell body [59]. Similar effects have been observed theoretically in the study of multiple particles sedimenting close to each other [77] and the study of two organisms swimming close to each other [59]. Bodies moving near each other in a viscous medium exhibit a translational speed above that observed in isolation.

Ramia *et al.* give an excellent explanation of the circling behavior of bacteria when swimming along a surface based on the hydrodynamics of the rotating flagella. They were able to show that when the model bacterium used in their study is started out initially parallel to a solid surface, asymmetry in the dependence of the thrust direction of the flagellum on the angle of rotation results in a net force parallel to the surface, but perpendicular to the body axis of the cell. All of these observations indicate that the change in the swimming speed for bacteria moving toward a solid surface at distances of between approximately 2 and 10 μm or for cells moving adjacent to the solid surface can be predicted by models that assume the interaction between the surface and bacterium is principally hydrodynamic.

However, two characteristics of bacterial motion are not predicted by models that consider only hydrodynamic interactions. Firstly, cells approaching the solid surface in this study at orientation angles between 135° and 180° do not "crash" into the surface as was predicted by the model of Ramia *et al.*, but change their orientation and begin to turn parallel to the surface at a distance of 2-4 μm from the surface as seen in Figure 4.48. (Subtracting the closest-approach distance of 4 μm from the distances in this figure, it can be seen that the distance to the surface when the orientation begins to drop from 135° at about 2.5 s is approximately 4 μm). Secondly, cells remain adjacent to the surface for relatively long periods of time, frequently executing tumbles and then continuing to move along the surface.

Examination of the interaction potentials calculated from the DLVO theory of colloid stability offers an explanation of the tendency of cells to remain adjacent to the surface. Shown in Figure 4.55 is the DLVO interaction potential, given by Equation 4.1, between the wild type cells and the glass surface in the buffer solution used in the tracking experiments. The experimentally determined zeta potentials found in Table 4.1 were used in the calculation.

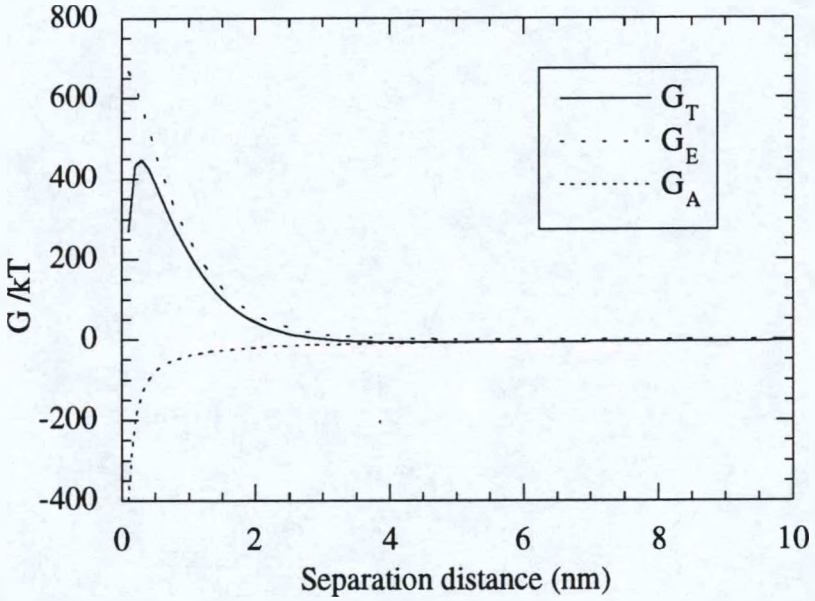

Figure 4.55: DLVO interaction potential as a function of separation distance. The potentials shown are those for van der Waals interaction G_A, electrostatic interaction G_E, and the sum of the two, G_T. for the wild type bacteria and glass in the phosphate buffer solution of ionic strength 0.19 M. The interaction potentials are normalized by k_BT.

The value of the Hamaker constant was taken as 1×10^{-21} J [61] and the particle radius was taken to be 1 μm. The relative permittivity of the medium was taken as 78.3. Figure 4.56 shows a close-up of the region near the origin. A secondary minimum exists in the interaction potential at approximately 4.5 nm from the surface and has a depth of approximately $7\,k_BT$. For comparison, using a bacterium mass of 4×10^{-13} g and a swimming speed of 50 μm/s at 30° C, the kinetic energy of a bacterium due to its swimming is only 1.05 x 10^{-4} k_BT. Its kinetic energy as a result of thermal motion is

$1.5\,k_BT$ [75]. Reversible bacterial adsorption in the secondary minimum would explain the tendency of cells to swim close and parallel to the solid surface. Another feature of the potential curve is the substantial energy barrier to the primary minimum, with a height of about $450\,k_BT$ at a distance of 1/2 nm. This barrier would prevent adsorption in the primary minimum and repel cells that get very close to the surface.

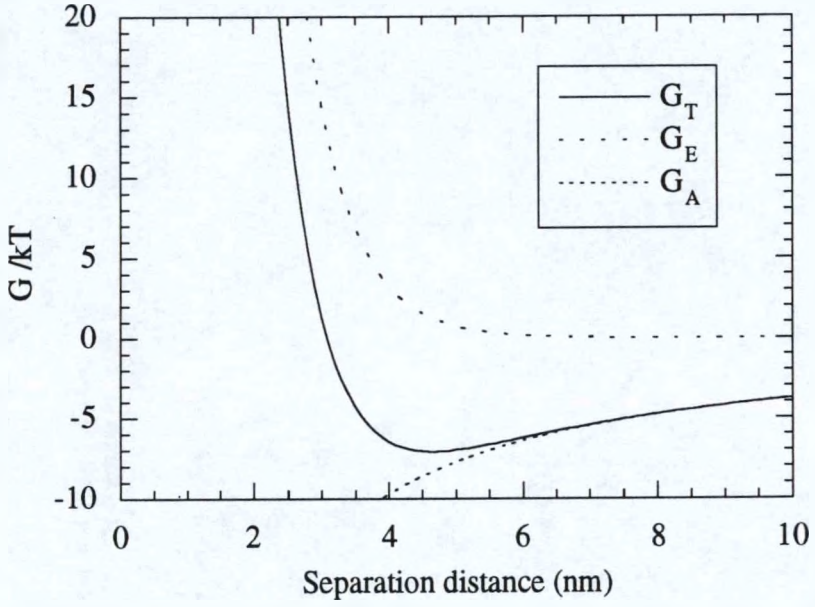

Figure 4.56: Expanded view of the DLVO interaction potential shown in Figure 4.55. A secondary minimum $7\,k_BT$ deep exists at approximately 4.5 nm from the solid surface.

The question remaining to be answered is how cells are able to turn parallel to the surface at distances of between 2 and 4 μm. The model bacteria of Ramia *et al.* do not turn parallel to the surface as they approach it. Also, the insignificance of electrostatic interactions between the cell body and the surface at this distance would seem to eliminate them as a possible explanation. However, two possible explanations exist based on hydrodynamic and electrostatic considerations. First of all, the hydrodynamic model solutions were applied to a spherical bacterium while *E. coli* are rod-shaped cells. There may be torque generated on a rod-shaped cell when it approaches the surface that would

reorient it toward the surface. Another possible explanation lies in the presence of extracellular material around the cell body. *E. coli* are known to be covered with hair-like pili that are 0.2 to 2.0 μm in length [53]. The pili may be reaching the region close to the surface where electrostatic repulsion is significant well before the cell body. The pili at the front of the cell would be repelled by this interaction, forcing the cell to rotate into an orientation parallel to the surface while the body of the cell is still some distance from the surface.

4.6 Conclusion

Motile bacteria moving within 10 μm of a solid surface show a decrease in their cell swimming speed for runs toward the surface. The dependence of the swimming speed on the surface-to-cell distance can be predicted by assuming that hydrodynamic interactions dominate. However as cells get within approximately 2-4 μm of a solid planar surface, they turn until they are aligned with the surface and typically continue to swim along the surface. Wild type cells are frequently able to move away from a solid surface by executing a tumble, although cells were often observed to tumble and continue to run adjacent to the surface as well. Runs adjacent to the surface for cells that do not tumble appear to the significantly longer. However, smooth swimming cells are also able to move away from the surface, indicating that tumbling may facilitate the movement of a bacterium from the surface, but is not necessary.

The theoretical model of Ramia *et al.* predicts the circular motion of bacteria swimming adjacent to a surface, but does not explain why bacteria tend to remain adjacent to the surface. The DLVO interaction potential shows a significant secondary minimum close to the surface that might explain this tendency. An unanswered question is why cells moving toward the surface at orientation angles of between 135° and 180° from the surface normal do not appear to collide with the surface, but begin to turn parallel to the surface at

distances of 2-4 μm from the surface. Two possible explanations, one with a hydrodynamic basis and the other based on the electrostatic repulsion of extracellular material, have been put forth but further study is required to answer this question.

Chapter 5

Summary and Concluding Remarks

This dissertation involves the comparison and validation of models and solution algorithms for the migration of populations of bacteria, and the study of the interactions of swimming bacteria with a solid surface. The major results of this work are summarized below.

5.1 Comparison and Validation of Models

In Chapter 2, a cellular level simulation was developed which can be applied to the problem of the migration of a population of bacteria in a fluid medium in the presence of chemical attractants or repellents. This simulation algorithm, termed cellular dynamics (CD), was used to probe the validity of a phenomenological macroscopic model for the migration of a population of bacteria in a one-dimensional attractant gradient, termed the RTBL model. An implicit assumption in the RTBL model is that bacterial motion is constrained to one dimension. In Chapter 3, a finite element solution method (FEM) was applied to a mathematically rigorous analogue of the RTBL model. The analogue equation is a simplification of Alt's general cell balance equation for time evolution of the density of

bacteria swimming in a fluid medium with an attractant gradient in one dimension. The full three-dimensional character of bacterial motion is preserved in the analogue equation. The FEM solution method was used to test the accuracy of population transport parameters obtained by applying the RTBL model to experimental data. The FEM solution was also used to probe the effect of different models for the modulation of the tumbling frequency of bacteria on the solution for the cell density profile.

Comparisons of CD solutions to RTBL solutions for the density of populations of bacteria responding to gradients of chemical attractants in a stopped-flow diffusion chamber show that the RTBL solutions agree (to within the noise level of the simulation) with the CD solution for the response of *E. coli* bacteria to an initial step gradient of an attractant. This agreement shows that a mathematical analysis based a perturbation expansion of the rigorous governing equation alone (see Section 2.4.2) is not a sufficient indicator of the ability of the RTBL model to accurately predict the solution for the density profile of a population of bacteria responding to relaxing step gradients of attractants. The CD methodology also illustrates the necessity of the use of the proper relationships between the experimentally measured swimming speed, v, and the chemotactic sensitivity χ_0^{3D} obtained from experiments and the one-dimensional analogues of these parameters, used in the solutions of one-dimensional models for bacterial motion such as RTBL.

In Chapter 3, a simplified form of Alt's general equation was applied to the problem of bacterial migration in the presence of a one-dimensional gradient of an attractant. Solution of the simplified form of Alt's general cell balance equation by FEM is a more efficient method than CD for validating one-dimensional phenomenological models. Comparisons to solutions generated with the CD algorithm, which is mathematically equivalent to the FEM solution method, show that the FEM solutions are accurate. The FEM solutions clearly illustrate the difference between the RTBL solution and the simplified form of Alt's equation. The application to experimental data from the stopped-flow diffusion chamber of RTBL and the FEM solution method of Alt's equation applied to

a one-dimensional attractant gradient shows that substantial errors can result if one-dimensional phenomenological models are used to obtain values from these experiments for the chemotactic sensitivity coefficient, χ_0.

The FEM solutions also demonstrate the importance of the correct choice of the model for the downgradient swimming behavior of bacteria on the value of χ_0 obtained from experiment. Some species of bacteria respond by returning to their zero-gradient (basal) tumbling frequency while other species continue to increase their tumbling frequency above the basal frequency when swimming in a direction opposing a concentration gradient of an attractant. This model must be chosen *a priori* since the FEM solutions show that while nearly identical solutions for the density profile can be generated using the "return-to-basal" and "increased-frequency" models for the downgradient behavior, the values of χ_0 required to obtain each of the solutions can differ by as much as 100%.

The FEM solutions also show that the assumption of a negligible partial derivative with respect to time in the total derivative of the number of bound attractant receptors is acceptable since solutions generated including and omitting this partial derivative are virtually indistinguishable for conditions of relevance to stopped-flow diffusion chamber experiments.

5.2 Bacteria-Surface Interactions

In Chapter 4, a tracking microscope was used to study the changes in the swimming behavior of bacteria when the cells encounter a solid surface. Analysis of the swimming behavior of wild type *E. coli* bacteria show that the mean swimming speed for bacteria moving toward a solid surface at orientation angles of greater than 135° and within 10 μm of the surface are lower than for cells with orientation angles less than 135° from the surface normal or for cells greater than 10 μm from the surface. Experimental measurements of the swimming speed of individual cells as a function of surface-to-cell

distance show that cells begin to decrease their swimming speed when they are 10 μm from a solid surface and are moving toward the surface at orientation angles greater than 135°. The rate at which their speed decreases is in agreement with the decrease in speed predicted by two theoretical solutions for spheres moving in a viscous medium toward a planar surface. As the surface-to-cell distance decreases to 2-3 μm, bacteria smoothly change their orientation until they are aligned parallel to the solid surface. Cells then frequently remain parallel to the surface longer than the mean run time of a wild type cell (0.8-0.9 s). In other words, surface trails may include 1-2 tumbles. (See for example Figure 4.24 where the cell tumbles while on the surface and then continues to move along the surface.). Wild type cells that exhibit very long runs tend to move along the surface for longer times than cells that tumble more frequently. Cells that tumble with a typical frequency (1.1-1.3 /s) tend to leave the surface more quickly than cells that exhibit very long runs, and often do so after tumbling. Observations of the swimming speed of smooth swimming (mutant) cells corroborate the observed decrease in cell swimming speed for cells approaching a surface and also showed that tumbling was not necessary for cells initially moving along a surface to leave the surface and return to the bulk fluid.

Cells swimming along the surface frequently swim in circles 30-50 μm in diameter. Consideration of the rotation of the flagella by *Ramia et al.* [59] show that circular paths are hydrodynamically favored for cells moving along a surface. However, hydrodynamic considerations are not sufficient to explain why cells seem to be constrained to move along the surface. Calculation of the interaction potential between the surface (glass in this study) and the bacteria reveals a secondary energy minimum between 4 and 5 nm from the surface and a substantial energy barrier to the primary minimum at less than 1 nm. Bacteria that approach very near the surface may become trapped in the secondary energy minimum and be constrained to motion only parallel to the surface plane until they are able to overcome the barrier and return to the bulk fluid, possibly as a result the tumbling process. However, it was observed in this study that tumbling is neither a sufficient nor necessary

condition for a cell to leave the surface, but tumbling while moving along the surface appears to increase the probability for cells to leave the surface.

5.3 Concluding Remarks

The results of these studies reveal the complex nature of bacterial motion both near a solid surface and far from surfaces in the bulk fluid. To be able to predict the behavior of a population of bacteria moving in the bulk fluid, it is essential to understand how to mathematically describe the physical situation. Questions concerning the response of bacteria to a chemical gradient must be answered before an attempt at modeling the behavior can be undertaken. For example, do bacteria change their tumbling frequency when moving down a chemical gradient or do they return to their basal tumbling frequency? This work shows that substantial errors can be introduced in the transport coefficients obtained from experiments if the correct assumption is not made, although the solution for the bacterial density profile may agree well with the experimental data. Models that assume the motion of the bacteria is one-dimensional, like the RTBL model, are more easily solved than more sophisticated models. Models for bacterial migration that give an accurate solutions quickly would be useful in designing processes such as *in situ* remediation schemes. However, before more simple models are used, it is necessary to determine if they are appropriate. Are there conditions that make the assumption of essentially one-dimensional motion valid? Simpler models should be benchmarked with more sophisticated models based on the general, three-dimensional cell balance equations under all expected actual or experimental conditions.

In the case of bacterial motion near surfaces, we have observed a spectrum of bacteria-surface interactions. Some wild type cells approach a solid surface, begin swimming along the surface while executing several tumbles and circular runs and then leave the surface. Other wild type cells make many circles on the surface in one long run.

The decrease in swimming speed observed as cells approach a surface at distances less than 10 μm is appropriately modeled by considering the hydrodynamic interactions between a sphere with a flagellum attached, a solid surface, and the surrounding fluid. However, understanding the tendency of cells to turn parallel to a surface and then move along the surface for significant periods of time is essential to characterizing cell-surface interactions. The model of Ramia *et al.*, which accounts for the hydrodynamic interactions between their model bacteria and solid surfaces, does not predict the gradual turning of cells until they are parallel to the surface. Although their work predicts that a bacterium with a spherical cell body will collide with the surface without the cell orientation changing significantly, a rod-shaped cell may turn parallel to the surface since the resistance to motion on the end of the cell closest to the surface would be greater than that at the end of the cell farthest from the surface. For a sphere, this force of resistance would be directed through the center of mass of the bacterium and would generate no torque. In a rod-shaped cell, this could cause the cell to rotate and align itself along the surface. In addition to this possibility, DLVO interactions between the surface and extracellular material (such as pili) could cause the fore end of rod-shaped cells to be repelled by the wall before the aft end. Both of these explanations could account for the tendency of cells to turn parallel to the surface and not collide with it, however more work is necessary to identify the proper mechanism for this phenomenon.

As an extension of this work, I would suggest performing tracking experiments in solutions with varying ionic strength. If it is true that adsorption in the secondary minimum is resulting in cells swimming very near the surface and parallel to it, then reducing the ionic strength could result in cells not swimming along the surface. Also, the ionic strength of the medium could be increased or perhaps another material could be used for the solid surface to reduce or remove the electrostatic barrier to the primary minimum. This would make it possible to test the conjecture that electrostatic repulsion of extracellular

material is possible for the tendency of bacteria not to collide with the solid surface, but to turn parallel to the surface.

At this point, it is not known why cells turn parallel to the surface and remain parallel to it, sometimes tumbling and continuing along the surface. A sufficient amount of tracking data might make it possible to obtain a reasonable stochastic representation of the motion of bacteria near the surface. One could obtain run time distributions for surface motion and probability distributions for the likelihood of a cell moving along the surface to return to the bulk fluid. However, it seems very possible that electrostatic interactions play a yet undetermined role in the motion of motile bacteria near solid surfaces. This would mean that near surface behavior would be a function of the composition of the media and the solid surface, making the prediction of the migration of bacteria in natural systems very difficult.

If it can be determined by what mechanism the turning and surface swimming behavior of bacteria occurs, it would then be possible to incorporate the interaction of the bacteria with the surface into a cell balance equation or simulation algorithm to describe the motion of bacteria in a porous media or other system including a solid phase. In either case, an analytical solution for the dependence of the swimming speed and path of the bacteria is not available. The inclusion of surface interactions into mathematical models of this type would require the additional solution of a model such as that of Ramia *et al.* that might also include a description of the electrostatic and van der Waals interactions. Solving this concurrently with a balance equation would not, at this time, be practical since it would require very intensive computer resources and would require an unrealistic amount of time to obtain a solution. However, it may be possible to solve a model for the reasonable number of discrete orientations and separation distances much as was done for the angle change distribution in the FEM solutions shown in this work. Then, if sufficient storage resources were available, it would be possible to include the dependence of the run speed

and cell swimming path on the separation distance in theoretical methods such as the CD and FEM solution methods developed in this study.

Bibliography

1. Aamand, J., *et al.*, *Microbial Adaptation to Degradation of Hydrocarbons in Polluted and Unpolluted Groundwater.* Journal of Contaminant Hydrology, 1989. **4**: p. 299-312.

2. Adler, J., *A Method for Measuring Chemotaxis and Use of the Method to Determine Optimum Conditions for Chemotaxis by Escherichia coli.* Journal of General Microbiology, 1973. **74**: p. 77-91.

3. Allaire, P.E., *Basics of the Finite Element Method.* 1985, Dubuque, IA: Wm. C. Brown.

4. Allen, M.P. and D.J. Tildesly, *Computer Simulations of Liquids.* 1987, New York: Oxford University Press.

5. Alt, W., *Biased Random Walk Models for Chemotaxis and Related Diffusion Approximations.* Journal of Mathmatical Biology, 1980. **9**: p. 147-177.

6. Batchelor, G.K., *An Introduction to Fluid Dynamics.* 1970, London: Cambridge University Press.

7. Beeman, R.E., S.H. Shoemaker, and J.R. Buttram. *In-Situ Demonstration of Anaerobic Bioremediation of Chlorinated Ethenes.* in *AIChE 1993 Summer National Meeting.* 1993. Seattle, Washington:

8. Berg, H.C., *How to Track Bacteria.* Review of Scientific Instruments, 1971. **42**(6): p. 868-71.

9. Berg, H.C., *Random Walks in Biology.* 1983, Princeton, NJ: Princeton University Press.

10. Berg, H.C., *A Physicist Looks at Bacterial Chemotaxis.* Cold Springs Harbor Symposia on Quantitative Biology, 1988. **53**: p. 1-9.

11. Berg, H.C. and D.A. Brown, *Chemotaxis in Escherichia coli Analysed by Three-Dimensional Tracking.* Nature, London, 1972. **239**: p. 500-504.

12. Berg, H.C. and D.A. Brown, *Chemotaxis in Escherichia coli Analyzed by Three-Dimensional Tracking.* Antibiotics and Chemotherapy, 1974. **19**: p. 55-78.

13. Berg, H.C. and L. Turner, *Movement of Microorganisms in Viscous Environments.* Nature, 1979. **278**: p. 349-351.

14. Berg, H.C. and L. Turner, *Chemotaxis of Bacteria in Glass Capillary Arrays.* Biophysical Journal, 1990. **58**(4): p. 919-930.

15. Bird, R.B. and H.C. Öttinger, *Transport Properties of Polymeric Liquids.* Annual Reviews of Physical Chemistry, 1992. **43**: p. 371.

16. Bornbusch, A.H., *Turning Field Size and Its Effects upon Computer Simulated Klinotactic Orientation.* Journal of Theoretical Biology, 1984. **107**: p. 151-163.

17. Bornbusch, A.H. and W.E. Conner, *Effects of Self-Steered Turn Size and Turn Bias upon Simulated Chemoklinotactic Behavior.* Journal of Theoretical Biology, 1986. **122**: p. 7-18.

18. Brebbia, C.A., J.F.C. Telles, and L.C. Wrobel, *Boundary Element Techniques: Theory and Applications in Engineering.* 1984, New York: Springer-Verlag.

19. Brenner, H., *The Slow Motion of a Sphere through a Viscous Fluid Towards a Plane Surface.* Chemical Engineering Science, 1961. **16**: p. 242-251.

20. Brown, D.A. and H.C. Berg, *Temporal Stimulation of Chemotaxis in Escherichia coli.* Proceeding of the National Academy of Science, 1974. **71**(4): p. 1388-1392.

21. Chet, I. and R. Mitchell, *Ecological Aspects of Microbial Chemotactic Behavior.* Microbiology, 1976. **30**: p. 221-239.

22. Corapcioglu, M.Y., M.A. Hossain, and M.A. Hossain, *Anaerobic Biotransformation of PCE and TCE in Groundwater: A Comparison of Experimental Data with Numerical Results.* Water Science Technology, 1991. **23**: p. 525-534.

23. Crank, J., *The Mathematics of Diffusion.* 2nd ed. 1979, Oxford: Clarendon Press.

24. Ellis, B., M.T. BAlba, and P. Theile, *Bioremediation of Oil Contaminated Land.* Environmental Technology, 1990. **11**: p. 443-455.

25. EPA, *Bioremediation in the Field,* Bioremediation. 1992, EPA:

26. Ford, R.M., *Quantitative Studies of Bacterial Motility and Chemotaxis Using a Stopped-Flow Diffusion Chamber Assay and an Individual cell-based Mathematical Model.* 1989, University of Pennsylvania:

27. Ford, R.M., *Mathematical Modeling and Quantitative Characterization of Bacterial Motility and Chemotaxis,* in *Metabolic and Physiologic Activities of Microorganisms,* C.J. Hurst, Editor. 1992, Wiley: New York. p. 177-215.

28. Ford, R.M. and P.T. Cummings, *On the Relationship between Cell Balance Equations for Chemotactic Cell Populations.* SIAM Journal of Applied Math, 1992. **52**(5): p. 1426-1441.

29. Ford, R.M. and D.A. Lauffenburger, *Measurement of Bacterial Random Motility and Chemotaxis Coefficients: II. Application of Single-Cell-Based Mathematical Model.* Biotechnology and Bioengineering, 1991. **37**: p. 661-672.

30. Ford, R.M., *et al.*, *Measurement of Bacterial Random Motility and Chemotaxis Coefficients: I. Stopped Flow Diffusion Chamber Assay.* Biotechnology and Bioengineering, 1991. **37**: p. 647-660.

31. Frymier, P.D., R.M. Ford, and P.T. Cummings, *Cellular Dynamics Simulations of Bacterial Chemotaxis.* Chemical Engineering Science, 1993. **48**(4): p. 687-699.

32. Greenberg, E.P. and E. Canale-Parola, *Motility of Flagellated Bacteria in Viscous Environments.* Journal of Bacteriology, 1977. **132**(1): p. 356-358.

33. Guell, D.C., *et al.*, *Hydrodynamic Forces and Band Formation in Swimming Magnetotactic Bacteria.* Journal of Theoretical Biology, 1988. **135**: p. 525-542.

34. Hammersley, J.M. and D.C. Handscomb, *Monte Carlo Methods*. 1964, New York: Wiley.

35. Harkes, G., J. Dankert, and J. Feijen, *Bacterial Migration along Solid Surfaces.* Applied and Environmental Microbiology, 1992. **58**(5): p. 1500-1505.

36. Hazelbauer, G.L., R.E. Mesibov, and J. Adler, *Escherichia coli Mutants Defective in Chemotaxis Toward Specific Chemicals.* Proceedings of the National Academy of Science, 1969. **64**: p. 1300-1307.

37. Hiemenz, P.C., *Principles of Colloid and Surface Chemistry.* 1986, New York: Marcel Dekker, Inc.

38. Kane, J.H., *Boundary element analysis in engineering continuum mechanics.* 1994, Englewood Cliffs, N.J.: Prentice Hall.

39. Keller, E.F. and L.A. Segel, *Model for Chemotaxis.* Journal of Theoretical Biology, 1971. **30**: p. 225.

40. Kelly, F.X., K. Dapsis, and D.A. Lauffenberger, *Effect of Bacterial Chemotaxis on Dynamics of Microbial Competition.* Microbial Ecology, 1988. **16**: p. 115-131.

41. Koshland, D.E., *Bacterial Chemotaxis as a Model Behavioral System.* 1980, New York: Raven Press.

42. Litton, G.M. and T.M. Olson, *Colloid Deposition Rates on Silica Bed Media and Artifacts Related to Surface Preparation Methods.* Environmental Science and Technology, 1993. **27**(1): p. 185-193.

43. Loeb, G.I., *The Properties of Nonbiological Surfaces and Their Characterization,* in *Bacterial Adhesion,* D.C.S.a.M. Fletcher, Editor. 1985, Plenum Press: New York. p. 111-129.

44. Lovely, P.S. and F.W. Dalquist, *Statistical Measures of Bacterial Motility and Chemotaxis.* Journal of Theoretical Biology, 1975. **50**: p. 477-496.

45. Macnab, R.M., *Sensing the Environment: Bacterial Chemotaxis,* in *Biological Regulation and Development,* R. Goldberger, Editor. 1980, Plenum Press: New York. p. 377.

46. Macnab, R.M. and D.E. Koshland, *The Gradient-Sensing Mechanism in Bacterial Chemotaxis.* Proceedings of the National Academy of Science, 1972. **69**: p. 2509-2512.

47. Macnab, R.M. and D.E. Koshland, *Persistence as a Concept in the Motility of Chemotactic Bacteria.* Journal of Mechanochemistry and Cell Motility, 1973. **2**: p. 141-148.

48. Matthess, G., A. Pekdeger, and J. Schroeter, *Persistence and Transport of Bacteria and Viruses in Groundwater- a Conceptual Evaluation.* Journal of Contaminant Hydrology, 1988. **2**: p. 171-188.

49. McDowell-Boyer, L.M., J.R. Hunt, and N. Sitar, *Particle Transport through Porous Media.* Water Resources Research, 1986. **22**(13): p. 1901-1921.

50. Mercer, J.R., *et al.*, *Growth Rate Effects on Fundamental Transport Properties of Bacterial Populations.* Biotechnology and Bioengineering, 1993. **42**: p. 1277.

51. Milton, J.S. and J.C. Arnold, *Introduction to Probability and Statistics: Principles and Applications for Enginnering and the Computing Sciences.* 1990, New York: McGraw-Hill.

52. Moore, A.T., A. Vira, and S. Fogel, *Biodegradation of trans-1,2-Dichloroethylene by Methane-Utilizing Bacteria in an Aquifer Simulator.* Environmental Science and Technology, 1989. **23**(4): p. 403-406.

53. Neidhardt, F.C., J.L. Ingraham, and M. Schaechter, *Physiology of the Bacterial Cell.* 1990, Sunderland, MA: Sinauer Associates, Inc.

54. Nickel, J.c., J. Downey, and J.W. Costerton, *Movement of Pseudomonas Aeruginosa Along Catheter Surfaces.* Investigative Urology, 1992. **29**(1): p. 93-96.

55. Norde, W. and J. Lyklema, *Protein Adsorption and Bacterial Adhesion to Solid Surfaces: A Colloid-Chemical Approach.* Colloids and Surfaces, 1989. **38**: p. 1-13.

56. Nossal, R. and S.H. Chen, *Effects of Chemoattractants on the Motility of Escherichia coli.* Nature New Biology, 1973. **244**: p. 253-254.

57. Othmer, H., S. Dunbar, and W. Alt, *Models of Dispersal in Biological Systems.* Journal of Mathematical Biology, 1988. **26**: p. 263-298.

58. Patlack, C.S., *Random Walk with Persistence and External Bias.* The Bulletin of Mathematical Biophysics, 1953. **15**: p. 311-338.

59. Ramia, M., D.L. Tullock, and N. Phan-Thien, *The Role of Hydrodynamic Interaction in the Locomotion of Microorganisms.* Biophysical Journal, 1993. **65**: p. 755-778.

60. Rifai, H.S., *et al.*, *Biodegradation Modeling at Aviation Fuel Spill Site.* Journal of Environmental Engineering, 1988. **114**(5): p. 1007-1029.

61. Rijnaarts, H.H.M., *et al.*, *Interactions Between Bacteria and Solid Surfaces in Relation to Bacterial Transport in Porous Media.* Colloids and Surfaces B: Biointerfaces, 1994. submitted for publication.

62. Rivero, M.A., *et al., Transport Models for Chemotactic Cell Populations Based on Individual Cell Behavior.* Chemical Engineering Science, 1989. **44**(12): p. 2881-2897.

63. Roberts, P.V., *et al., A Field Evaluation of In-Situ Biodegradation of Chlorinated Ethenes: Part 1, Methodology and Field Site Characterization.* Ground Water, 1990. **28**(4): p. 591-604.

64. Rosenberg, M., *Basic and Applied Aspects of Microbial Adhesion at the Hydrocarbon:Water Interface.* Critical Reviews in Microbiology, 1991. **18**(2): p. 159-173.

65. Rutter, P.R. and B. Vincent, *Physicochemical Interactions of the Substratum, Microorganisms and the Solid Phase,* in *Microbial Adhesion and Aggregation,* K.C. Marshall, Editor. 1984, Springer-Verlag: Berlin.

66. Segel, L.A., *A Theoretical Study of Receptor Mechanisms in Bacterial Chemotaxis.* SIAM Journal of Applied Mathematics, 1977. **32**: p. 653-665.

67. Segel, L.A., *On Deducing the Nature and Effect of Attractant-Receptor Binding from Population Movements of Chemotactic Bacteria,* in *Physical Chemical Aspects of Cell Surface Events in Cellular Regulation,* C.D.a.R. Blumenthal, Editor. 1979, Elsevier: New York. p. 293-302.

68. Semprini, L., *et al., Field Evaluation of In-Situ Biodegradation of Chlorination Ethenes: Part2, Results of Biostimulation and Biotransformation Experiments.* Ground Water, 1990. **28**(5): p. 715-727.

69. Song, H.-G., X. Wang, and R. Bartha, *Bioremediation Potential of Terrestrial Fuel Spills.* Applied and Environmental Microbiology, 1990. **56**(3): p. 652-656.

70. Spudich, J.L. and D.E. Koshland, *Quantitation of the Sensory Response in Bacterial Chemotaxis.* Proceedings of the National Academy of Science, 1975. **72**: p. 710-713.

71. Staffeld, P.O. and J.A. Quinn, *Diffusion-Induced Banding of Colloid Particles via Diffusiophoresis: 1. Electrolytes.* Journal of Colloid and Interfacial Science, 1989. **130**: p. 69.

72. Strauss, I., *Bacterial Chemotaxis in the Presence of Multiple Stimuli.* 1992, University of Virginia: Master's thesis.

73. Tankersley, R.A. and W.E. Conner, *Not-So-Random-Walks-Computer Simulations of Chemo-orientation Behavior.* Bioscience, 1990. **40**: p. 392-395.

74. van Loosedrecht, M.C., *et al., Electophoretic Mobility and Hydrophobicity as a Measure to Predict the Initial Steps of Bacterial Adhesion.* Applied and Environmental Microbiology, 1987. **53**(8): p. 1898-1901.

75. van Loosedrecht, M.C.M., *et al., Bacterial Adhesion: A Physicochemical Approach.* Microbial Ecology, 1989. **17**: p. 1-15.

76. van Loosedrecht, M.C.M., *et al., Hydrophobic and Electrostatic Parameters in Bacterial Adhesion.* Aquatic Science, 1990. **52**: p. 103-114.

77. Vincent, J., N. Phan-Thien, and T. Tran-Cong, *Sedimentation of Multiple Particles of Arbitrary Shape*. Journal of Rheology, 1991. **35**(1): p. 1-27.

Appendix A

Relating Mean Run Time and Attractant Gradient

Brown and Berg [11] observed that the mean run time $\langle \tau \rangle$ of cells in an attractant gradient increased exponentially with the rate of change in the number of bound receptors over the mean run time measured in the absence of a gradient, $\langle \tau_0 \rangle$. Rivero *et al.* [62] expressed this relationship by the equation:

$$\ln \frac{\langle \tau \rangle}{\langle \tau_0 \rangle} = \upsilon \frac{DN_b}{Dt} \tag{A.1}$$

υ is a proportionality constant describing the fractional change in mean run time per unit time rate of change in cell surface receptors that are bound to attractant molecules and DN_b / Dt is the material derivative of the number of bound receptors,

$$\frac{DN_b}{Dt} = \frac{\partial N_b}{\partial t} + v\hat{\mathbf{s}} \cdot \vec{\nabla}_r N_b = \frac{dN_b}{da}\frac{\partial a}{\partial t} + v\hat{\mathbf{s}} \cdot \vec{\nabla}_r a \frac{dN_b}{da} \tag{A.2}$$

In the RTBL model, it is assumed that $\partial a / \partial t \ll v\hat{\mathbf{s}} \cdot \vec{\nabla}_r a$. Under this assumption, we can write:

$$\frac{dN_b}{dt} \approx v\hat{\mathbf{s}} \cdot \vec{\nabla}_r a \frac{dN_b}{da} \tag{A.3}$$

For a single population of homogeneous receptors, Rivero *et al.* assume the following form for the dependence of the change in the number of bound receptors on the attractant concentration:

$$\frac{dN_b}{da} = \frac{N_T K_d}{(K_d + a)^2} \tag{A.4}$$

where K_d is the dissociation constant for the attractant-receptor binding and N_T is the total number of receptors. Substituting Equations A.3 and A.4 into Equation A1 gives:.

$$\ln \frac{\langle \tau \rangle}{\langle \tau_0 \rangle} = \upsilon v \frac{N_T K_d}{(K_d + a)^2} \hat{\mathbf{s}} \cdot \vec{\nabla}_r a \tag{A.5}$$

Rivero *et al.* define a chemotactic sensitivity coefficient, χ_0, as:

$$\chi_0^{3D} = \upsilon v^2 N_T \tag{A.6}$$

where the superscript 3D has been included to indicate explicitly that this is the definition for motion in three dimensions. Using the definition of χ_0^{3D}, Equation A.6, one can write Equation A.5 as:

$$\ln \frac{\langle \tau \rangle}{\langle \tau_0 \rangle} = \frac{\chi_0^{3D}}{v} \frac{K_d}{(K_d + a)^2} \hat{\mathbf{s}} \cdot \vec{\nabla}_r a \tag{A.8}$$

In the one-dimensional RTBL model based on the Segel equations, Rivero *et al.* defined one-dimensional analogues of the above equations leading to:

$$\ln\frac{\langle\tau^{\pm}\rangle}{\langle\tau_0\rangle}=\frac{\chi_0^{1D}}{s}\frac{K_d}{(K_d+a)^2}\frac{\partial a}{\partial z} \tag{A.9}$$

where the positive/negative sign is used for bacteria moving in the positive/negative z direction, s is the one-dimensional swimming speed and:

$$\chi_0^{3D}=\upsilon v^2 N_T \tag{A.10}$$

Attention is now turned to the relationship between $p^{\pm}$ defined in the one-dimensional Segel equations, Equations 2.3 and 2.4, and the corresponding quantities one would obtain by considering the more accurate three-dimensional description of bacterial motion with symmetry in two (x and y) of the three spatial directions. The latter problem was considered at length by Ford and Cummings [28] and the main relevant results are simply quoted in this Appendix. Equations (3.18) and (3.19) of Ford and Cummings give expressions for n^+ and n^-, the densities of cells moving in the positive and negative z-directions, as:

$$\begin{aligned} n^+(z,t)&=\int_0^{\pi/2}\int_0^{2\pi}\int_{-\infty}^{\infty}\int_{-\infty}^{\infty} n(\mathbf{r},\hat{\mathbf{s}},t)\,dx\,dy\,d\phi\sin\theta\,d\theta \\ &=\int_0^{\pi/2} n_z(z,\theta,t)\sin\theta\,d\theta \end{aligned} \tag{A.11}$$

Likewise, the density of cells moving in the negative z direction is given by:

$$\begin{aligned} n^-(z,t)&=\int_{\pi/2}^{\pi}\int_0^{2\pi}\int_{-\infty}^{\infty}\int_{-\infty}^{\infty} n(\mathbf{r},\hat{\mathbf{s}},t)\,dx\,dy\,d\phi\sin\theta\,d\theta \\ &=\int_{\pi/2}^{\pi} n_z(z,\theta,t)\sin\theta\,d\theta \end{aligned} \tag{A.12}$$

In these equations, $n(\mathbf{r},\hat{\mathbf{s}},t)$ is the density of cells at point $\mathbf{r}$ at time t moving in direction $\hat{\mathbf{s}} = (\sin\theta\cos\phi, \sin\theta\sin\phi, \cos\theta)$ (θ and ϕ are the usual angles for spherical coordinates). The quantity $n_z(z,\theta,t)$ is the density of cells moving with z-coordinate z whose velocity is at an angle θ to the z-axis and is defined by:

$$\begin{aligned} n_z(z,\theta,t) &= \int_0^{2\pi}\int_{-\infty}^{\infty}\int_{-\infty}^{\infty} n(\mathbf{r},\hat{\mathbf{s}},t)\,dx\,dy\,d\phi \\ &= 2\pi\int_{-\infty}^{\infty}\int_{-\infty}^{\infty} n(|x|,|y|,z,\theta,y)\,dx\,dy \end{aligned} \tag{A.13}$$

By integrating the three-dimensional balance equations over the x and y coordinate directions [28] and comparing with the Segel equations, one can derive an expression for the terms n^+p^+ and n^-p^- in Equations 2.3 and 2.4. Consider the equation for n^+p^+:

$$\begin{aligned} n^+p^+ = \int_0^{\pi/2}\int_{\pi/2}^{\pi} n_z(z,\theta,t)\beta_0 \exp\left[-\frac{\chi_0^{3D}}{v}\frac{K_d}{(K_d+a)^2}\hat{\mathbf{s}}\cdot\nabla a\right] \\ \times K(\theta,\theta')\sin\theta'\,d\theta'\sin\theta\,d\theta \end{aligned} \tag{A.14}$$

where $K(\theta,\theta')$ is the reduced turn probability distribution which gives the probability that a bacterium moving at angle θ to the z-axis moves at angle θ' after tumbling. Details of this can be found in Ford and Cummings [28]. A similar expression can be developed for n^-p^-. From these expressions it is evident that p^+ and p^- do not reduce to the simple one-dimensional expressions, Equations 2.7 and 2.12. Thus, we should regard Equation 2.12 as a mathematical approximation in the RTBL model.

Appendix B

Turn Angle Probability Distribution

Berg and Brown [11] observed the direction change that *E. coli* bacteria exhibit when tumbling. They generated a plot of the number of bacteria turning into each 10° interval from 0° to 180°. We used this experimental data to generate a turn angle probability distribution by fitting a polynomial to the data and then normalizing the distribution. Let the direction in which a bacterium is moving prior to tumbling, $\hat{\mathbf{s}}$, be given by $\hat{\mathbf{s}} = (\sin\theta\cos\phi, \sin\theta\sin\phi, \cos\theta)$ and the direction in which a bacterium is moving after tumbling, $\hat{\mathbf{s}}'$, be given by $\hat{\mathbf{s}}' = (\sin\theta'\cos\phi', \sin\theta'\sin\phi', \cos\theta')$. Let α be defined such that $\cos(\alpha) = \hat{\mathbf{s}} \cdot \hat{\mathbf{s}}'$. The polynomial we used to represent the normalized probability distribution for α is

$$p(\alpha) = \sum_{i=1}^{n-1} c_i \alpha^i (\pi - \alpha)^{n-i} \tag{B.1}$$

where c_i are coefficients chosen by the method of least squares to best fit the data and n is the order of the polynomial. The polynomial is written in this form so that $p(\alpha = 0) = p(\alpha = 2\pi) = 0$ in agreement with the experimental data. We found that a seventh order polynomial of this type generated the best fit. The relationship between $p(\alpha)$ and $p(\cos\alpha)$ is:

$$p(\cos\alpha) = \frac{p(\alpha)}{\sin\alpha} \tag{B.2}$$

This is used to generate the distribution function:

$$F(\cos\alpha) = \int_{-1}^{\cos\alpha} p(\cos\alpha')\, d(\cos\alpha') \tag{B.3}$$

When a cell tumbles, we choose $\cos\alpha$ from this distribution using standard techniques [34]. If the angle of rotation of the new direction vector $\hat{\mathbf{s}}'$ around the direction vector before tumbling $\hat{\mathbf{s}}$ is γ, then the angle γ is chosen at random from a uniform distribution on $[0,2\pi]$. The new direction $\hat{\mathbf{s}}'$ is then found from

$$\hat{\mathbf{s}}' = \mathbf{M}\hat{\mathbf{s}} \tag{B.4}$$

where M is the coordinate transformation matrix between (θ,ϕ), (α,γ), and (θ',ϕ') and can be found in Patlack [58].

Appendix C

Direction Change Distribution

The direction change distribution $k(\mathbf{r},\hat{\mathbf{s}}',t;\hat{\mathbf{s}})$ found in Equation 3.1 is the probability that a bacterium originally moving in the direction $\hat{\mathbf{s}}'$ at time t and at position $\mathbf{r}$ prior to tumbling moves in the direction $\hat{\mathbf{s}}$ after tumbling where $\hat{\mathbf{s}} = (\sin\theta\cos\phi, \sin\theta\sin\phi, \cos\theta)$ and $\hat{\mathbf{s}}' = (\sin\theta'\cos\phi', \sin\theta'\sin\phi', \cos\theta')$ and as shown in Figure C.1.

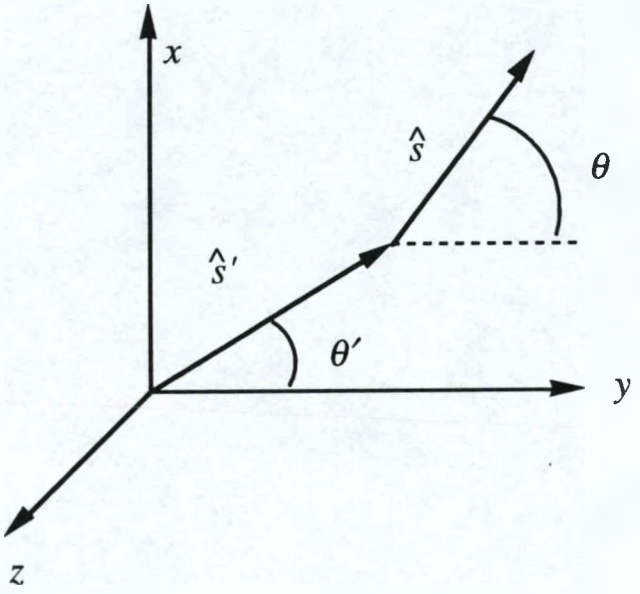

Figure C.1: This is an illustration of the relationship between the direction vectors, $\hat{\mathbf{s}}$ and $\hat{\mathbf{s}}'$ and the angles θ and. θ'.

Macnab and Koshland [46] observed experimentally that $k(\mathbf{r},\hat{\mathbf{s}}',t;\hat{\mathbf{s}})$ is independent of the presence of an attractant, so that $k(\mathbf{r},\hat{\mathbf{s}}',t;\hat{\mathbf{s}}) = k(\hat{\mathbf{s}}';\hat{\mathbf{s}})$. The direction change distribution $K(\theta',\theta)$ found in the balance equation for one-dimensional attractant gradients, Equation 3.1, and defined in Equation A.1, is the probability that a bacterium originally moving in a direction with angle θ' off the z-axis prior to tumbling moves in a direction with the angle θ off the $z-$axis after tumbling. The distributions $k(\hat{\mathbf{s}}';\hat{\mathbf{s}})$ and $K(\theta',\theta)$ are related by

$$K(\theta',\theta) = \frac{1}{2\pi}\int_0^{2\pi}\int_0^{2\pi} k(\hat{\mathbf{s}}',\mathbf{s})\,d\phi'\,d\phi \tag{C.1}$$

The distribution $k(\hat{\mathbf{s}}';\hat{\mathbf{s}})$ is calculated from the turn angle distribution $p(\alpha)$ where $\cos(\alpha) = \hat{\mathbf{s}}\cdot\hat{\mathbf{s}}'$. The distribution $p(\alpha)$ was determined experimentally for *E. coli* by Berg and Brown [11]. A seventh order polynomial of the type:

$$p(\alpha) = \sum_{i=1}^{6} c_i \alpha^i (\pi - \alpha)^{7-i} \tag{C.2}$$

was used, where the c_i are coefficients chosen by the method of least squares to best fit the experimental data for the distribution of turn angles (see also Frymier *et al.* [31]). The use of the seventh-order polynomial is simply for numerical convenience and does not imply any physical or mechanistic model for the reduced direction change distribution. Since the reduced direction change distribution, $K(\theta',\theta)$, is independent of the attractant concentration and therefore of time, a substantial time savings can be realized if $K(\theta',\theta)$ is tabulated at the control points for two point Gaussian integration on each element so the values can be called on when needed without recalculation.

Appendix D

Genotype of HCB437

This information was provided by Linda Turner of the Rowland Institute, Cambridge, MA. Following are the mutations which affect gene function in the smooth swimming bacteria, HCB437:

thr(AM)1	-requires threonine.
leuB6	-requires leucine.
thi1	-require thiamine.
his4	-requires histidine.
lacY1	-cannot metabolize lactose, arabinose, xylose or maltose as carbon sources.
ara14	- " " " " "
xyl5	- " " " " "
mtl1	- " " " " "
metF(AM)159	-requires methionine.
tsx78=T6	-phage T6 and T1 receptors, this strain lacks or has nonfunctional receptors for this phage.
tonA31=T1	- " " " " "
rpsL136 Sm(r)	-streptomycin resistant.

DE2209(cheA-cheZ)	-this is a deletion for the chemotaxis genes from cheA to cheZ.
DE7021(tsr)	-this is a deletion for the tsr gene (receptor for serine).
DE100(trg)	-transducer for ribose and galactose.
zdb::Tn5 Kn(R)	-kanamycin resistant.

The original reference for this strain is:

Wolf *et al.*, 1987, Journal of Bacteriology, Vol. 169, 1878-1885.

Appendix E

Growth Media and Buffer Solution Compositions

Minimal growth medium composition (per liter distilled water):

K_2HPO_4	11.2	g
KH_2PO_4	4.8	g
$(NH_4)_2S0_4$	2.0	g
$MgSO_4$-$7H_20$	0.25	g
$Fe_2(SO_4)$-$5H_2O$)	0.0006	g

Thiamine solution (per ml distilled water):

0.5 mg thiamine

Galactose solution (per ml distilled water):

100.0 mg galactose

Minimal medium preparation:

1. Add 50 ml of stock solution to 250 ml shaker flask.
2. Autoclave to sterilize. Cool to room temperature.
3. Add 0.5 ml each of thiamine and galactose solutions, filtered through a 0.2 μm filter.
4. Add 100 μl of frozen *E. coli* stock.
5. Incubate at 30° C until $ABS(\lambda_{590}) = 0.8 - 1.0$ (approximately 11 hr)

Phosphate buffer solution composition (per liter distilled water):

K_2HPO_4	11.2	g
KH_2PO_4	4.8	g
EDTA	0.029	g

Tryptone broth composition (per liter distilled water):

10 g Difco Bacto-Tryptone
5 g NaCl

Appendix F

Additional Wild Type and Smooth Swimming Bacterial Traces

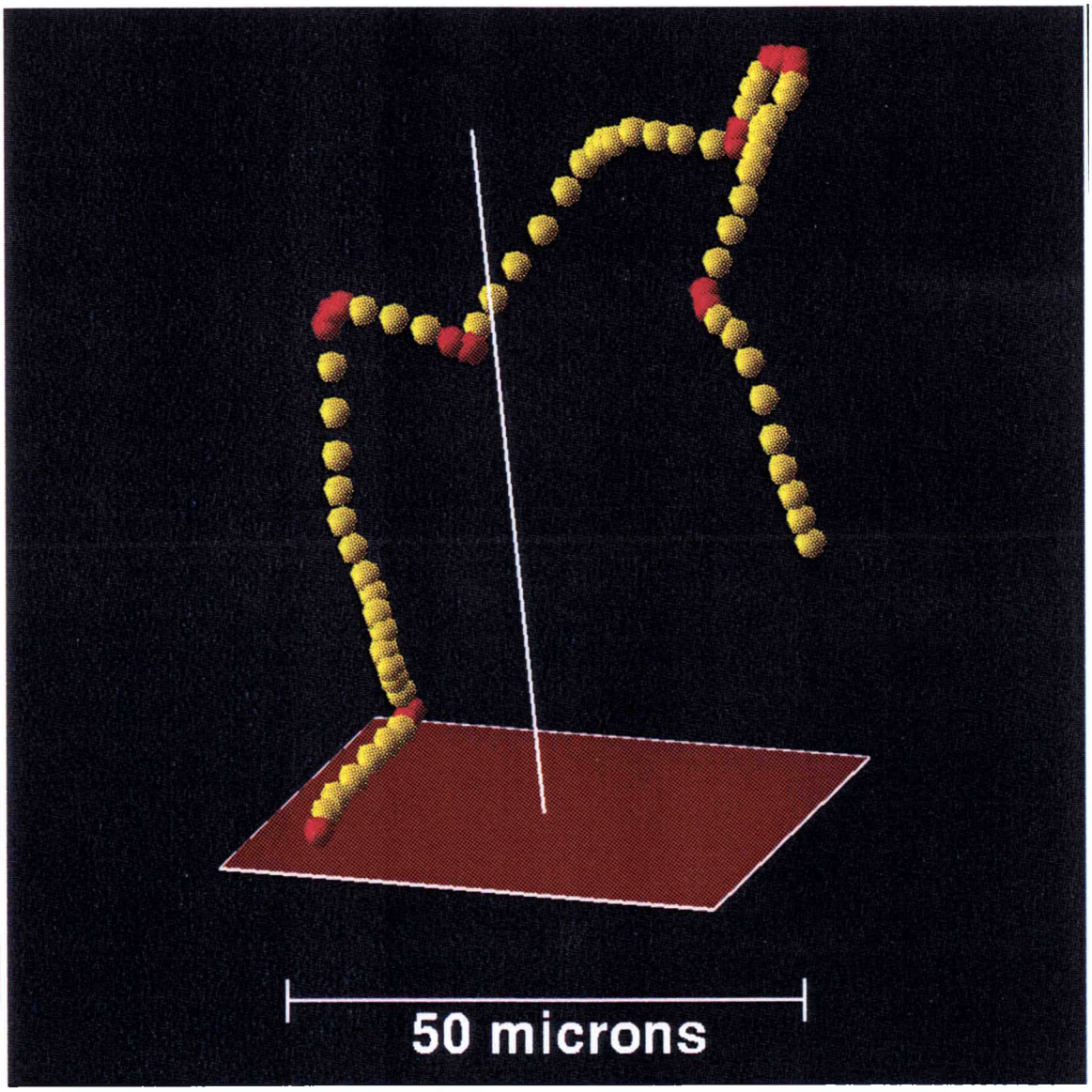

Figure F.1: Wild type bacterial trace 6.

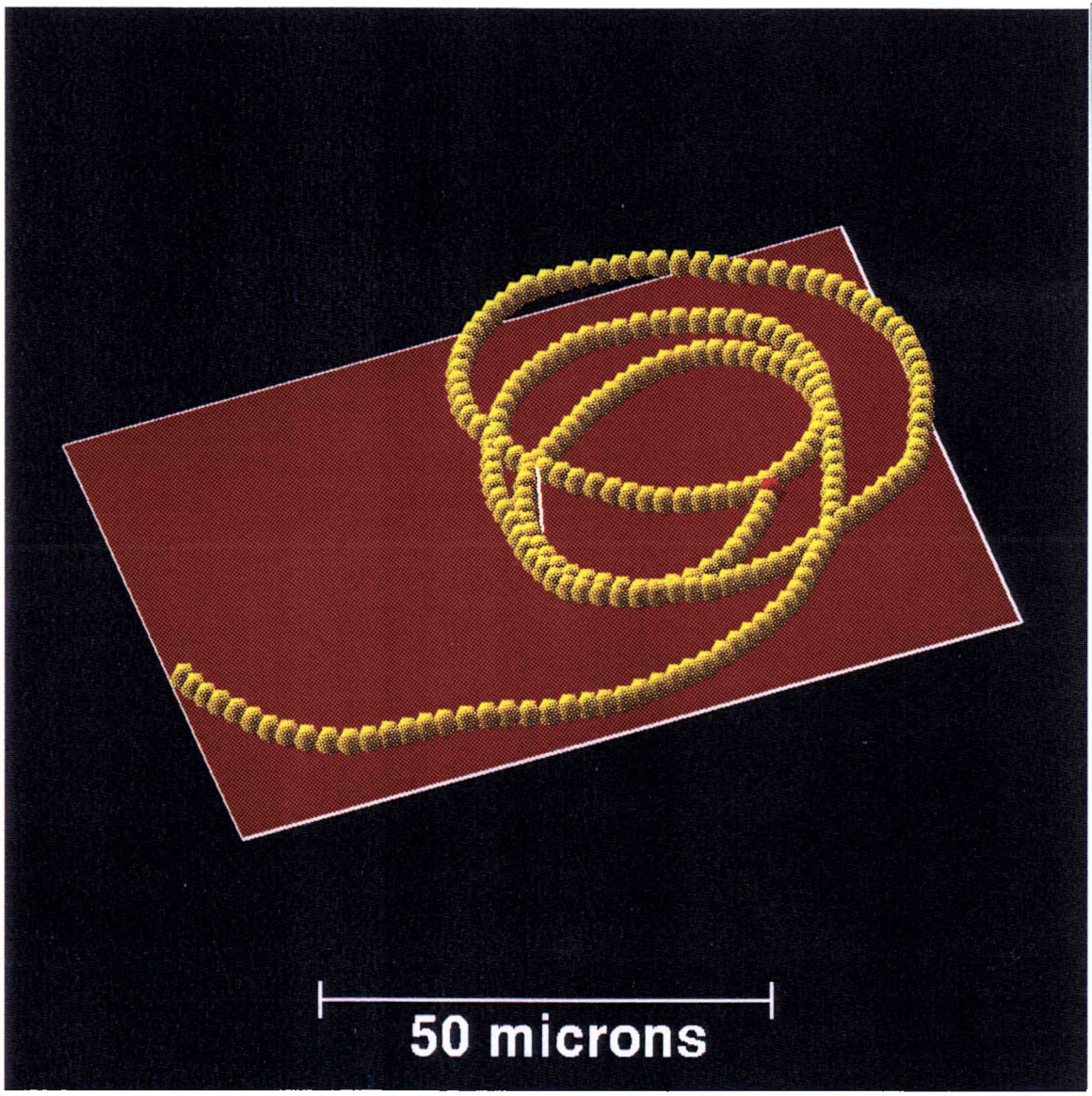

Figure F.2: Wild type bacterial trace 7.

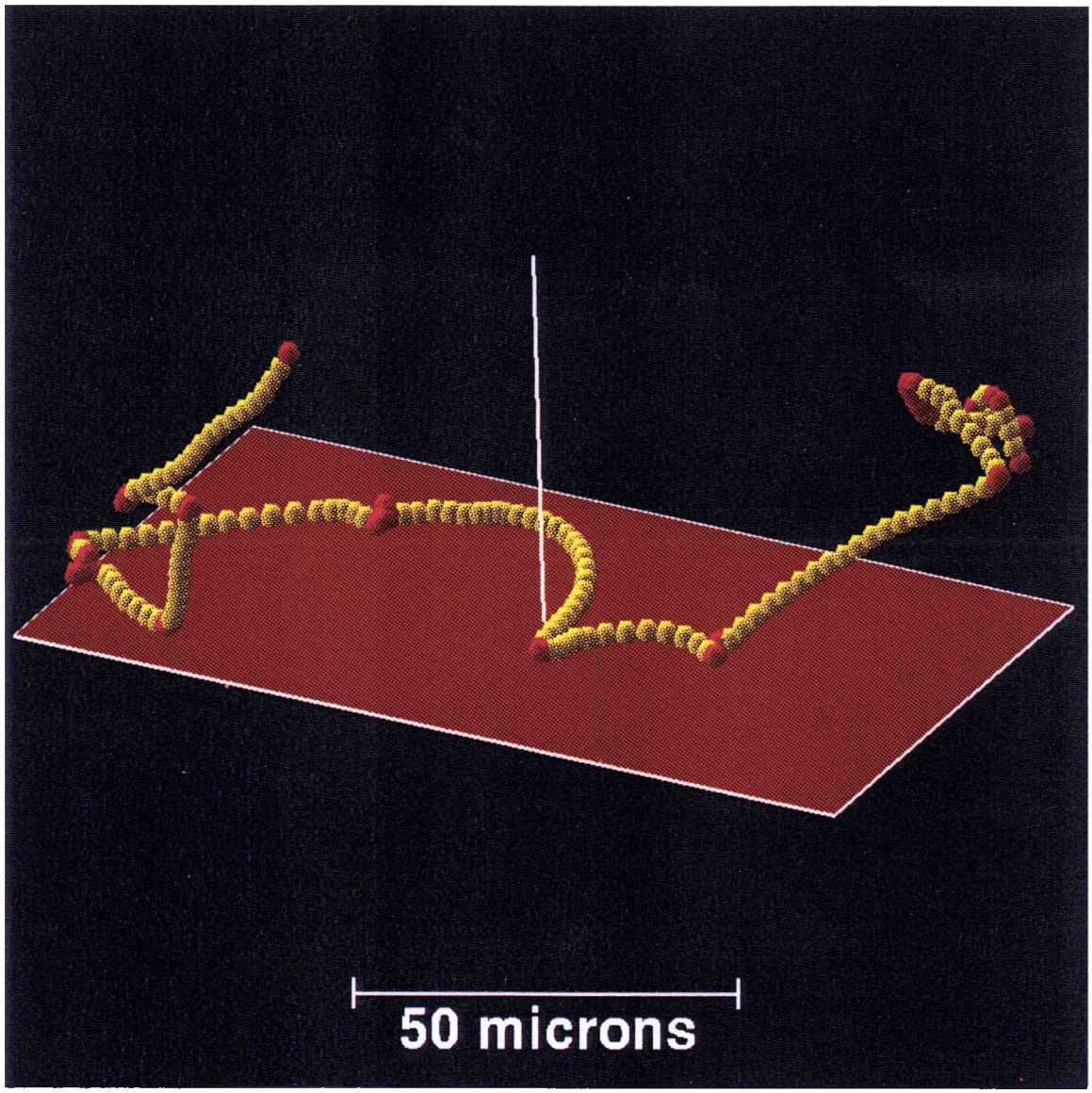

Figure F.3: Wild type bacterial trace 8.

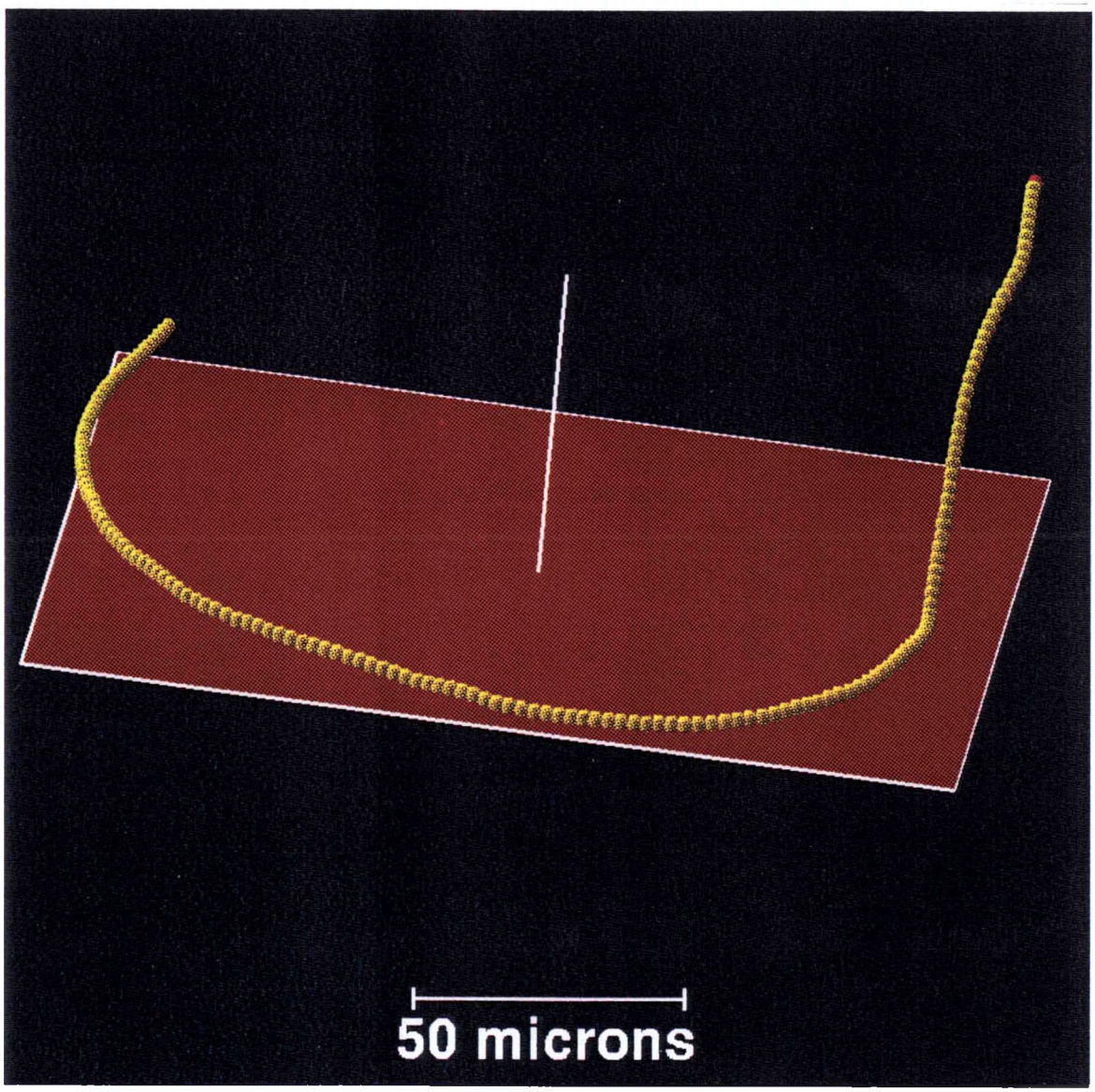

Figure F.4: Smooth swimming bacterial trace 4.

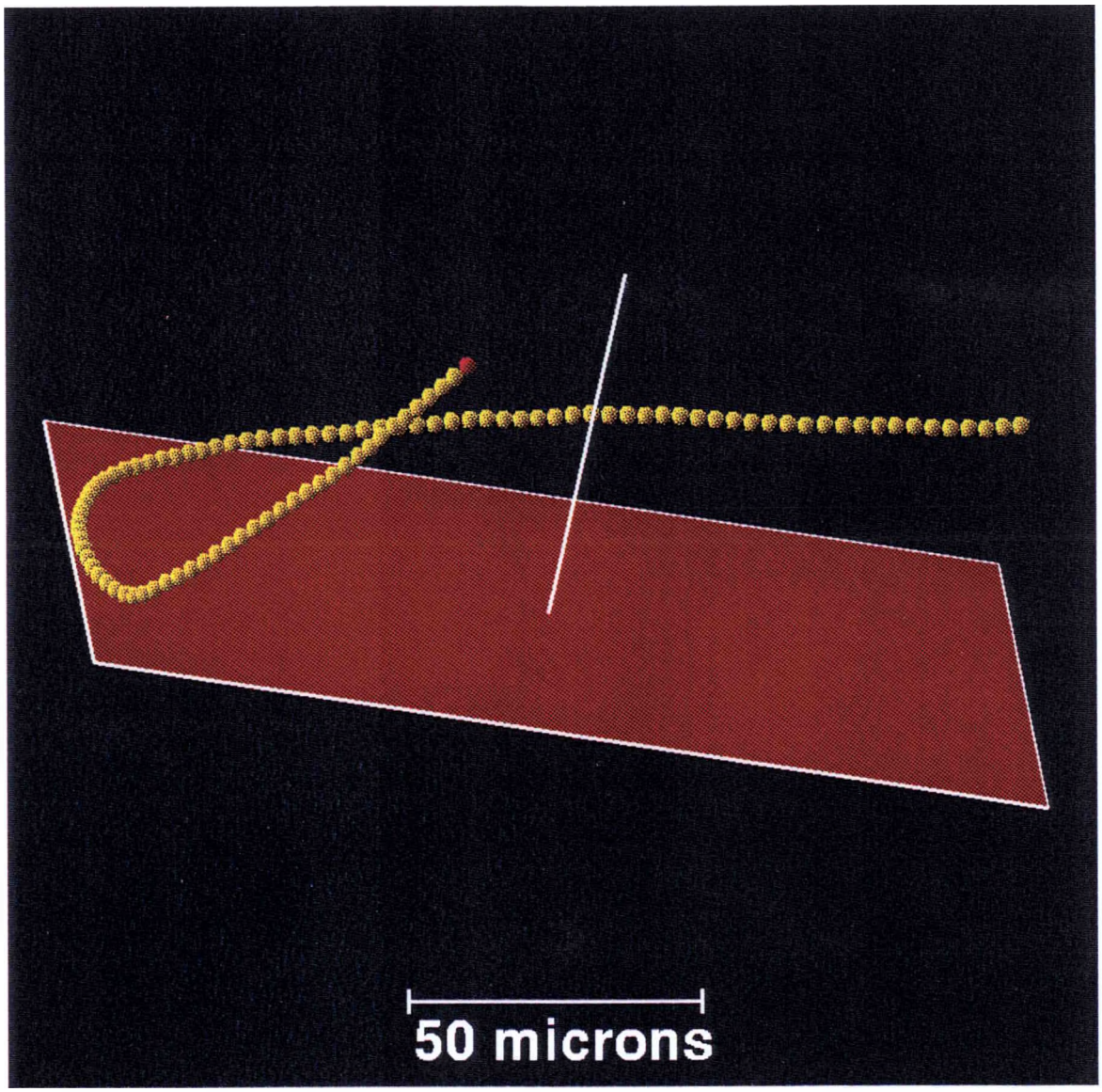

Figure F.5: Smooth swimming bacterial trace 5.

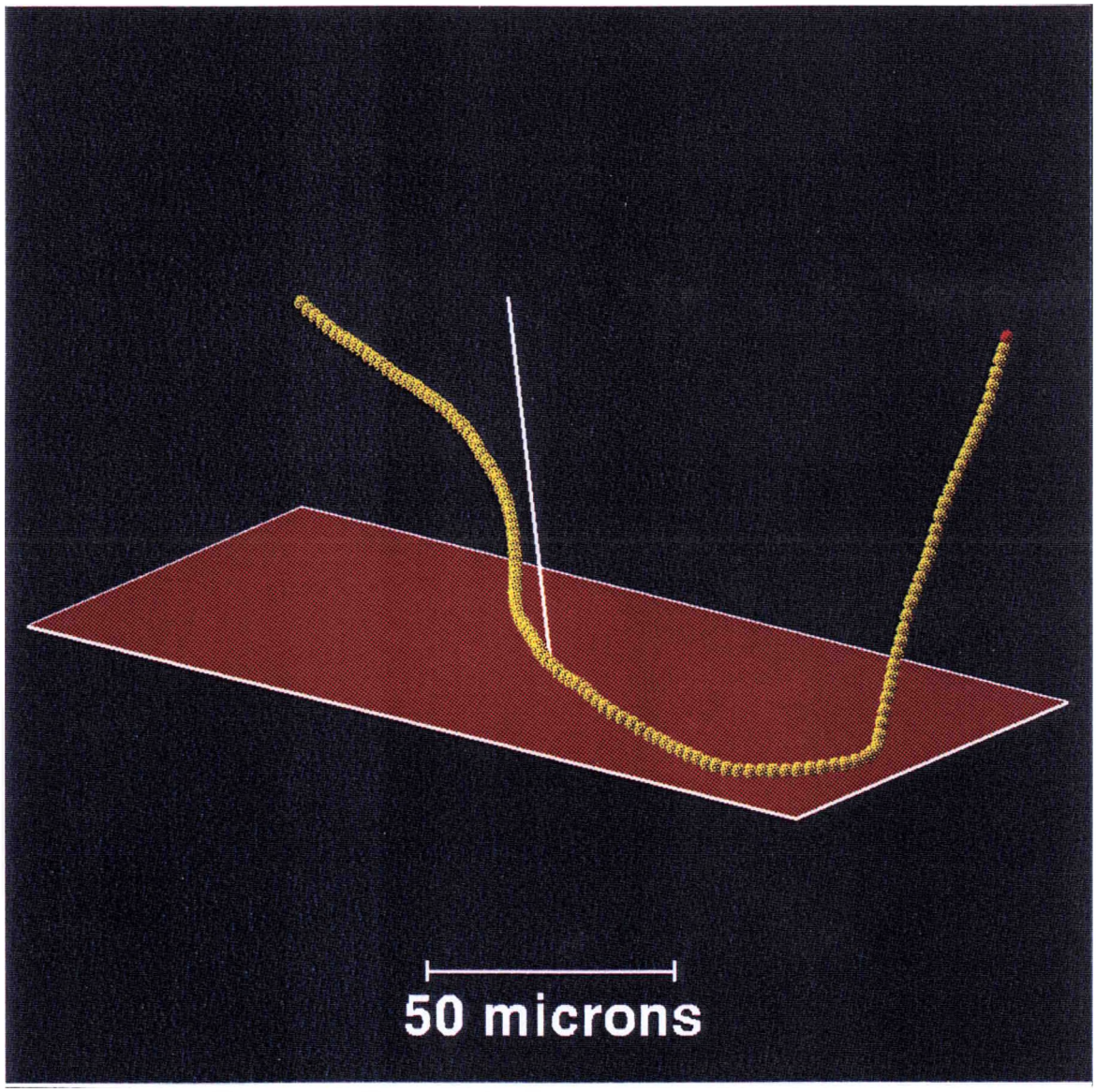

Figure F.6: Smooth swimming bacterial trace 6.

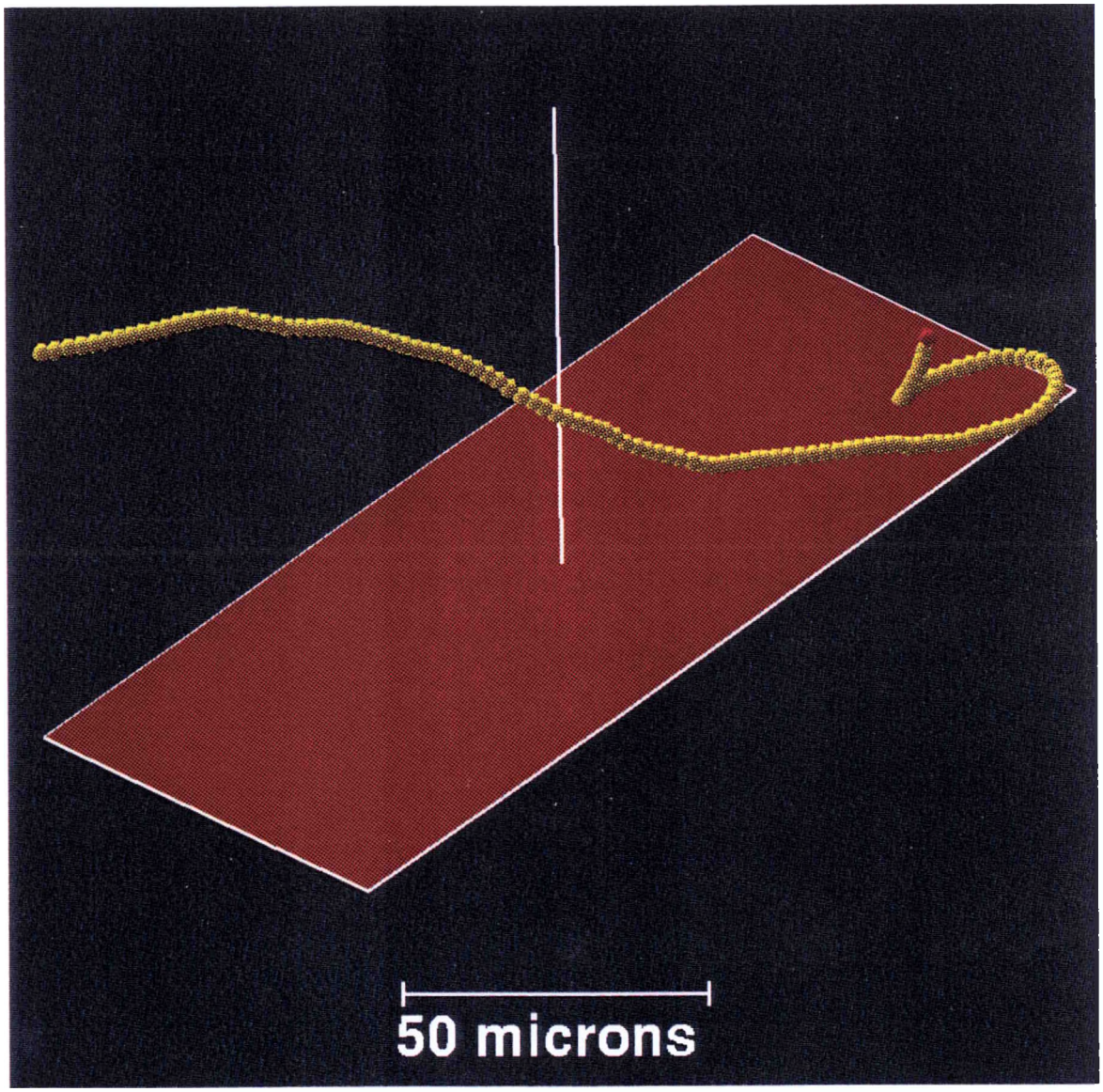

Figure F.7: Smooth swimming bacterial trace 7.